Synthesis and Profiling of Antimalarial Side-chain Modified Pyrido[1,2-*a*]benzimidazoles

A dissertation submitted to the University of Cape Town in fulfillment of the requirements for the degree

Masters in Chemistry

By Linley Nicole Barnard

Supervisor: Professor Kelly Chibale

Department of Chemistry
University of Cape Town
Rondebosch
7701
South Africa

March 2017

Declaration

I hereby declare that ***Synthesis and Profiling of Antimalarial Side-chain Modified Pyrido[1,2-a]benzimidazoles*** is my own work and has not been presented for the award of any degree at any university. I understand what plagiarism means and I know that it is wrong. Therefore I declare that all the work in this document is my original work.

_____

Linley Nicole Barnard

March 2017

Acknowledgments

This dissertation is not the product of a one-man-effort in any way. There are so many people who have contributed to this product and there will never be enough words to thank them. To my beloved parents, Teresa and Nico Barnard, I have no words to express my deep gratitude and love for you. You have been my rock, my support, my inspiration and the people closest to my heart. Thank you for always believing in me and sacrificing so much to give me the very best. From the bottom of my heart I want to thank my supervisor, Prof. Kelly Chibale, for his tenderhearted mentorship since day 1. I am forever grateful for the wisdom and knowledge you have shared with me in our meetings. You have given me an incredible example of passion, leadership and above all, humility. Thank you for investing in me and giving me the most tremendous opportunities. You have been one of the biggest blessings from God. To my PBI team – Kawaljit Singh, Ferdinand Ndubi, Godfrey Mayoka, John Okombo and Christel Brunschwig. Your support and encouragements have been a constant light in my life. To the people who helped me solve problems and attempt new things in this dissertation – Mathew Njoroge, Lauren Arendse, Nicole Sykes, Steven Fienberg and Neil Ravenscroft – you have been valuable treasures and my heart overflows with gratitude for your kindness and willingness to help. To precious friends that became family – Tracy-Lee Flowers, Merilyn Sandnes, Chanel Samuels, Gayle Watters, Nicci Scheepers, Jessica Akester, Josh Beretta, Margaret Paton and Mo Motala – you have all been such a light during the dark times. I treasure your hearts of gold and I will never be able to thank you enough for all that you do and all that you are to me. As I look over the past two years, I see the grace of God carrying me through this beautiful journey. All the effort and hours that have been put into this dissertation is for You Jesus, my King. He has blessed me abundantly with incredible opportunities, with the most precious people mentioned above, and with His grace and love that I am not worthy of. Thank you Lord for never giving up on me. Thank you for loving me at my most unlovable. Your grace is sufficient for me, for Your power is made perfect in

my weakness. Psalm 16:8 “I have set the Lord always before me; because He is at my right hand, I will not be shaken.”

Publications

Singh, K.; Okombo, J.; Brunschwig, C.; Ndubi, F.; Barnard, L.; Wilkinson, C.; Njogu, P.M.; Njoroge, M.; Laing, L.; Machado, M.; Prudeñcio, M.; Reader, J.; Botha, M.; Nondaba, S.; Birkholtz, L-M.; Lauterbach, S.; Churchyard, A.; Coetzer, T. L.; Burrows, J. N.; Yeates, C.; Denti, P.; Wiesner, L.; Egan, T. J.; Wittlin, S. and Chibale K. Antimalarial Pyrido[1,2-a]benzimidazoles: Lead Optimization, Parasite Life Cycle Stage Profile, Mechanistic Evaluation, Killing Kinetics, and in Vivo Oral Efficacy in a Mouse Model. *J. Med. Chem*. **2017**, *60* (40), 1432-1448.

Okombo, J.; Singh, K.; Mayoka, G.; Ndubi, F.; Barnard, L.; Njogu P. M.; Njoroge, M.; Gibhard, L.; Brunschwig, C.; Vargas, M.; Keiser, J.; Egan, T. J.; and Chibale, K. Antischistosomal Activity of Pyrido[1,2-a]benzimidazole Derivatives and Correlation with Inhibition of β-Hematin Formation. *ACS Infectious Diseases* **2017**, *3* (6), 411-420.

Conferences

January 2016 – Poster Presentation:

Improving Physicochemical Properties of Antimalarial Pyrido[1,2-a]benzimidazoles at the **Keystone Symposia on Drug Discovery for Parasitic Diseases**, 24 - 28 January 2016, Granlibakken Resort, Tahoe City, California, USA.

November 2016 – Poster Presentation:

Improving Physicochemical Properties of Antimalarial Pyrido[1,2-a]benzimidazoles at the **H3D Symposia on Malaria, Tuberculosis and Neglected Tropical Diseases**, 15 – 18 November 2016, Goudini Spa, Western Cape, South Africa.

Abstract

The currently available malaria drugs in the market are unsatisfactory in many respects. Shortcomings include costly treatments, toxicity and various side effects. The rapid rise of resistant strains of *Plasmodium falciparum*, particularly in South-East Asia, has rendered even the most promising treatment regimens ineffective. Therefore, there is an urgent need to explore and develop new antimalarial drugs preferably with novel mechanisms of action, multistage activity, good safety profiles and efficacy at low doses. To address this need, structure activity relationship (SAR) and structure property relationship (SPR) studies were carried out on a novel antimalarial chemotype, namely the pyrido[1,2-*a*]benzimidazoles (PBI) class of compounds. A frontrunner compound based on the PBI scaffold was previously found to possess potent antiplasmodial activity *in vitro* [IC_{50}(Pf NF54) = 0.11 μM; IC_{50}(Pf K1) = 0.12 μM] and promising oral efficacy (95% at 4×50 mg/Kg p.o) in the *in vivo* mouse *P. berghei* model. However, pharmacokinetic (PK) studies showed oral-limited absorption attributed to poor dissolution or solubility. Thus a series of derivatives was synthesized by making structural modifications to the parent PBI scaffold by distorting the symmetry through introduction of small groups in the C-2 position (Figure i), in an effort to identify derivatives with improved solubility properties, while retaining antiplasmodial activity. The synthesized derivatives displayed good antiplasmodial activity against the chloroquine-sensitive (NF54) strain of *P. falciparum* and selected compounds against the multi-drug resistant (K1) strain. However, substitutions at the C-2 position resulted in derivatives with improved solubility at the expense of antiplasmodial activity and metabolic stability. In an effort to investigate the factors responsible for improvement in solubility, the dihedral angles of the optimized structures were derived using density functional theory (DFT) calculations (B3LYP/6-31G*). The calculated dihedral angle of compound **6.4** was compared to the experimentally determined dihedral angle from the single X-ray crystal structure of **6.4**. A weak correlation (R^2 = 0.4) between kinetic solubility and dihedral angle was observed and this suggests that there are many factors that influence

solubility and that dihedral angle is just one them.

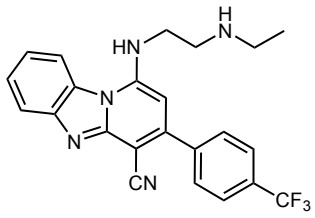

A

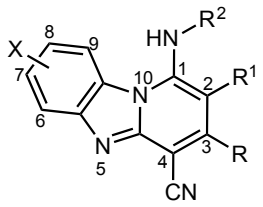

B

Figure i: The structures of the parent PBI compound (**A**) and the general PBI scaffold (**B**) representing synthesized structural derivatives.

Abbreviations

°C	degree Celsius
*μ*g/ml	microgram per milliliter
*μ*L	microliter
*μ*M	micromolar
Å	angstrom
ACT	artemisinin combination therapy
APCI	Atmospheric Pressure Chemical Ionization
ASU	asymmetric unit
BHI	*β*-hematin inhibition
$CDCl_3$	deuterated chloroform
CD_3OD	deuterated methanol
CHO	Chinese Hamster Ovary
CSD	Cambridge Structural Database
CYP	cytochrome P450
DCM	dichloromethane
DDD	drug discovery and development
DFT	density functional theory
DMF	*N,N*-dimethylsulfoxide
DMSO-d_6	deuterated dimethyl sulfoxide
EtOAc	ethyl acetate
ESI	Electron Spray Ionization
Hb	haemoglobin
HCl	hydrochloric acid
Hex	hexane
HLM	Human Liver Microsomes
HPLC	High Performance Liquid Chromatography
Hz	Hertz
IC_{50}	inhibitory concentration required to inhibit growth of 50 % of the organism
ip	intraperitoneal
IUPAC	International Union of Pure and Applied Chemistry

LC/MS	Liquid chromatography–mass spectrometry
MeOH	methanol
Mg	Magnesium
MHz	Megahertz
MLM	Mouse Liver Microsomes
mm	millimeter
mmol	millimole
m.p.	melting point
MS	Mass Spectrometry
MTT	3-(4,5-dimethylthiazol-2-yl)-2,5-diphenyltetrazolium-bromide
m/z	mass to charge ratio
NH_4OAc	ammonium acetate
nm	nanometer
NMR	Nuclear Magnetic Resonance
PBI	pyrido[1,2-*a*]benzimidazoles
PBS	Phosphate Buffered Saline
PK	pharmacokinetics
po	orally
$POCl_3$	Phosphorus(V) oxychloride
ppm	parts per million
R_f	retention factor
RMSD	root-mean-square deviation
SAR	structure-activity relationship
SD	standard deviation
SI	Selectivity Index
TDR	Tropical Disease Research
THF	tetrahydrofuran
TLC	Thin Layer Chromatography
t_R	retention time
WHO	World Health Organization
δ	NMR chemical shift

Table of Contents

CHAPTER 1: INTRODUCTION AND LITERATURE REVIEW

1.1 Malaria

1.1.1 Etiology

Malaria is a life threatening, mosquito-borne disease responsible for ubiquitous morbidity and mortality. The infectious disease is caused by five strains of the *Plasmodium* parasite. Four of these are responsible for human malaria namely *P. falciparum*, *P. vivax*, *P. malariae* and *P. ovale*. The female *Anopheles* mosquito functions as the malaria vector that transports the parasite from one person to another. Of the 400 species, only 30 species of *Anopheles* mosquito are considered important vectors.[1]

The fifth strain of *Plasmodium* parasite, *P. knowlesi*, is known to cause malaria in monkeys in South-East Asia. Current research has shown that *P. knowlesi* malaria may be transferred between humans and monkeys when an *Anopheles* mosquito, infected by a monkey, bites a human.[1]

P. falciparum is predominantly found in the African region and is responsible for most malaria fatalities. *P. vivax* is the most widespread because it can develop in the *Anopheles* mosquito vector at lower temperatures and survive at higher altitudes. However, it is mostly found outside of the African region due to many African populations who lack a protein which *P. vivax* requires to invade red blood cells.[1]

1.1.2 Epidemiology

Malaria is largely distributed in tropical areas of the world with most cases found in sub-Saharan Africa and the South-East Asia regions. The World Health Organization (WHO) reported 212 million cases of malaria in 2015, with 90% of these cases occurring in the WHO African region (see Table 1).

Table 1: **A Table of the global trends in malaria incidence and mortality reported for 2015.**

WHO Region	% Malaria cases	% Malaria deaths
Africa	90	92
South-East Asia	7	6
Eastern Mediterranean	2	2

Young children remain exceedingly vulnerable to this disease with about 70 % of the 438 000 malaria deaths of 2015 occurring in children under the age of 5 and 292 000 of these deaths were in children from the WHO African Region. This makes malaria the fourth highest cause of death in children with 10% of child deaths in sub-Saharan Africa attributed to malaria.[2]

Amongst the 95 endemic countries and territories that continue to fight the ongoing battle against malaria, the global burden is heavily distributed in Africa where an estimated 80% of malaria cases and 78% of deaths are accounted for in 15 countries.[2]

1.1.3 Life cycle and pathogenesis

The *Plasmodium* parasite is an obligatory intracellular protozoan with specialized methods of traveling across tissue membranes and invading host cells in the mosquito vector and human host. The female *Anopheles* mosquito carries the motile forms of the parasite, known as sporozoites, in the salivary glands (Figure 1.1).[3]

Upon biting the human host during a blood meal, the sporozoites are injected into the bloodstream (1) and travel to the liver where they invade hepatocytes (2).[4] The asymptomatic liver stage will last for about 6 days and involves sporozoites growing and dividing in each hepatocyte to produce thousands of haploid forms known as merozoites.[5] Hepatocytes rupture to release merozoites into the bloodstream where they invade erythrocytes and start asexual replication to produce new merozoites in the intraerythrocytic cycle

(3).[6] This is known as the asexual blood stage of the infection and it is the pathogenic stage where the host will present clinical symptoms (4).[7] During the asexual blood stage, parasites replicate to produce 8-20 new merozoites every 48 hours and thus cause parasite numbers to increase to 10^{13} per host.[5] Merozoites in the infected erythrocytes will eventually leave the asexual multiplication stage and develop into the sexual forms that will circulate in the bloodstream as male and female gametocytes (5).[7] The sexual stage parasites are nonpathogenic but are transmissible to the mosquito vector.[5]

A mosquito that bites an infected human will ingest gametocytes with its blood meal (6). The gametocytes will travel to the gut of the mosquito where the human erythrocyte will burst to release the gametocytes (7). The gametocytes will develop into male and female gametes that will fuse to form diploid zygotes that develop into motile ookinetes that can travel to the midgut wall of the mosquito.[8] Once they reach the midgut they form oocysts that grow and divide to form thousands of haploid forms known as sporozoites. After 1-2 weeks, oocysts burst to release sporozoites that travel to the salivary glands of the mosquito where the infection cycle will continue.[5]

The development of the parasite within the host brings about various structural, biochemical and functional changes in the erythrocytes that may include changes in shape, membrane rigidity and permeability to ions. These changes occur in response to proteins secreted by the parasite and interactions with erythrocyte membrane proteins. These effects allow the parasite to survive within the host cell for extended time periods and enhance the virulence of the disease which may lead to cerebral malaria and anemia.[9]

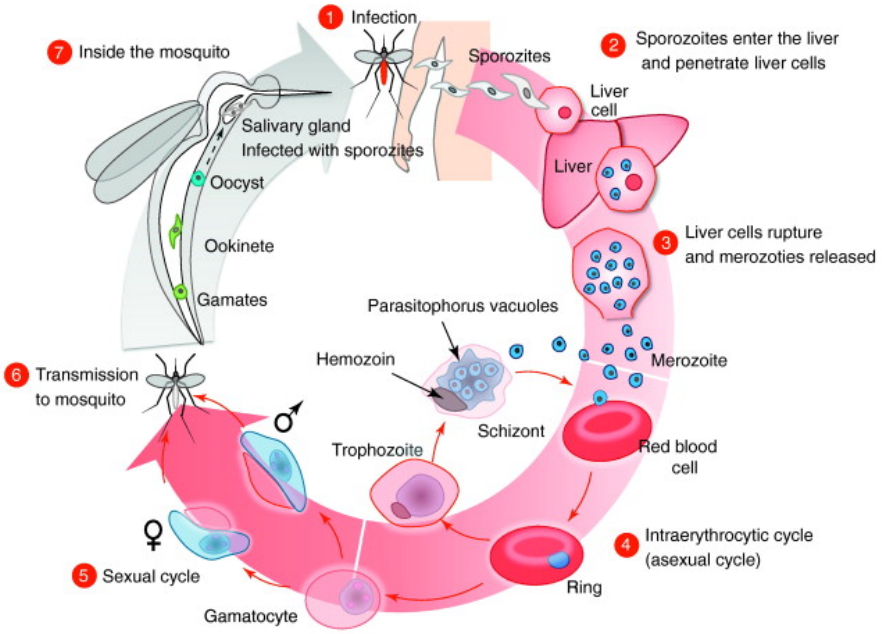

Figure 1.1. Life cycle of the *Plasmodium* parasite.[6]

1.1.4 Chemotherapy and treatment challenges

Cost-effective interventions can lead to the treatment and control of malaria. Such measures involve case management for early detection and prompt diagnosis, vector control that aims to reduce the transmission of the disease between parasite and human and chemoprevention to suppress the infection in humans.[1]

One of the first agents used for the treatment of malaria was the bark of the Cinchona tree. The structure of one of the active components in the bark, quinine (**1**), was elucidated in 1908.[10] Due to the side effects associated with the toxicity of quinine such as diarrhea, nausea, stomach cramps and vomiting, as well as its requirement for multiple dosages, structure-activity relationship (SAR) studies led to the development of the successful derivative chloroquine (**2**).[11] Chloroquine was first synthesized in 1934 and became the most common first-line treatment for a variety of parasites due to its low cost, high efficacy and easy accessibility.[12] The first case of chloroquine-resistant *P. falciparum* was reported in 1961 in Colombia.[13] Chloroquine-resistance escalated dramatically and led to the development of the structurally related,

quinoline-based synthetic derivatives that include mefloquine (**3**) and halofantrine (4), as seen in Figure 1.2.[14]

These compounds are highly active against chloroquine-resistant strains albeit parasite-resistance to these drugs has developed rapidly. Furthermore, these drugs are known to cause unfavorable side effects. Halofantrine is known to cause diarrhea, vomiting and headaches and mefloquine may cause dizziness, anxiety, hallucinations and depression.[15,16]

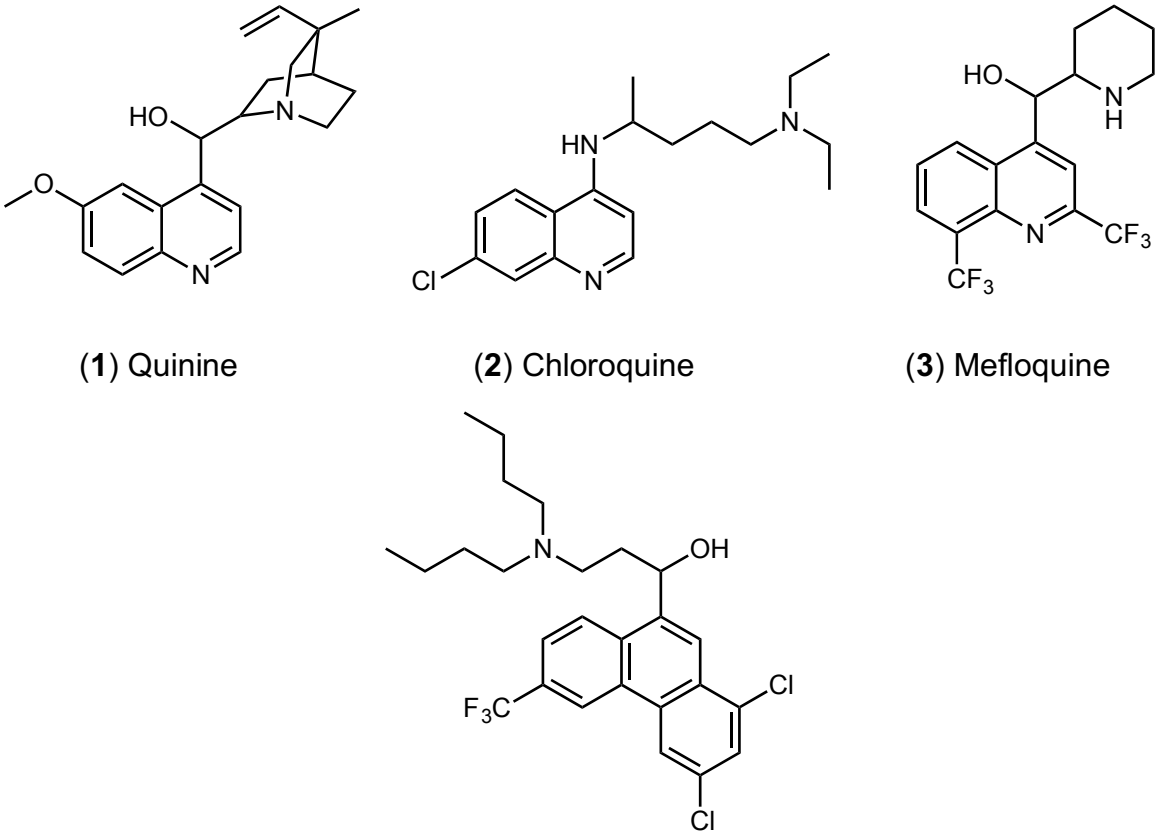

(**1**) Quinine (**2**) Chloroquine (**3**) Mefloquine

(**4**) Halofantrine

Figure 1.2. Structures of quinoline-based antimalarial drugs.

Artemisinins have been identified as non-quinoline-based antimalarial drugs. The parent drug, artemisinin (**5**), is derived from the sweet wormwood *Artemisia annua*. The antimalarial properties of this sesquiterpene lactone were discovered in the 1970s by Chinese scientists. It is the fastest acting drug against *P. falciparum*. However, the short half-lives and rapid clearance of artemisinin and its semi-synthetic derivatives is a drawback to effective deployment.[17]

Although their mode of action is still not well understood, artemisinins are unique in the fact that they target the asexual parasites of the blood stage infection and cause rapid clearance. In addition, these drugs target gametocytes, which are responsible for transmission.[18] By the 1990s, artemisinin monotherapies were widely used in Asia. In 2001, the WHO recommended replacement of artemisinin monotherapies with artemisinin combination therapies (ACTs) to stop the spread of drug-resistant strains.[19]

In ACT treatment, the artemisinin derivative (**6**) is paired with a long acting partner drug that has a different mechanism of action. The purpose of combination therapy is to minimize opportunities for drug resistance to develop and spread.[18] By 2012, 99% of ACT deliveries consisted of fixed-dose combination ACTs, which consist of two active drugs combined into a single tablet. This type of delivery allows for improved patient adherence.[20]

The first ACT, artemether-lumefantrine (Figure 1.3), was registered in 1992 and administered as a single tablet.[17] By 2010, 56 countries were using artemether-lumefantrine as a first- or second-line treatment. There are five combinations of ACTs that are currently recommended to treat malaria namely: artemether-lumefantrine, artesunate-amodiaquine, artesunate-mefloquine, artesunate-sulfadoxine-pyrimethamine and dihydroartemisinin-piperaquine. The choice of treatment is dependent on the therapeutic efficacy of the combination therapy in a particular region.[21]

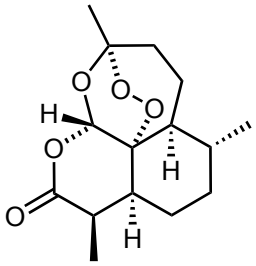

(**5**) Artemisinin

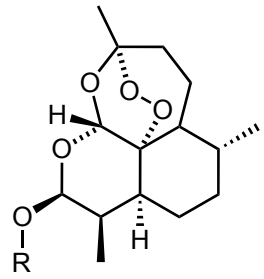

Artemisinin Derivative	R
Artemether	Methyl
Artether	Ethyl
Artesunate	$CO(CH_2)_2CO_2H$

(**6**) Artemisinin Derivatives

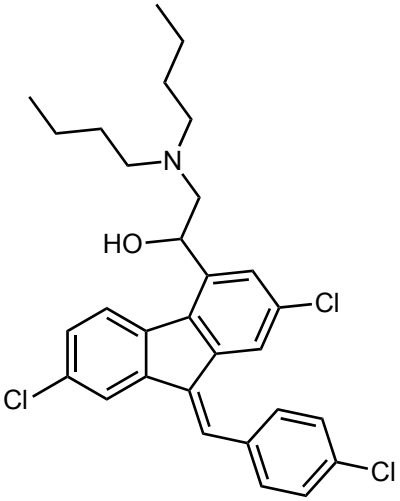

(**7**) Lumefantrine

Figure 1.3. Structures of artemisinin (**5**), artemisinin derivatives (**6**) and the partner drug, Lumefantrine (**7**).

Resistance to artemisinins has been reported in Cambodia, Thailand, Vietnam, Myanmar and the Lao People's Democratic Republic.[22] Until now, the partner drug in the combination therapy has ensured that patients still respond effectively to ACT treatment. Thus resistance to the partner drug will have serious consequences for ACT treatment regimens.[1]

Atovaquone (**8**) is an antimalarial agent that inhibits mitochondrial electron transport in the parasite. Despite its excellent efficacy, the rapid development of parasite resistance means it is typically used in prophylaxis in a synergistic combination with proguanil (**9**) (Figure 1.4). This fixed-dose combination therapy has fewer side effects but comes at a high cost.[23]

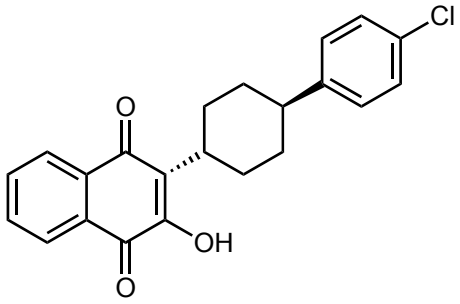

(**8**) Atovaquone

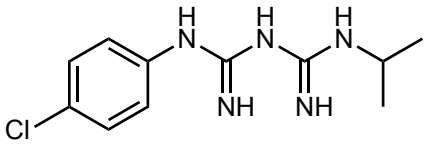

(**9**) Proguanil

Figure 1.4. Structures of atovaquone (**8**) and proguanil (**9**).

Tetracycline (**10**) and lincomycin (**11**) are antibiotics that have played an important role in the development of antimalarial drugs (Figure 1.5). Doxycycline (**12**) is a synthetically derived tetracycline used as a prophylactic drug for travellers. It can be used to treat malaria when used in conjunction with a fast acting schizontocidal agent. Quinine can be used with doxycycline to treat chloroquine-resistant malaria caused by *P. falciparum* and *P. vivax.* This combination therapy is especially successful to treat the disease in areas where chloroquine- and multidrug-resistant malaria limits treatment options.[24]

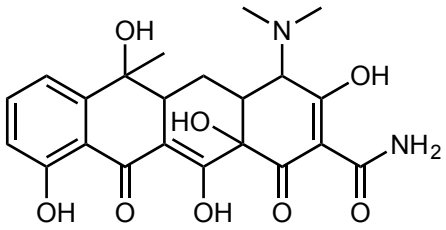

(**10**) Tetracycline

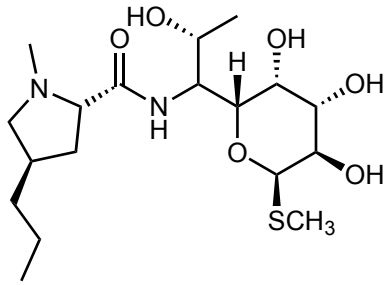

(**11**) Lincomycin

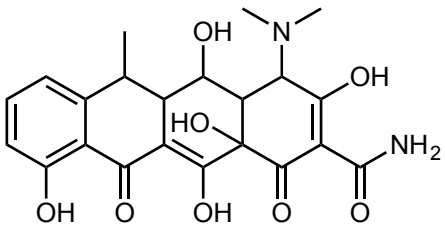

(**12**) Doxycycline

Figure 1.5. Structures of antibiotics used as antimalarial drugs.[24]

The advantage of antibiotics is that the safety concerns regarding pregnant women is known and thus they can be used to treat pregnant women in their

first trimester of pregnancy. However, there are concerns regarding the development of resistant strains.[25]

The high cost, toxicity and rising emergence of resistant strains of the *Plasmodium* parasite are limiting the use of the available and potential antimalarial treatments. Due to the fact that there are few alternatives to ACTs, there is an urgent need for new antimalarial drugs with novel mechanisms of action as well as better safety and resistance profiles.

1.2 Strategies in Antimalarial Drug Discovery

1.2.1 Introduction

A combination of scientific and technological advancements has transformed drug discovery over the past 100 years. Early drug discovery approaches were focused on observing the phenotypes that substances induced in humans and animals. The rise of the technological age in the late 1990s saw major advancements in the knowledge of how drugs produce a phenotype and led to the emergence of the target-based screening approach. This section focuses on the efficiencies of these major strategies, as well as targeting the host hemoglobin degradation as a valuable tool in antimalarial drug discovery.

1.2.2 Target-based screening

Target-based screening is a strategy that investigates the chemical response induced by a compound when it acts on a particular biological target.[26] With the advancement of biochemistry and the pioneering of genomics in the 1980's, target-based screening started generating interest as it began replacing the standard approach of phenotypic screening.[27]

This approach received increased attention as structural biology and computational tools developed that allowed for more structure-based drug

discovery. This technology meant that compounds could be designed to specifically bind to a particular target and therefore provide more information regarding the mechanism of action of the drug, which phenotypic screening lacked at the time.[28]

However, compounds identified through this approach have occasionally displayed inactivity against the whole cell or in whole organism assays.[29] Recent years have seen a decline in the use of target-based approaches as researchers have concluded that it may limit the breadth of new findings.[27]

1.2.3 Phenotypic whole-cell screening

Phenotypic screening is an approach that involves the successive testing of compounds in a biological system (e.g. cells, tissues, whole organisms) to induce a desired effect or phenotype.[26] Despite many opinions regarding which approach is superior, between target-based and phenotypic whole-cell screening, the contribution of first-in-class small molecule drugs developed between 1999 and 2008 by phenotypic screening surpassed the amount by the target-based approach. [30]

The advantage of phenotypic screening is the potential of identifying biologically active compounds that act on a novel target or simultaneously act on more than one target and thus reduce the likelihood of resistance. This approach has the additional advantage of producing hits with important drug-like properties (e.g. cell penetration) as it takes into account the real biological environment in which compounds will have to interact with targets.[27,31] Furthermore, phenotypic screening provides the advantage of discovering new disease biology in the cases where it is not well understood.[32]

The well-known challenges of phenotypic screening that has rendered it “the road less travelled” to many drug discovery teams are the difficulties accompanied with identifying the relevant target(s) of the drugs and understanding the mechanism of action.[33] The resurgence of phenotypic screening over the last few years is as a result of new technologies in

chemogenetics and chemical proteomics that have been developed to advance target identification techniques.[34–36] A review by Guiguemende *et al.*[37] reports on how phenotypic whole cell screening has played a key role in the malaria drug discovery programs over the last few years.[37]

1.2.4 Hemoglobin degradation

When the malaria parasite enters the host bloodstream, it invades the erythrocytes. It then ingests the hemoglobin (Hb) from the erythrocyte through a process known as pinocytosis (Figure 1.6).[38] Once the Hb enters the food vacuole (FV) of the parasite, it is digested by protease enzymes resulting in the release of small peptides, which are a nutrient source for the parasite.[39] Simultaneously, free heme [Fe(II)PPX] is released and is subsequently oxidized to hematin (ferriprotoporphyrin IX, [Fe(III)PPX]), known to be toxic to the parasite. To overcome this hematin toxicity, the parasite uses an inherent heme detoxification system. This system allows the parasite to convert toxic hematin [Fe(III)PPX] to a non-toxic crystalline form known as hemozoin.[40]

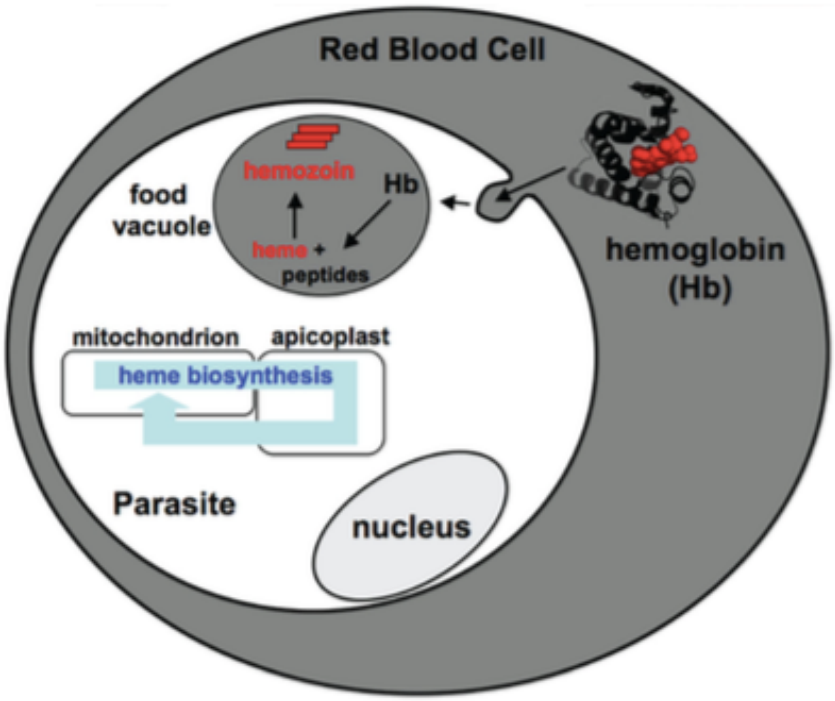

Figure 1.6: The pathway of hemozoin formation.[40]

Antimalarial drugs, such as chloroquine, are known to act through inhibition of the formation of the non-toxic hemozoin by forming π-π complexes with heme. This results in the accumulation of toxic heme in the food vacuole of the parasite, which leads to parasite death.[41]

The availability of assays based on *β*-hematin, the synthetic equivalent of hemozoin, has facilitated screening for inhibition of *β*-hematin formation. The strategy for the rational drug design of novel antimalarial *β*-hematin inhibitors (BHI) requires compounds that form strong complexes with heme and thus inhibit the formation of *β*-hematin. In addition, compounds need to accumulate in the food vacuole of the parasite.[42]

1.3 Solubility

1.3.1 Introduction

Solubility is a physicochemical property that describes the ability of a compound to dissolve in a solvent at equilibrium. It has a major impact on the bioavailability of a drug. Early stage solubility information is essential for analyzing SAR studies of lead compounds to allow for structure-solubility relationships to be explored.[43]

Early on in the drug discovery and development (DDD) process, solubility may be used as a parameter to determine whether a class of compounds is viable for SAR studies in the hit-to-lead stage. In the lead optimization stage, solubility becomes a major issue because molecular modifications made to improve target-protein binding may become detrimental to the physicochemical properties of the molecule such as solubility.[44]

Since poor solubility may lead to assay inaccuracies and developmental challenges, a more holistic approach is favorable as the focus is then divided between activity and drug-like properties. This approach yields better drug

candidates because a less potent drug may have improved drug-like properties that translate to superior *in vivo* results.[43]

1.3.2 Strategies to improve solubility

Structural properties determine the *in vivo* physicochemical and biochemical properties, pharmacokinetics and toxicity of a drug.[43] Various strategies can be employed to improve solubility. Structural modification strategies include the addition of ionizable groups, polar groups, hydrogen bonding, reducing molecular weight, reducing logP, disruption of molecular planarity and symmetry or constructing a pro-drug. However, these strategies may not always have the desired outcomes.

The common approach of introducing hydrophilic groups to improve aqueous solubility may result in decreased target protein-drug interactions. This is the case when the newly introduced hydrophilic groups form new hydrogen bonds that induce tighter crystal packing. In addition, the aforementioned strategy may not be viable in the case where solubility and hydrophobicity need to be improved.[45]

The aqueous solubility of a solid solute depends on the crystal packing of the solute as well as the ability of the solute to interact with water.[46] Therefore, disruption of the crystal packing could be considered as a unique alternative to improve aqueous solubility. Due to the fact that molecular planarity and symmetry affect crystal packing, it can be hypothesized that disruption of molecular planarity would result in less efficient crystal packing which may lead to decreased melting point and improved solubility of the compound.[45]

Ishikawa *et al.*[45] published work that focused on improving aqueous solubility by disrupting molecular planarity and symmetry through various chemical modifications. These modifications included removal of aromaticity, introduction of substituents into benzylic positions, twisting of fused rings and increasing dihedral angles. Disrupting molecular planarity by introducing small hydrophobic substituents in *ortho* positions of aromatic rings increases the

dihedral angle and lowers the crystal packing energy. This results in a decreased melting point and an increase in solubility.[45]

Melting point, dihedral angles and retention time on reverse-phase HPLC were used to examine any changes in physicochemical properties. Fluorine was reported to be an optimal substituent to disrupt molecular planarity and improve aqueous solubility owing to its small Van der Waals radius, next to hydrogen. Therefore, it is expected to have the least impact on target protein-drug interactions. This approach also allows for aqueous solubility to improve without increasing the molecular size, which may have unfavorable pharmacokinetic consequences.[45]

1.4 Drug Metabolism

1.4.1 Introduction

Drug metabolism is the process whereby a xenobiotic is chemically modified by enzymes to clear the compound from the body. The purpose of this biotransformation process is to increase the clearance of the drug and reduce exposure, which results in low bioavailability. Metabolism of all xenobiotics occurs mainly in the liver and other major organs such as the kidneys, lungs, skin and blood-brain barrier.[43,47]

Metabolism is divided into three phases. Phase I metabolism involves structural modifications, mainly catalyzed by cytochrome P450 (CYP) enzymes through oxidation, reduction and dealkylation. Phase II metabolism results in the conjugation of phase I metabolites with other hydrophilic molecules, which ultimately increase the aqueous solubility of these products in order to promote excretion from the body via bile and urine.[48,49] Phase III metabolism consists of drug transporters located in the epithelial and endothelial cells of the liver, gastrointestinal tract, kidney and blood-brain barrier. They transport drugs across cellular membranes and are thus responsible for the concentrations of the drug at the target site.[50]

1.4.2 Metabolic stability of drug candidates

Metabolic stability is a vital property in drug discovery that directly affects the pharmacokinetics (PK) of a drug. Quantitative metabolic stability studies are used to prioritize compounds for *in vivo* studies by evaluating the extent of metabolic breakdown. Qualitative metabolite structure studies are used to determine metabolic soft spots in order to design structural modifications that may sterically hinder the site of metabolism in an effort to improve the stability of the compound.[43]

In vitro models have been developed to allow the study of drug metabolism and metabolite identification during the drug discovery and development process. Since the liver is the predominant organ for metabolism, several *in vitro* human liver models have been developed in an effort to resemble metabolism *in vivo* in the liver. These *in vitro* human liver models are designed to reduce complexity of the study system.[51]

Pooled liver microsomes, liver S-9 fractions and hepatocytes are the three most commonly used *in vitro* models in the lead optimization and development process.[52] Liver microsomes are the most frequently used *in vitro* models. Though they don't possess as many metabolizing enzymes as hepatocytes, they include the important cytochrome P450 enzymes which are involved in the metabolism of 60 – 80 % of marketed drugs.[51]

Different animal liver microsomes are used to determine the best *in vivo* model for further testing. The transgenic mouse is a common efficacy model used to determine dosing concentrations for proof-of-concept studies. The rat is used for safety studies while *in vitro* work in the human model is used to make predictions for clinical studies.[43,51]

Drug optimization needs to be carried out with pharmacological activity, safety and metabolic stability in mind in order to ensure more efficient and successful drug discovery and development projects.[53]

CHAPTER 2: SYNTHESIS AND PHARMACOLOGICAL EVALUATION OF SIDE-CHAIN MODIFIED PYRIDO[1,2-*a*]BENZIMIDAZOLES

2.1 Introduction

This chapter describes the synthesis of pyrido[1,2-*a*]benzimidazole (PBI) derivatives obtained by performing SAR studies around a previously identified parent compound. These derivatives are aimed at improving antiplasmodial activity and solubility. The synthesized compounds were evaluated for solubility and *in vitro* antiplasmodial activity against the chloroquine-sensitive (NF54) strain, and selected compounds against the multidrug resistant (K1) strain, of *Plasmodium falciparum.* Towards elucidating the mechanism of action, compounds were also tested for *β*-hematin inhibition activity. Factors affecting solubility were also investigated.

2.2 Background

PBIs are compounds made up of a tricyclic nucleus. Their heterocyclic framework consists of a pyridine ring fused to a benzimidazole moiety (Figure 2.1). In naming this system, the benzimidazole moiety takes precedence as the base because it is made up of more rings than the pyridine ring. The 3 characters in the square bracket are the locants and they indicate which bond is common to both rings. The first 2 numbers in the square brackets (i.e. 1,2) refer to the numbers in the pyridine ring and the third character is an alphabetical character which refers to the bond as viewed from the benzimidazole ring. The numbering is assigned such that the lowest numerals and alphabet characters are chosen.[54]

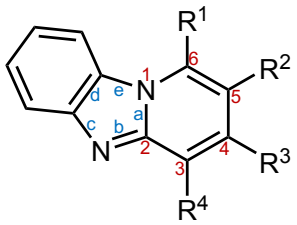

Figure 2.1: The general structure of pyrido[1,2-a]benzimidazoles.

2.2.1 Biological activity of pyrido[1,2-a]benzimidazoles

The numerous biological activities of, and diverse synthetic routes to, PBI compounds have attracted interest from medicinal chemists in recent years. The biological activities range from anticancer[55] (**13**), antifungal (**14**)[56], antimycobacterial (**15**)[57], antiviral[58] (**16**), anxiolytic[59] (**17**) and antiparasitic[60] (**18**). In addition, mechanistically they have shown potential as DNA intercalators[61] and perforin inhibitors[62] (Figure 2.2).

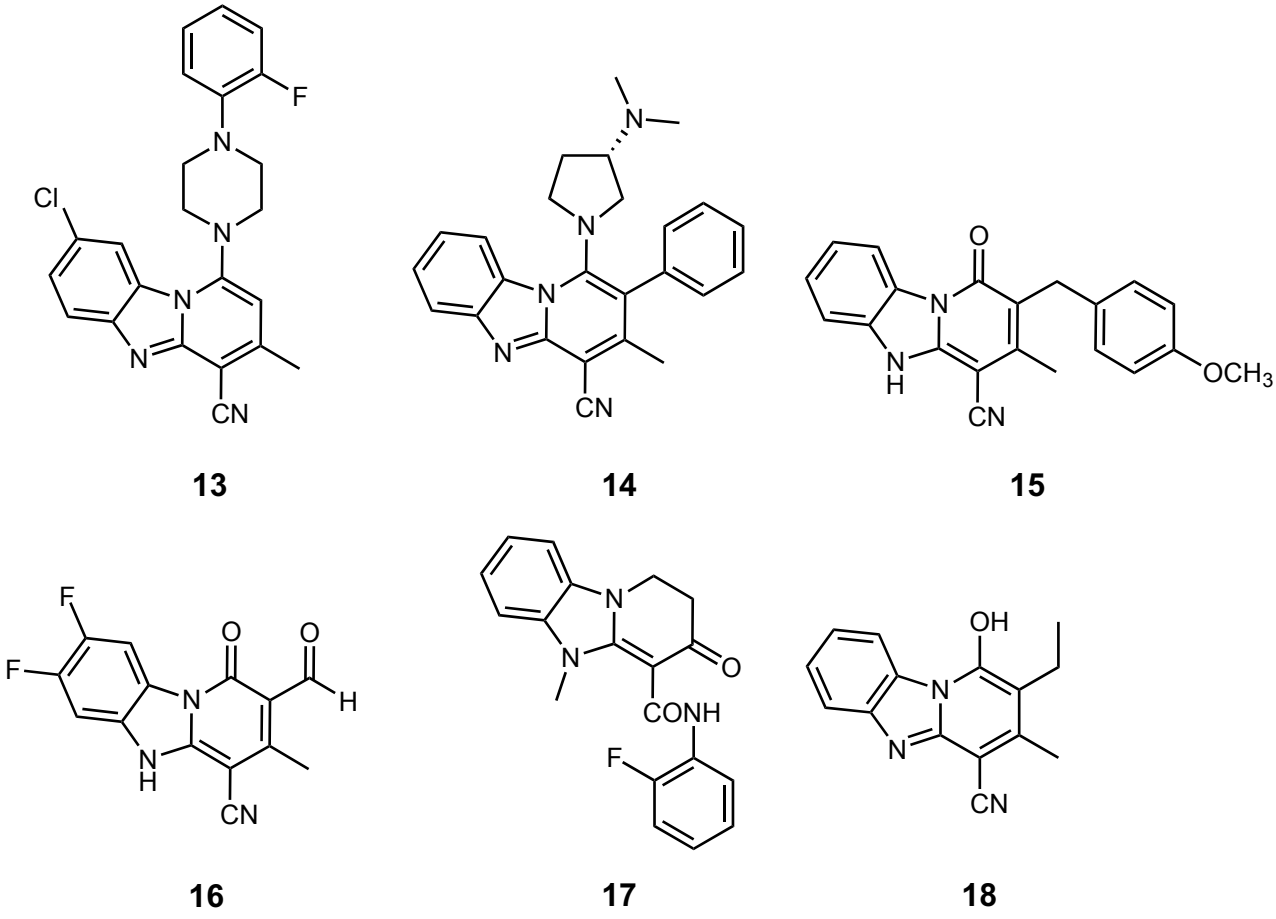

Figure 2.2: Structures of biologically active PBIs.

2.2.2 Pyrido[1,2-a]benzimidazoles as antimalarial agents

In 2011, Ndakala *et al.*[63] reported, for the first time, the antimalarial activity of PBIs. A small library of diverse compounds had previously been screened *in vitro* against a group of protozoa and the moderate antiplasmodial activity of PBIs was identified (Figure 2.3).

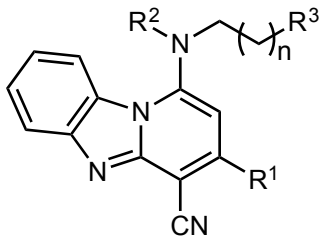

Figure 2.3: The PBI scaffold used for SAR exploration by Ndakala *et al*.[63]

Further SAR studies led to the identification of a more potent PBI derivative (**19** with IC_{50} values of 0.11 μM and 0.047 μM against NF54 and K1 strains, respectively. Compound **19** also showed significant efficacy in *Plasmodium berghei* infected mice following both intraperitoneal (ip) and oral (po) administration, with >90% inhibition of parasitemia (4 x 25 mg/kg). However, *in vitro* metabolic stability studies showed that **19** has a high rate of metabolic degradation and compound **20** was identified as its major metabolite, formed through *N*-dealkylation (Figure 2.4), with antiplasmodial activity comparable to **19**. However, *in vivo* (mouse) pharmacokinetic studies of compound **20** indicated that the oral absorption becomes saturated at relatively low doses, most likely because of poor dissolution or solubility.[63]

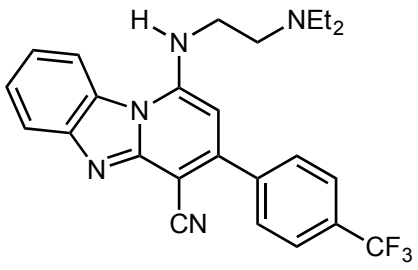

19

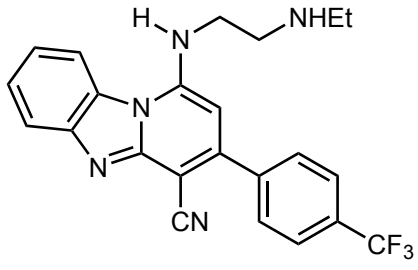

20

Figure 2.4: The structure of the lead compound (**19**) as well as the metabolite (**20**) identified during SAR studies.

2.3 Rationale

As indicated above, *in vivo* pharmacokinetics studies revealed an apparent solubility-limited absorption of compound **20**. Therefore, the main focus of this study was to improve the solubility of **20** while also expanding SAR studies on parts around the PBI core not previously explored.

As mentioned in Chapter 1, various approaches can be used to improve solubility. The main approach used in this study involves disrupting the molecular planarity and/or symmetry of the molecule by introducing small hydrophobic substituents, such as a methyl or fluorine group, in appropriate positions of the PBI core. Thus in order to further explore SAR studies, various substituents were introduced at various positions around the core.

2.4 Research Question

The research question is whether it will be possible to identify novel PBI-based antimalarial drug leads with favorable solubility, whilst retaining and/or improving desirable pharmacological properties.

2.5 Objective

The objective of this study was to optimize side-chain modified antimalarial PBIs with respect to solubility, metabolic stability and antiplasmodial activity. An attendant objective was mechanistic evaluation of compounds with respect to inhibition of *β*-hematin formation.

2.6 Specific Aims

i. Synthesis of PBI target compounds.
ii. Characterization of target compounds using spectroscopic and analytical techniques.
iii. *In vitro* profiling with respect to antiplasmodial activity, cytotoxicity, solubility, metabolic stability and *β*-hematin inhibition.

iv. Determination and evaluation of factors that may be responsible for improved solubility and deduce relationships.

2.7 Synthesis and Characterization

2.7.1 Introduction

Initial SAR studies were designed to determine the effect of incorporating small and large hydrophobic groups at C-2 (Figure 2.5) as this was postulated to be the optimal position for disruption of planarity in an effort to improve solubility.

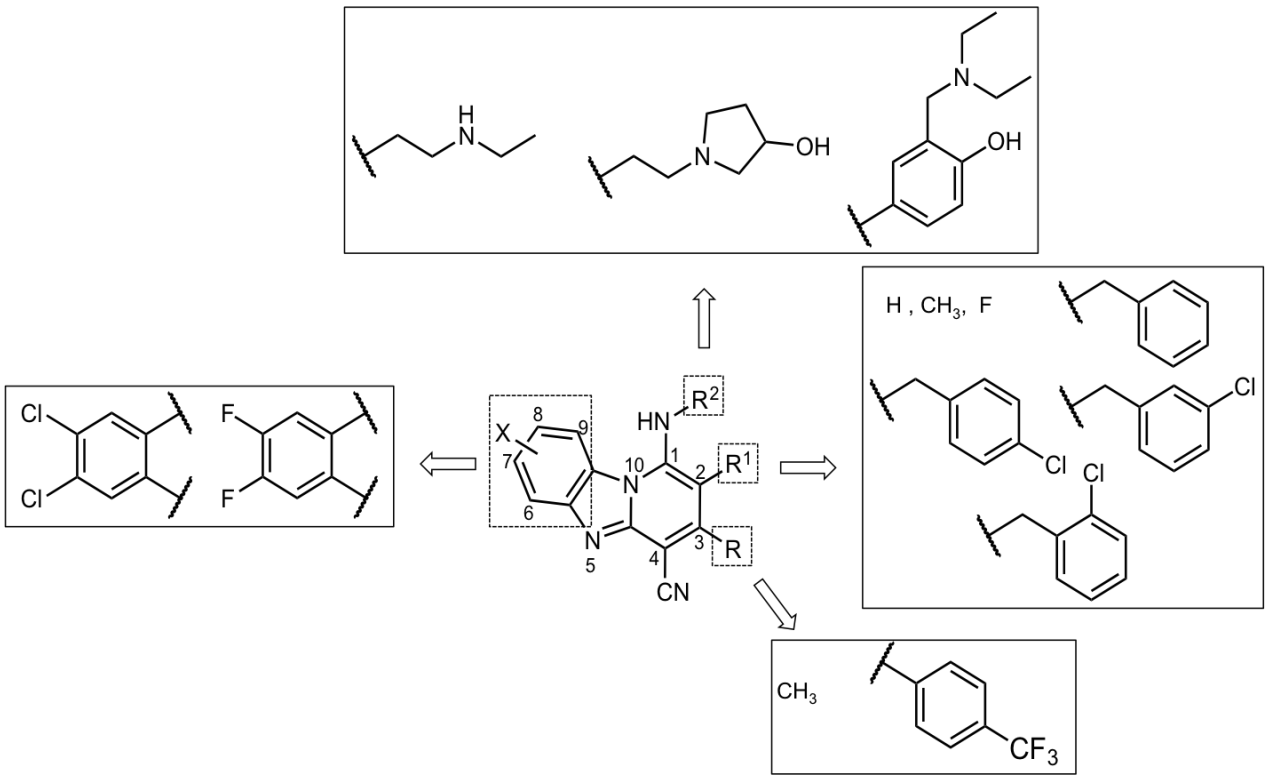

Figure 2.5: PBI scaffold used for SAR exploration.

The amine side-chains were selected based on their potential to improve solubility. The 2-aminoethyl-3-pyrrolidinol moiety can act as a hydrogen bond donor and acceptor, and as such has potential to improve solubility. The Mannich base side-chain is a well-known moiety found in antimalarial drugs such as amodiaquine, amopyroquine and tebuquine (Figure 2.6). This side-chain is able to form an intramolecular hydrogen bond network that is expected to benefit solubility.

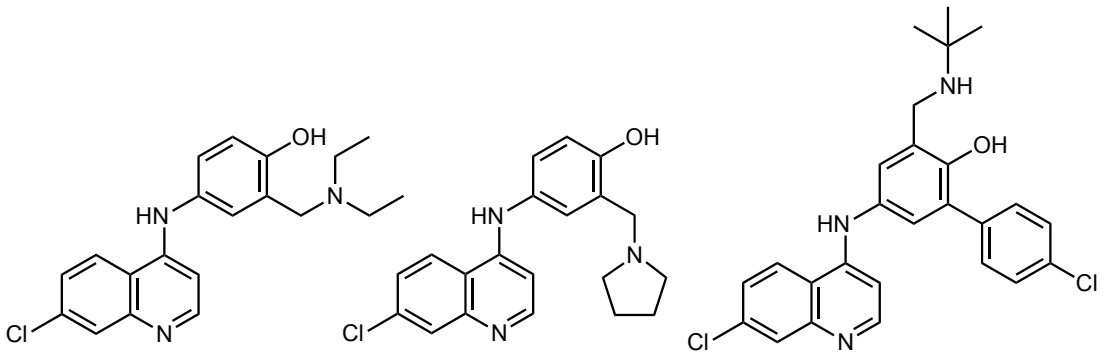

21 **22** **23**

Figure 2.6: Structures of (**21**) amodiaquine, (**22**) amopyroquine and (**23**) tebuquine with Mannich base side-chains.

Unlike large hydrophobic substituents such as methyl and benzylic groups, fluorine has the smallest Van der Waals radius next to hydrogen and is less likely to interfere with protein-drug interactions due to its small size. Thus, a fluorine atom is more likely to increase the dihedral angle without loss of biological activity.[45]

A recent publication by our group revealed that appropriate modifications on the benzimidazole moiety of the PBI core (X in Figure 2.5) improved the *in vitro* antiplasmodial activity and metabolic stability.[64] Substitutions were made at this position, whilst simultaneously incorporating substitutions at C-2.

2.7.2 Synthesis of target pyrido[1,2-a]benzimidazoles

The retrosynthetic analysis of the PBI target compounds is outlined in Scheme 1.

The target compounds (**viii**) were synthesized through a nucleophilic substitution reaction of the chlorinated intermediates with the appropriate amine. The chlorinated intermediates (v**ii**) were synthesized by reacting the hydroxyl intermediates with phosphorus oxychloride ($POCl_3$) in a dehydration reaction.

A condensation reaction between the benzimidazole intermediates (**iv**) and the respective *β*-keto esters (**v**) afforded the hydroxy intermediates (**vi**).[63]

Substituted benzimidazole intermediates (**iv**) were synthesized in a condensation reaction between ethyl-2-cyanoacetate (**i**) and the appropriate diamine (**ii**). The substituted *β*-keto esters (**v**) were synthesized from **iii** using literature methods.[57,65]

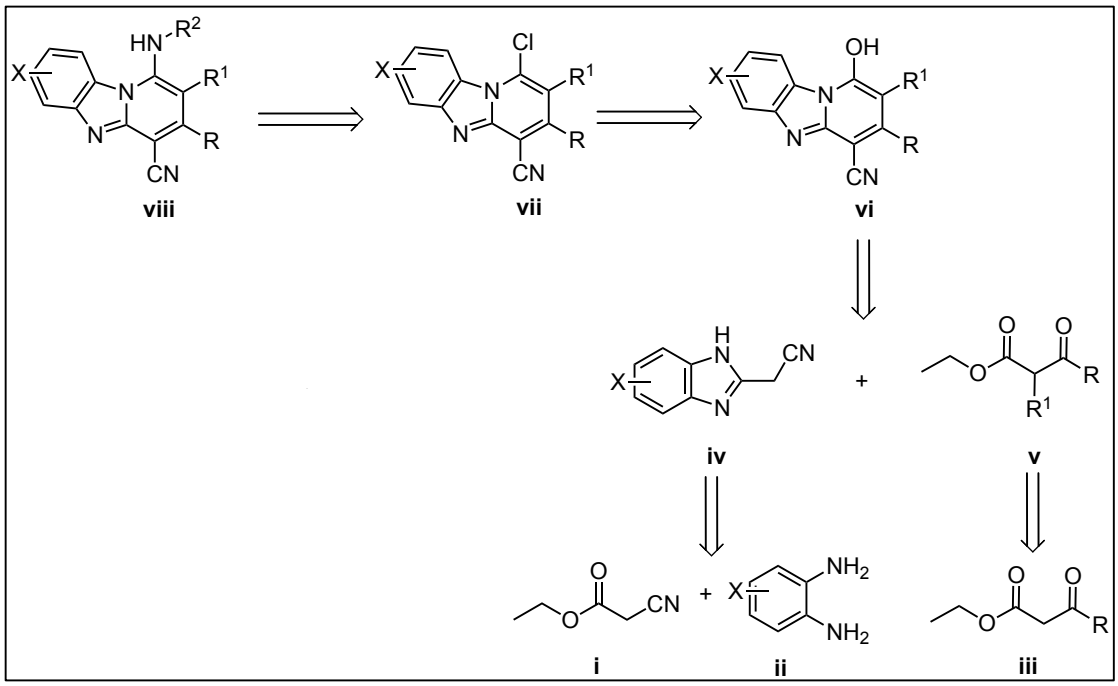

Scheme 1: Retrosynthetic analysis of PBI target compounds.

The reaction scheme for the synthesis of the PBI target compounds can be seen in Schemes 2. Target compounds were obtained in low to moderate yields (Table 2).

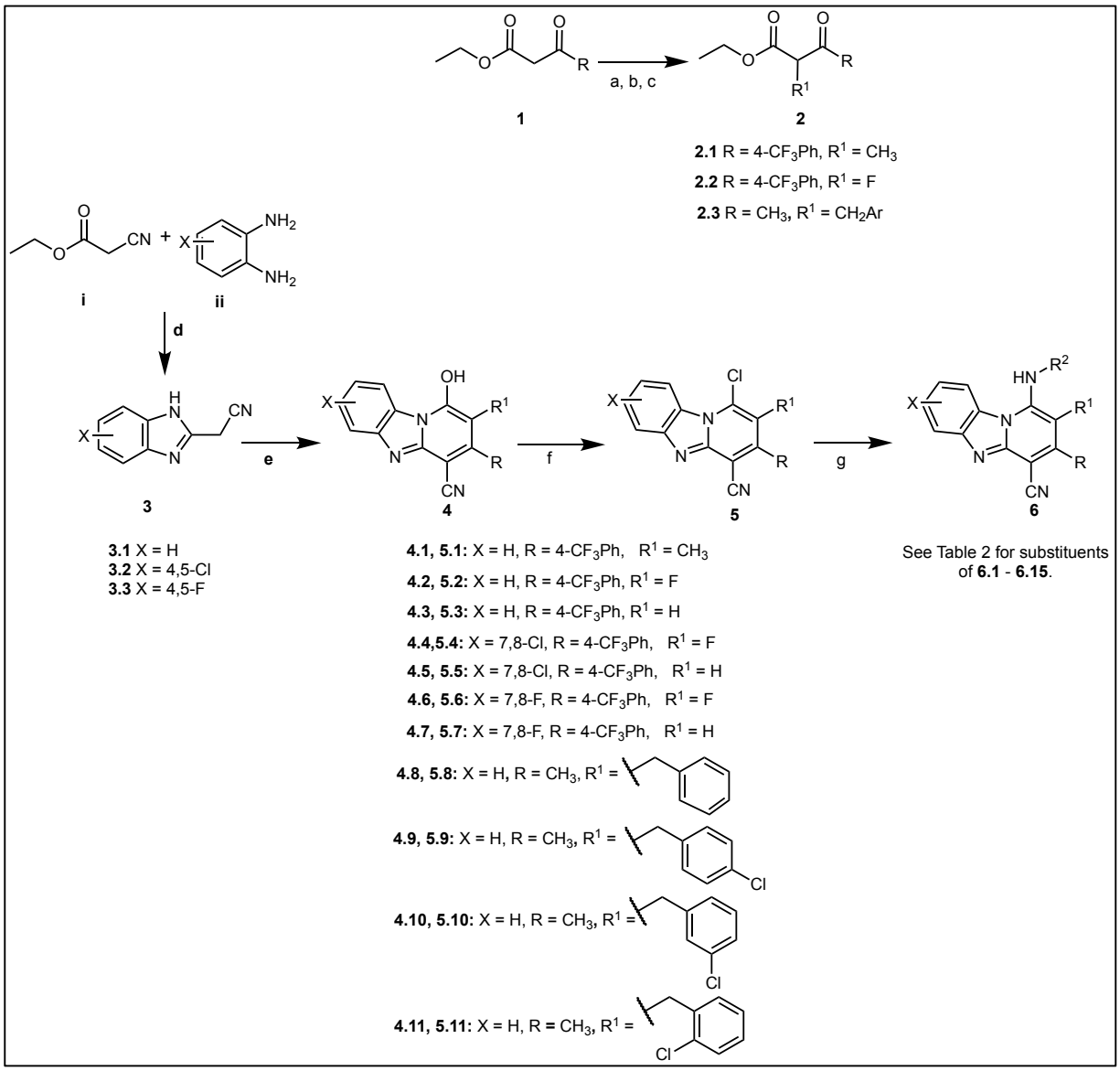

Scheme 2: General synthetic approach for the synthesis of target compounds, **6.1** – **6.15.** *Reagents and conditions:* (a) MeI, K_2CO_3, MeCN, 50°C, 2 h; (b) Selectfluor, MeCN, microwave (150 W), 82°C, 10 min; (c) appropriate benzyl halide, *t*BuOK, *t*BuOH, THF, 70°C, 8 - 24 h, (d) DMF, 150°C, 2 h; (e) NH_4OAc, 145°C, 1 h; (f) $POCl_3$, 130°C, 2 - 8 h; (g) appropriate amine, THF, Et_3N, microwave (150 W), 80°C, 20 – 40 min.

Table 2: Target Compounds with Isolated Yields

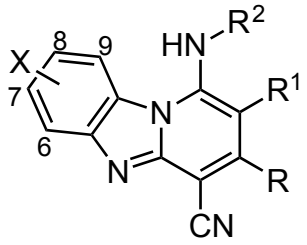

Compound	X	R^1	R^2	R	Yield (%)	Expected mass m/z	Observed mass m/z
6.1 (LB 10)	H	CH_3	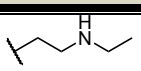	4-CF_3Ph	65	437.2	438.2 $[M+1]^+$
6.2 (LB 20)	H	F	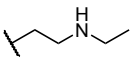	4-CF_3Ph	19	441.2	442.1 $[M+1]^+$
6.3 (LB 29)	H	CH_3	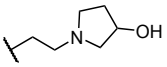	4-CF_3Ph	56	479.2	480.2 $[M+1]^+$
6.4 (LB 34)	H	F	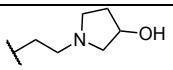	4-CF_3Ph	44	483.2	484.2 $[M+1]^+$
6.5 (LB 27)	H	H	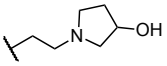	4-CF_3Ph	32	465.2	466.2 $[M+1]^+$
6.6 (LB 97)	H	F	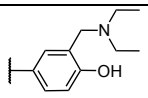	4-CF_3Ph	11	547.2	548.1 $[M+1]^+$
6.7 (LB 76)	7,8-Cl	F	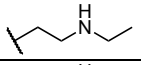	4-CF_3Ph	28	509.1	510.1 $[M+1]^+$
6.8 (LB 75)	7,8-Cl	H	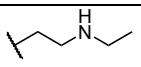	4-CF_3Ph	24	491.1	492.1 $[M+1]^+$
6.9 (LB 94)	7,8-F	F	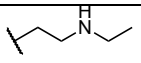	4-CF_3Ph	5	477.1	478.1 $[M+H]^+$
6.10 (LB 85)	7,8-F	H	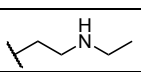	4-CF_3Ph	71	459.2	460.2 $[M+1]^+$
6.11 (LB 88)	7,8-F	H	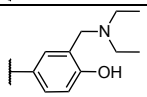	4-CF_3Ph	26	565.2	566.2 $[M+1]^+$
6.12 (LB 45)	H	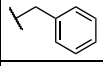	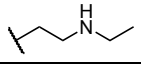	CH_3	7	383.5	384.2 $[M+1]^+$
6.13 (LB 49)	H	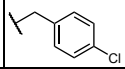	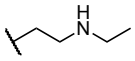	CH_3	20	417.2	418.1 $[M+1]^+$
6.14 (LB 53)	H	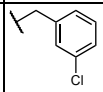	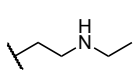	CH_3	31	417.2	418.1 $[M+1]^+$
6.15 (LB 59)	H	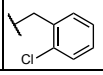	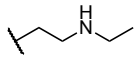	CH_3	20	417.2	418.1 $[M+1]^+$

The synthesis of **6.6 (LB76)** is used as an illustrative example to explain reaction mechanisms and compound characterisation.

2.7.2.1 Synthesis of benzimidazole intermediates

For the synthesis of the benzimidazole moiety substituted compounds, the initial step in the synthetic route involves a condensation reaction to afford the substituted benzimidazole.

The reaction mechanism for the formation of intermediate **3.2**, involves attack by the lone pair electrons of the nitrogen of the dichloro diamine phenyl (**a**) on the carbonyl carbon of ethyl cyanoacetate, followed by a proton transfer and the subsequent loss of ethanol (**b**) to yield intermediate **c** (Scheme 3). The lone pair of electrons on the other nitrogen atom of **c** attacks the carbonyl carbon, which leads to the formation of the 5-membered ring intermediate (**d**). A second proton transfer generates a hemi-aminal (**e**) and subsequent loss of a water molecule from intermediate **f** affords the benzimidazole intermediate **g** (**3.2**).

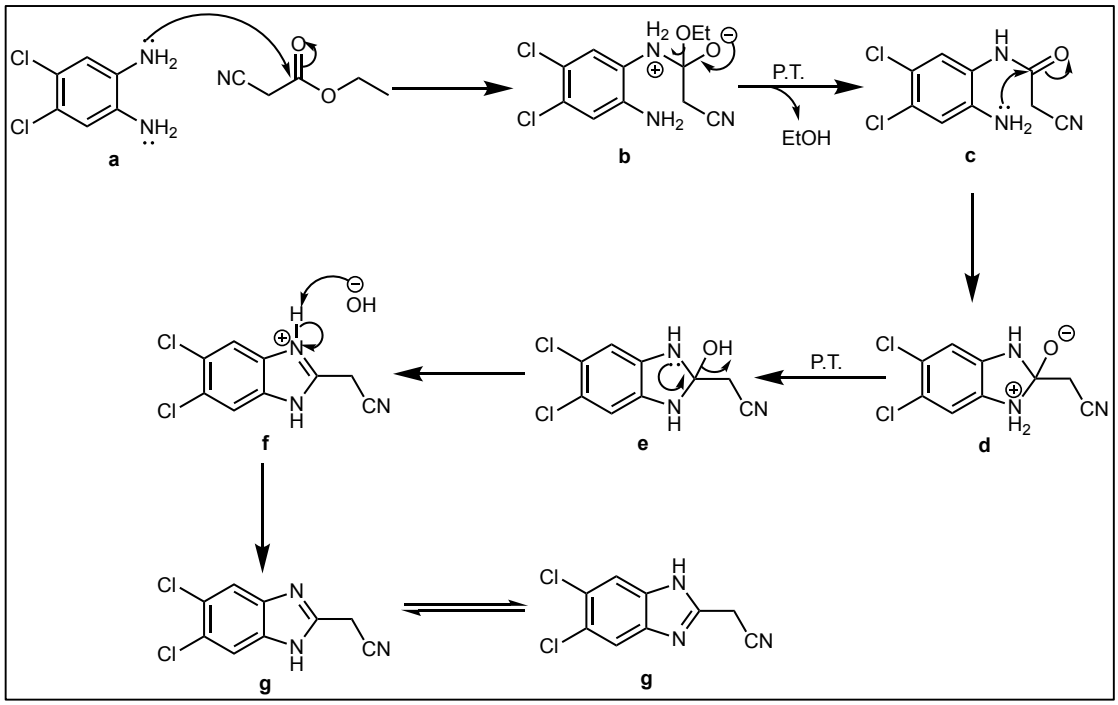

Scheme 3: Synthetic route for the synthesis of the benzimidazole intermediates.

Spectroscopic analysis of the benzimidazole intermediate 3.2

The ^{1}H NMR (400 MHz, DMSO) spectrum of **3.2** confirmed the presence of signals in the region of δ 12.0 – 13.0 corresponding to NH, two aromatic protons and the two aliphatic protons of the acetonitrile moiety (Figure 2.7).

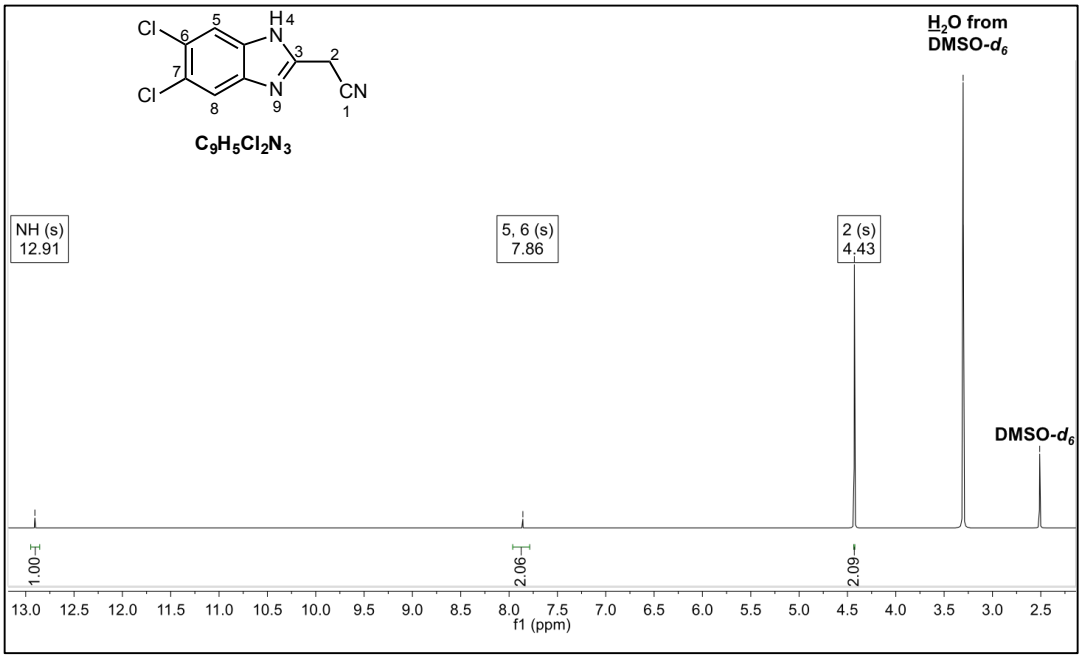

Figure 2.7: ^{1}H NMR (400 MHz, DMSO-d_6) spectrum of the benzimidazole intermediate, **3.2**.

2.7.2.2 Synthesis of the hydroxy intermediate 4.4

In the condensation reaction to form the hydroxy intermediate **4.4**, ammonium acetate deprotonates the carbon of acetonitrile **3.2** to form a carbanion (**i**), as seen in Scheme 4. This carbanion attacks the electrophilic carbonyl carbon of the substituted *β*-keto ester. Intramolecular cyclization (**k-o**) followed by the loss of water and ethanol results in the intermediate, **p** (**4.4**).

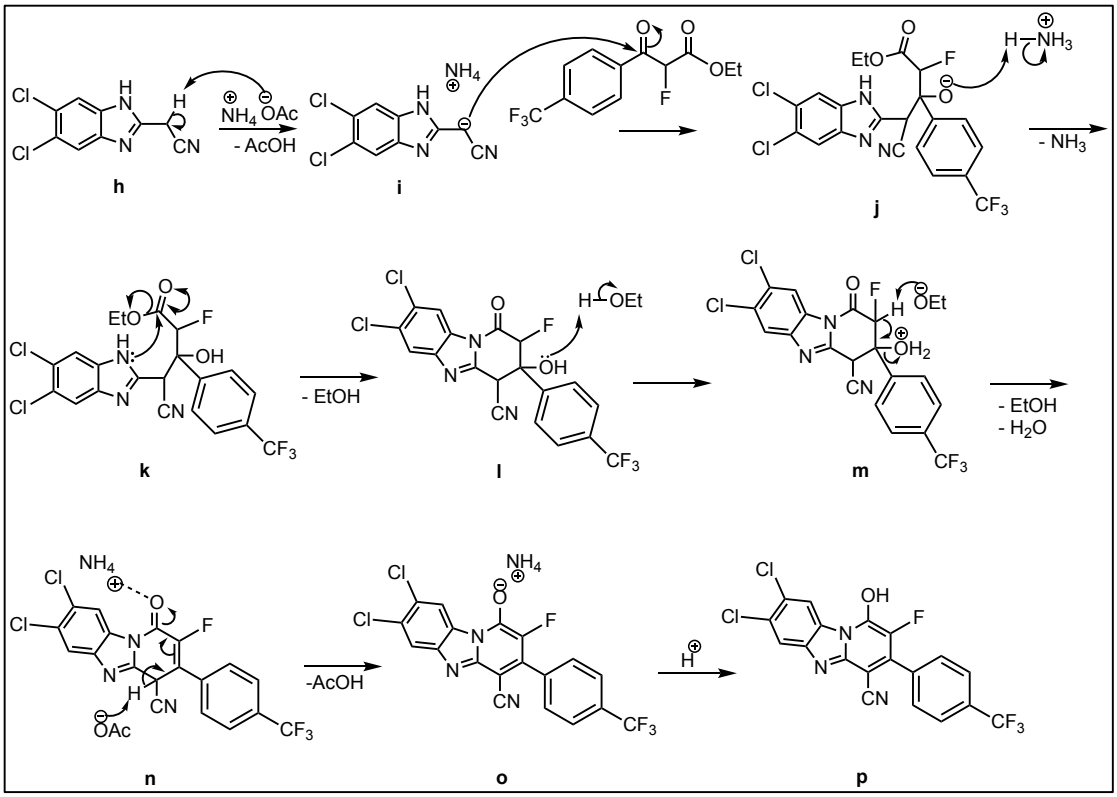

Scheme 4: Synthetic route for the synthesis of the hydroxy intermediate, **4.4.**

Spectroscopic analysis of the hydroxy intermediate 4.4.

The structure of the hydroxy intermediate was confirmed by ^{1}H NMR (400 MHz, DMSO-d_6), as seen in Figure 2.8. The spectrum of **4.4** shows the presence of 6 aromatic signals in the region δ 7.7 – 8.7. The distinctive splitting pattern of the four protons of the *para*-substituted benzene ring is seen as the pair of doublets (J = 7.8 Hz) that arises due to the symmetry of this moiety.

According to Ndakala *et al.*[63], the ^{13}C spectrum of this intermediate corresponds to the enol tautomer with a signal at δ 157.9 for C-1. However, other groups have published it as the keto tautomer (Figure 2.9) with a ^{13}C signal in the region of δ 158-159, along with a ^{1}H signal corresponding to the N<u>H</u> at δ 13.46.[66] Since the ^{1}H spectra of the PBI intermediates in this project display no signals that correspond to a N<u>H</u>, we have chosen to represent these intermediates as the enol tautomer.

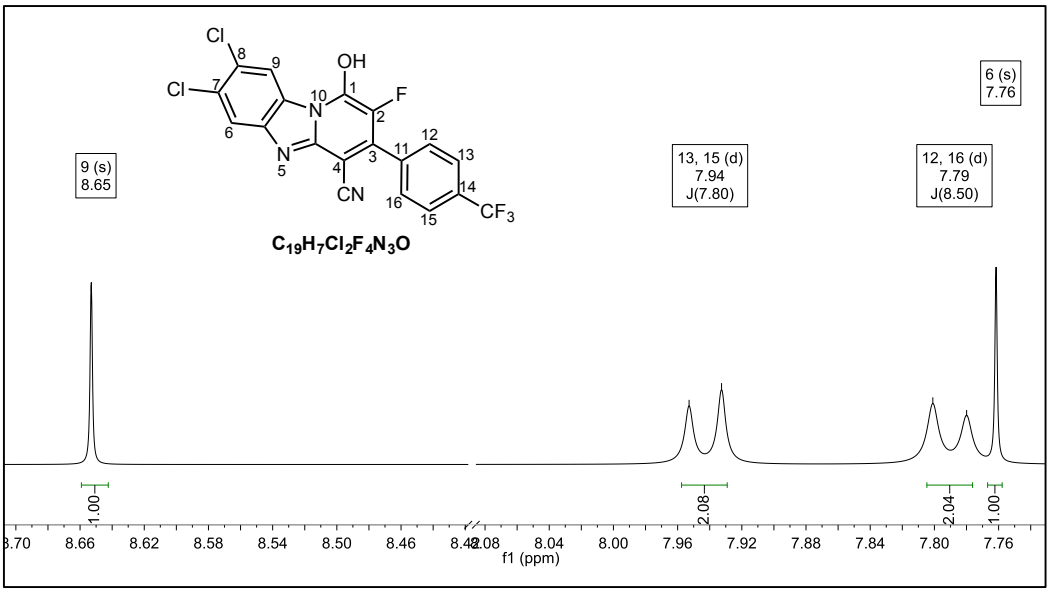

Figure 2.8: ^{1}H NMR (400 MHz, DMSO-d_6) spectrum of the hydroxy intermediate, **4.4**.

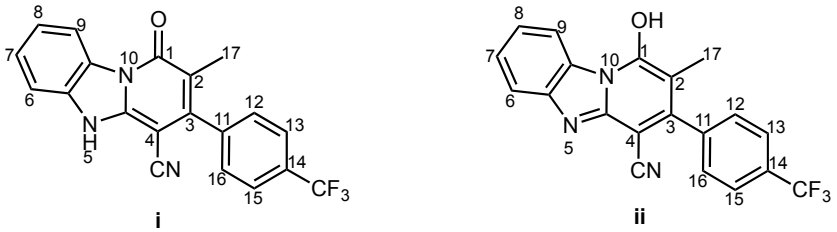

Figure 2.9: Keto **(i)** and enol **(ii)** tautomer of **4.1**

2.7.2.3 Synthesis of the C-1 chlorinated intermediate 5.4

The hydroxy intermediate **4.4** was reacted with phosphorus oxychloride ($POCl_3$) to afford the chlorinated intermediate **5.4** (Scheme 5). Mechanistically, the lone pair of electrons of the hydroxyl oxygen attacks the electrophilic phosphorus of $POCl_3$ (**q**) and the subsequent electron transfer results in the loss of a chloride ion (**r**). The electron deficiency of the oxygen enhances the electrophilicity of the electrophilic carbon and the chloride ion attacks the electrophilic carbon of this phosphorous intermediate (**s**). The subsequent loss of HCl and PO_2Cl results in the formation of the chlorinated intermediate, **5.**

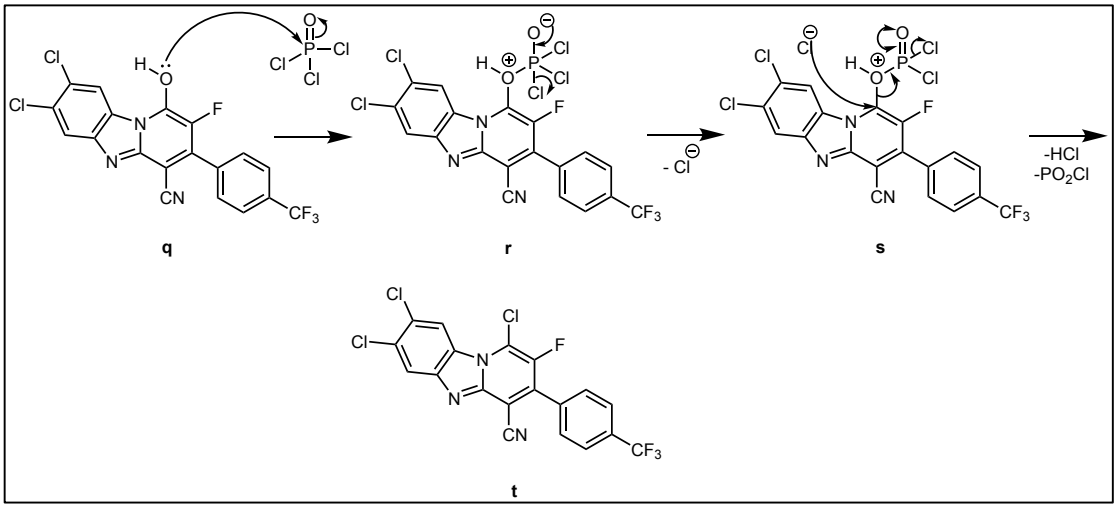

Scheme 5: Synthetic route for the synthesis of the C-1 chlorinated intermediate, **5.4.**

Spectroscopic analysis of the chlorinated intermediate 5.4.

The ^{1}H NMR (400 MHz, DMSO) of **5.4** confirmed the successful formation of the chlorinated intermediate (Figure 2.10). The 6 aromatic protons are observed in the region δ 7.9 – 8.3, slightly downfield from the hydroxy intermediate (Figure 2.8). Since the chloro group is electron-withdrawing, it deshields the protons more than the hydroxyl group and thus the proton signals shift downfield.

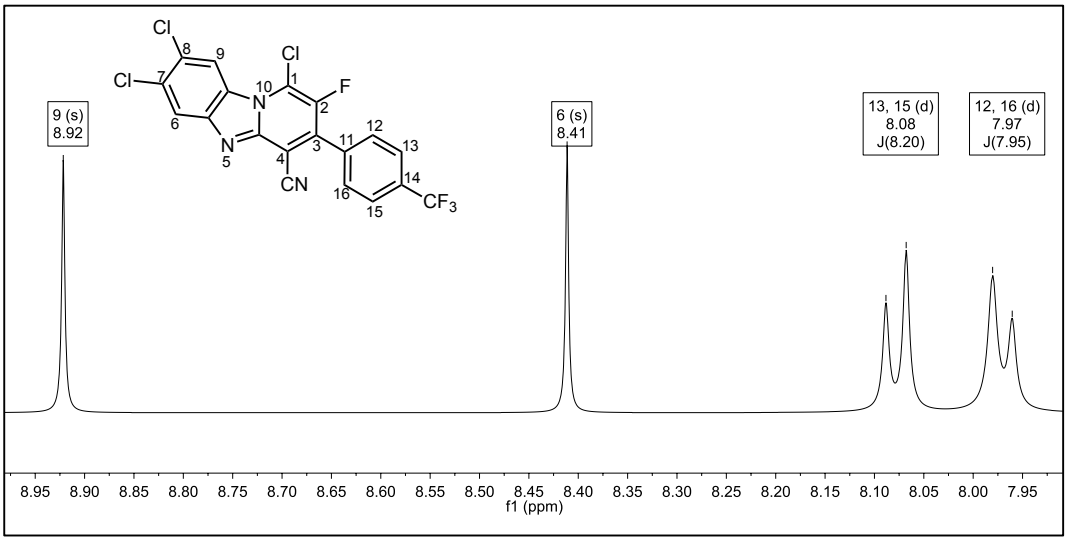

Figure 2.10: ^{1}H NMR (400 MHz, DMSO-d_6) spectrum of the chlorinated intermediate, **5.4**.

2.7.2.4 Synthesis of the target compound 6.7

The final step in the synthetic route involves amination of the chlorinated intermediate, **5.4**, via a nucleophilic substitution reaction to obtain the desired target compound **6.7**, as illustrated in Scheme 6. The nucleophilic amino nitrogen of *N*-ethylethylenediamine attacks the electrophilic carbon (**u**). This causes electrons from the pyridine ring to move in such a way that a negative charge resides on the nitrile nitrogen due to the extended conjugation. As electrons move back into the pyridine ring through the resonance effect, the chloride ion, being a good leaving group, is displaced in a nucleophilic aromatic substitution reaction (**v**). Triethylamine mops up the liberated HCl produced alongside the target compound (**6.7**).

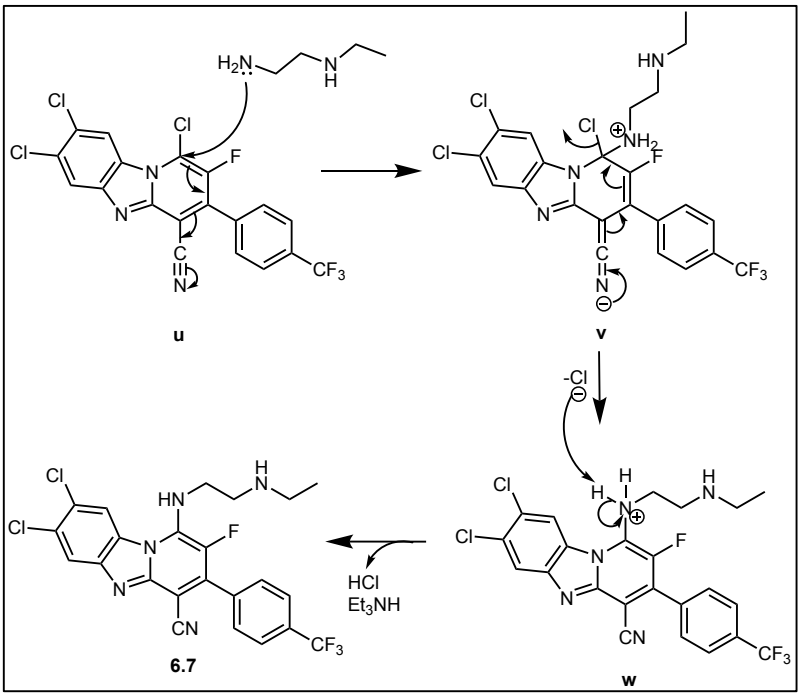

Scheme 6: Synthetic route for the synthesis of the target compound, **6.7**.

Spectroscopic analysis of selected target compounds.

The structure of the target compound (**6.7**) was confirmed using 1D and 2D NMR spectroscopy (Figure 2.11). The diagnostic feature of the ^{1}H NMR spectrum of **6.7** is the appearance of the aliphatic proton signals of the alkylamine side-chain in the region δ 1.2 – 4.5.

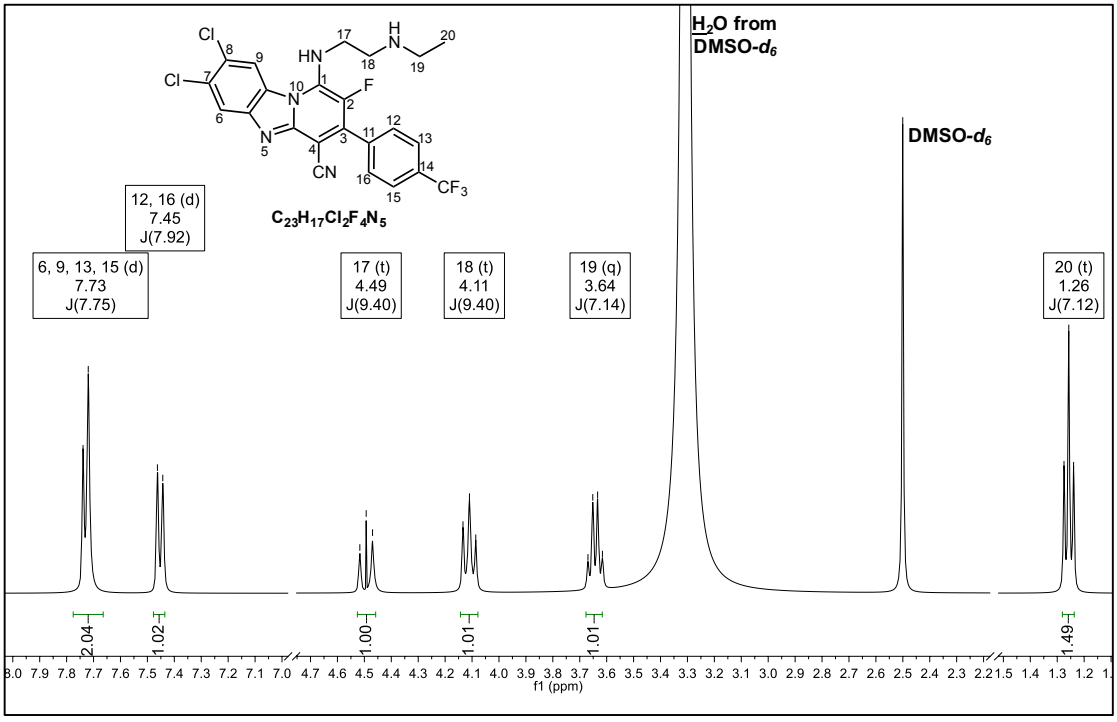

Figure 2.11: ^{1}H NMR (400 MHz, DMSO-d_6) spectrum of the target compound, **6.7**.

In the case of target compound **6.11**; the protons of the benzene ring of the Mannich base were assigned using the relative coupling constants (Figure 2.12). The *ortho* coupling observed between H^{21} and H^{22} gives rise to a coupling constant of $^{3}J_{HH\text{-}o}$ = 8.5 Hz for the doublet assigned to H^{21}. The *meta* coupling between H^{18} and H^{22} results in a coupling constant of $^{4}J_{HH\text{-}m}$ = 2.6 Hz for the doublet of H^{18}. Due to H^{22} coupling with two non-equivalent neighbors, H^{18} and H^{21}, the signal appears as a doublet of doublets.

As seen in Figure 2.12, the signals for the two protons on the fluorine substituted benzimidazole moiety, H^{6} and H^{9}, each appear as a doublet of doublets compared to one doublet for the same protons on the 7,8-dichloro

substituted target compound, **6.7,** above (Figure 2.11). This is attributed to the spin active nature of ^{19}F, which has a nuclear spin of $\frac{1}{2}$ that allows for *ortho* coupling ($^3J_{HF\text{-}o}$ = 11.5 Hz) between H^9 and the vicinal fluorine on C-8 as well as *meta* coupling ($^4J_{HF\text{-}m}$ = 8.7 Hz) to the fluorine of C-7. A similar trend is observed for H^6. These two protons, being in chemically similar environments, were assigned based on the through space effects from the NH to H^9. The H^9 is deshielded by hydrogen bonding with the NH nearby.

Furthermore, the protons of the alkylamine moiety of the Mannich base appear as one quartet and one triplet signal owing to the symmetry of this region. Therefore, H^{24} and H^{26} are in a similar chemical environment and the same is true for H^{25} and H^{27}. The singlet at δ 4.08 corresponds to the methylene linker and the singlet at δ 5.59 corresponds to the aromatic proton on C-2.

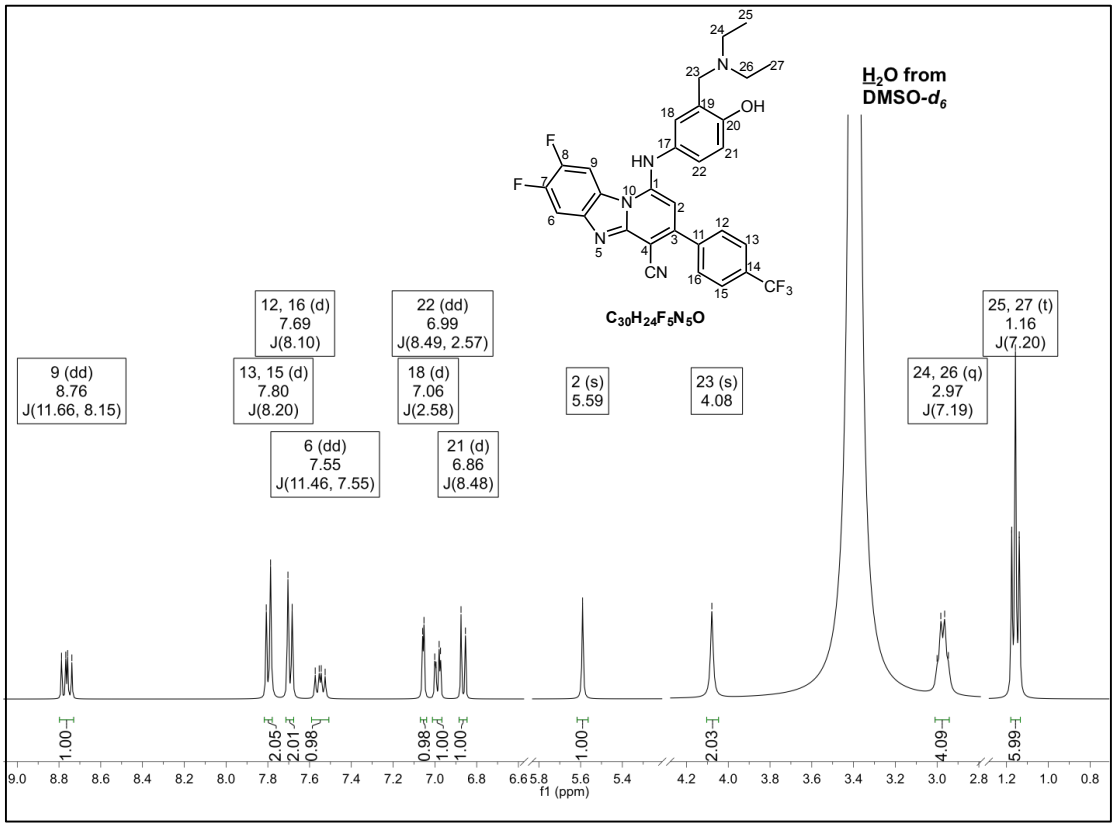

Figure 2.12: ^1H NMR (400 MHz, DMSO-d_6) spectrum of the target compound, **6.11**.

The pyrrolidinol target compounds (**6.3** – **6.5**) were obtained as a racemic mixture as expected. The pyrrolidinol side chain has a stereogenic centre at

C-20. As seen in the ^{1}H NMR spectrum of **6.4** in Figure 2.13, the signal of the stereogenic proton (H^{20}) appears as a multiplet in the region of δ 4.25 – 4.35 due to its diastereotopic nature. The signals for the other protons of the pyrrolidinol ring seem to be affected by the diastereotopicity because they do not show defined splitting patterns but are instead observed as multiplets. Further structure confirmation is provided by the crystal structure of **6.4** in which the oxygen atom of the hydroxyl group was disordered over two positions (see 2.9.2).

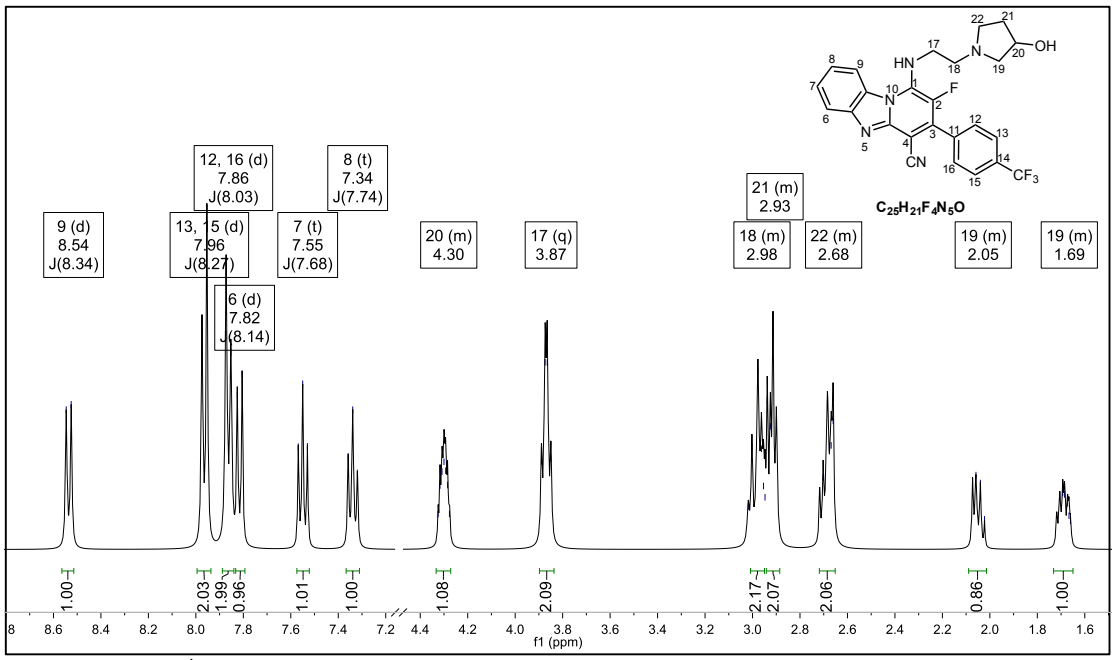

Figure 2.13: ^{1}H NMR (400 MHz, DMSO-d_6) spectrum of the target compound, **6.4**.

The protons of the *para*-substituted phenyl ring were assigned based on the substitution of the electron withdrawing trifluoromethyl group. This group removes electron density at the *ortho*- and *para*-positions and thus these sites are more deshielded. On this basis, H^{13} and H^{15} are more deshielded than H^{12} and $H^{16.}$

2.8 Pharmacological Evaluation and Physicochemical Properties

2.8.1 Antiplasmodial, β-hematin and cytotoxicity evaluation

The synthesized target compounds were evaluated for *in vitro* antiplasmodial activity against the chloroquine-sensitive (NF54) strain of *P. falciparum* and for cytotoxicity against the Chinese Hamster Ovary (CHO) mammalian cell line. The IC_{50} values obtained are displayed in Table 3.

Due to their flat heterocyclic nature like that of chloroquine, it was hypothesized that PBIs could act by inhibiting the formation of hemozoin. Therefore, compounds were tested in the *β*-hematin inhibition assay (BHIA) which is used to determine whether a compound is able to inhibit the formation of *β*-hematin and to quantify the *β*-hematin inhibition (Table 3). A compound with a BHIA IC_{50} value below 100 *μ*M is considered to be a *β*-hematin inhibitor.[67]

Table 3: *In Vitro* Antiplasmodial Activity, Cytotoxicity and BHIA Evaluation of Pyrido[1,2-*a*] benzimidazole Derivatives

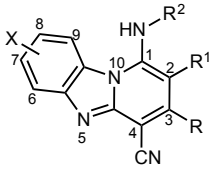

Compound	X	R^1	R^2	R	Antiplasmodial Activity (NF54) IC_{50} (μM)	Antiplasmodial Activity (K1) IC_{50} (μM)	Cytotoxicity (CHO) IC_{50} (μM)	SI	BHIA	
									IC_{50} (μM)	SD
Chloroquine					0.021	0.194			16.52	1.04
Emetine							0.095(±0.002)			
Amodiaquine									16.25	4.37
Pyrimethamine									NI[a]	NI[a]
20	H	H	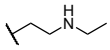	4-CF_3Ph	0.12	ND[b]	1.56 (±0.03)	13	40.5	0.59
6.1 (LB 10)	H	CH_3	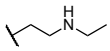	4-CF_3Ph	1.28	ND[b]	8.3 (±3.7)	6.5	200.6	25.73
6.2 (LB 20)	H	F	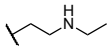	4-CF_3Ph	5.53	ND[b]	>227	41	245.4	61.51
6.3 (LB 29)	H	CH_3	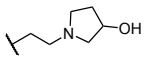	4-CF_3Ph	0.55	ND[b]	25 (±3.8)	45.5	269.0	42.74
6.4 (LB 34)	H	F	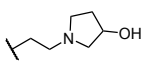	4-CF_3Ph	0.19	ND[b]	>207 (ND[b])	>1000	106.4	31.88
6.5 (LB 27)	H	H	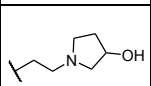	4-CF_3Ph	0.04	ND[b]	6.12 (±1.2)	153	85.3	2.5
6.6 (LB97)	H	F	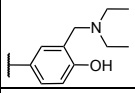	4-CF_3Ph	0.35	ND[b]	>100 (ND[b])	>288	12.2	1.27
6.7 (LB 76)	7,8-Cl	F	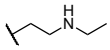	4-CF_3Ph	0.78	0.92	7.40 (0.5)	9.4	30.8	ND[b]
6.8 (LB 75)	7,8-Cl	H	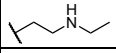	4-CF_3Ph	0.02	ND[b]	3.39 (±0.7)	188.3	35.4	1.11
6.9 (LB 94)	7,8-F	F	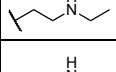	4-CF_3Ph	3.95	ND[b]	56.94 (±17.8)	14.4	1061.4	147.34
6.10 (LB 85)	7,8-F	H	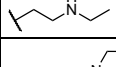	4-CF_3Ph	0.03	0.03	0.43 (±0.1)	13.7	13.0	2.20
6.11 (LB 88)	7,8-F	H	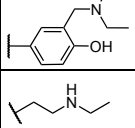	4-CF_3Ph	0.07	0.07	>100 (ND[b])	>1538.5	9.4	2.23
6.12 (LB 45)	H		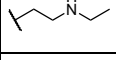	CH_3	5.15	ND[b]	75.08 (±10.6)	14.6	1372.8	102.72
6.13 (LB 49)	H	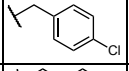	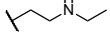	CH_3	2.18	ND[b]	2.41 (±0.9)	1.1	987.4	67.37
6.14 (LB 53)	H		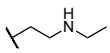	CH_3	1.94	ND[b]	5.98 (±2.4)	3.1	287.3	37.78
6.15 (LB 59)	H		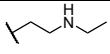	CH_3	2.36	ND[b]	ND[b]	ND[b]	9269.1	875.94

[a] NI: No inhibition
[b] ND: Not determined

From the results in Table 3, it is evident that many of the target compounds showed good antiplasmodial activity against the chloroquine sensitive (NF54) strain of *P. falciparum* with activity in the sub-micromolar range.

Substitution on the benzimidazole ring of the PBI core results in improvement of antiplasmodial activity compared to the parent compound (**20**), with the exception of **6.7** and **6.9**. The most active compound, **6.8** (IC_{50} = 0.02 μM), displayed activity comparable to the antimalarial drug chloroquine (IC_{50} = 0.021 μM) and was found to be 6-fold more potent than **20** (IC_{50} = 0.12 μM). Dichloro substituted compounds (**6.7** [IC_{50} = 0.78 μM] and **6.8** [IC_{50} = 0.02 μM]) displayed enhanced activity as compared to their fluorine analogous (**6.9** [IC_{50} = 3.95 μM] and **6.10** [IC_{50} = 0.03 μM]).

Substituting the *N*-ethylethane-diamino side-chain of **20**, with 2-aminoethyl-3-pyrrolidinol (**6.5**) and the Mannich base (**6.11**) side-chain, improved the activity of the lead compound by 3-fold and 1.7-fold, respectively.

The three compounds with the 2-aminoethyl-3-pyrrolidinol side-chain, **6.3**, **6.4** and **6.5** (IC_{50}: **6.3** = 0.55 μM; **6.4** = 0.19 μM; **6.5** = 0.04 μM), displayed improved activity compared to the corresponding *N*-ethylethane-diamino analogues **20**, **6.1** and **6.2** (IC_{50}: **20** = 0.12 μM; **6.1** = 1.28 μM; **6.2** = 5.53 μM). However, earlier microsomal metabolic stability studies showed that compounds with this side-chain were metabolically unstable in mouse liver microsomes and it was decided to continue investigations with compounds containing the *N*-ethylethane-diamino side-chain.

The five most potent compounds are all unsubstituted at C-2. Thus, upon substitution at this position there is a reduction in antiplasmodial activity. Compound **6.4** showed the highest activity (IC_{50} = 0.19 μM) of the C-2 substituted analogues (R^1 = F).

The BHIA results in Table 3 suggest that *β*-hematin inhibition contributes to the mechanism of action of all the C-2 unsubstituted analogues. Generally the C-2 substituted analogues were not found to inhibit the formation of *β*-hematin with the exception of **6.7** (BHI IC_{50} = 30.8 *μ*M). The two Mannich base analogues, **6.6** (BHI IC_{50} = 12.2 *μ*M) and **6.11** (BHI IC_{50} = 9.4 *μ*M), displayed the highest activity in the BHIA.

Figure 2.14 demonstrates the linear relationship (R^2 = 0.55) between *in vitro* antiplasmodial activity and BHI, with a P value of 0.0009. This relationship infers that all the compounds with sub-micromolar antiplasmodial activity are classified as *β*-hematin inhibitors. Thus the less potent compounds possessing antiplasmodial activity above 1 *μ*M are non-*β*-hematin inhibitors.

Generally, an R-squared value greater than 0.8 infers a strong positive correlation is present. Since the R-squared value of the graph in Figure 2.14 is 0.55, it suggests that the correlation is weak and that there are other factors (e.g. other mechanisms or targets involved, physicochemical properties, accumulation, permeability in infected red blood cells etc.) that also influence the *in vitro* antiplasmodial activity, with BHI being just one of the contributing factors. It is noteworthy that this graph does not factor in the different *in vitro* environments of the BHIA and the antiplasmodial studies. The BHIA does not require the compound to cross any membranes whereas the antiplasmodial activity assay requires the compound to cross the membranes of infected erythrocytes and the parasite to reach the target in the digestive food vacuole.

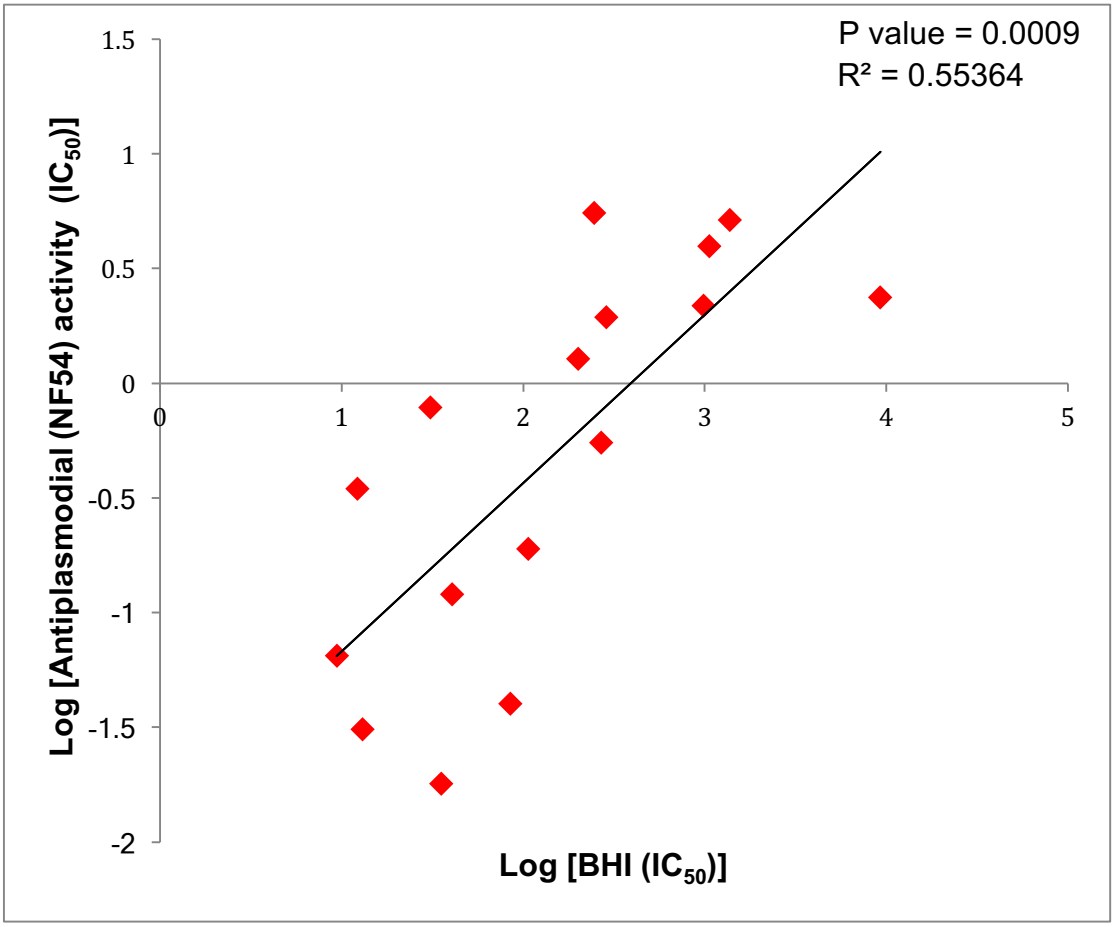

Figure 2.14: Relationship between antiplasmodial activity and BHI of the PBI target compounds.

The similar antiplasmodial activity against the chloroquine-resistant strain (K1) of the parasite on selected compounds suggests that the compounds show no evidence of cross-resistance since the compounds are equipotent against both strains.

2.8.2 Microsomal metabolic stability profiling

The *in vitro* metabolic stability of selected target compounds was assessed using the one point assay in mouse liver microsomes (MLM) and human liver microsomes (HLM) (Table 4).

The stability of the compounds was classified as follows:

- < 45 % remaining after 30 minutes = metabolically unstable
- 45 – 90 % remaining after 30 minutes = moderately stable
- > 90 % remaining after 30 minutes = metabolically stable

Table 4: *In Vitro* Microsomal Stability of Pyrido[1,2-*a*]benzimidazole Derivatives in Mouse and Human Liver Microsomes

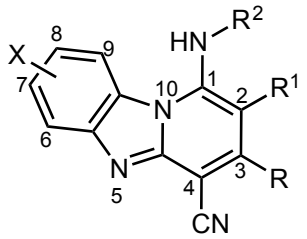

Compound	X	R^1	R^2	R	MLM: % remaining after 30 min		Projected half-life (min)	HLM: % remaining after 30 min		Projected half-life (min)
					Average	SD		Average	SD	
Propranolol					5.7	0.4	<10	60.5	4.8	41
Midazolam					0.1	0.1	<10	0.1	0	<10
MMV390048					84.6	0.1	>150	93.1	3.7	>150
20	H	H	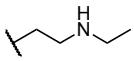	4-CF_3Ph	97	9	>150	ND[a]	ND[a]	ND[a]
6.1 (LB 10)	H	CH_3	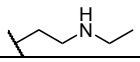	4-CF_3Ph	80	2	100	85	4	131
6.2 (LB 20)	H	F	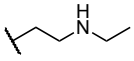	4-CF_3Ph	35	0.7	26	39	2	22
6.3 (LB 29)	H	CH_3	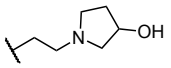	4-CF_3Ph	16	2	ND[a]	23	2	ND[a]
6.4 (LB 34)	H	F	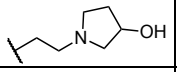	4-CF_3Ph	37	3	28	ND[a]	ND[a]	ND[a]
6.5 (LB 27)	H	H	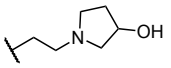	4-CF_3Ph	51	1	31	13	1	ND[a]
6.7 (LB 76)	7,8-Cl	F	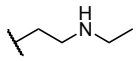	4-CF_3Ph	91	5	ND[a]	90	8	ND[a]
6.8 (LB 75)	7,8-Cl	H	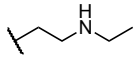	4-CF_3Ph	81	6	132	95	7	>150
6.10 (LB 85)	7,8-F	H	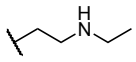	4-CF_3Ph	67	10	ND[a]	79	7	ND[a]
6.11 (LB88)	7,8-F	H	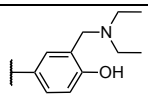	4-CF_3Ph	30	3	ND[a]	35	3	ND[a]

[a] ND: Not determined

The C-2 unsubstituted compounds displayed moderate to high levels of metabolic stability, except for the Mannich base (**6.11**). The major metabolite of compound **20** resulted from terminal *N*-deethylation**,** while *N*-dealkylation and oxidation of the pyrrolidinol ring were observed as routes of metabolism for compound **6.5** (Figure 2.15).

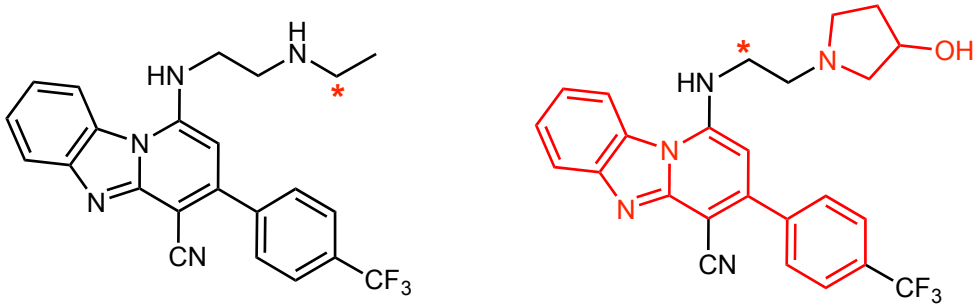

Figure 2.15: The metabolic soft spots (denoted in red) of the PBI analogues that are unsubstituted at position C-2**.**

Most of the compounds that are substituted at the C-2 position displayed moderate to high rates of metabolic degradation. Substitution at this position appears to render the PBI core/phenyl ring vulnerable to oxidation, as seen in Figure 2.16, and thus dramatically lowers the metabolic stability of these compounds.

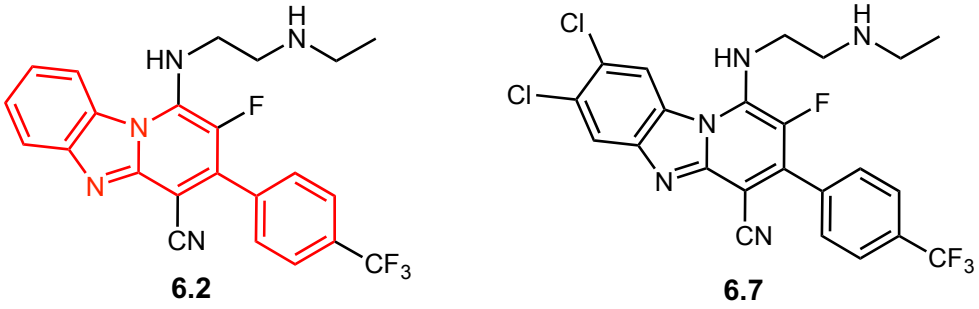

Figure 2.16: The metabolic soft spots (denoted in red) of **6.2**, which is substituted at position C-2, and the chemical structure of compound **6.7**.

Compound **6.7** (Figure 2.16) is the only C-2 substituted analogue that showed metabolic stability with more than 90 % remaining after 30 minutes in mouse

and human liver microsomes. This is presumably due to the presence of the two chloro-groups substituted on the benzimidazole moiety pf the PBI core.

2.8.3 Solubility

Kinetic and equilibrium solubility studies were carried out on all PBI target compounds (Table 5). These two assays differ in that the equilibrium solubility assay measures the amount of compound still in solution after incubation whereas the kinetic assay measures the amount of compound that precipitates out of solution.[43,68]

Due to the short incubation time of the kinetic assay, it can be carried out in a high throughput fashion and is thus ideal for rapid compound assessment and to guide SAR studies in the hit to lead stage.[68] This assay can produce solubility results that are higher than in the equilibrium solubility assay because the formation of a supersaturated solution inspires that more time is required for precipitation to occur.[69]

Since equilibrium solubility does not require the compound to be made up as a stock solution in an organic solvent, it mimics the crystal forces of the solid and the mixing that takes place in the gastrointestinal tract. This assay is also advantageous in that it is conducted for a longer time period (24 - 72 hours) than the kinetic assay to allow for equilibrium to be reached. For these reasons the equilibrium solubility assay is favored for the lead optimization stage to determine whether structural modifications are improving solubility.[68]

In kinetic solubility assays, it is generally accepted that compounds with solubility less than 1 μM are considered to be highly insoluble, those with solubility between 1 - 100 μM are moderately soluble and compounds with solubility greater than 100 μM are considered to be highly soluble.[70]

Equilibrium solubility is ranked as follows based on 200 μM preparations:

- ≥ 150 μM = high
- 5 – 150 μM = moderate
- 5 – 49 μM = low
- < 5 μM = very low

Table 5: Solubility Data for Target Compounds

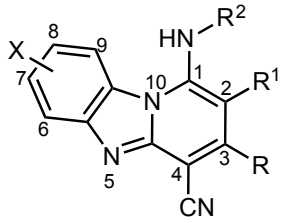

Compound	X	R^1	R^2	R	Kinetic Solubility (μM)	Equilibrium Solubility: PBS (pH 6.5) μM
Reserpine (negative control)					1-5	<5
Hydrocortisone (positive control)					>200	>200
20	H	H	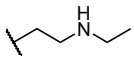	4-CF_3Ph	10-20	<5
6.1 (LB 10)	H	CH_3	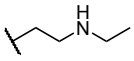	4-CF_3Ph	40-80	16.5 (±0.9)
6.2 (LB 20)	H	F	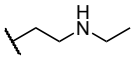	4-CF_3Ph	>100	160
6.3 (LB 29)	H	CH_3	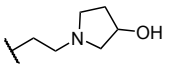	4-CF_3Ph	10-20	<5
6.4 (LB 34)	H	F	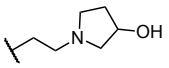	4-CF_3Ph	5-10	80
6.5 (LB 27)	H	H	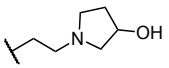	4-CF_3Ph	5-10	<5
6.6 (LB 97)	H	F	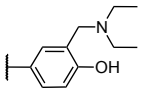	4-CF_3Ph	5-10	<5
6.7 (LB 76)	7,8-Cl	F	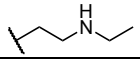	4-CF_3Ph	40-80	23.4 (±1.2)
6.8 (LB 75)	7,8-Cl	H	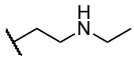	4-CF_3Ph	10-20	10
6.9 (LB 94)	7,8-F	F	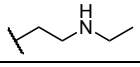	4-CF_3Ph	>200	>200
6.10 (LB 85)	7,8-F	H	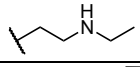	4-CF_3Ph	10-20	<5
6.11 (LB 88)	7,8-F	H	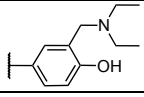	4-CF_3Ph	10-20	<5
6.12 (LB 45)	H		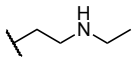	CH_3	80-160	146.5 (±2.0)
6.13 (LB 49)	H	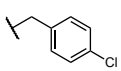	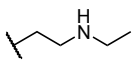	CH_3	10-20	<5
6.14 (LB 53)	H	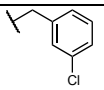	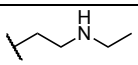	CH_3	20-40	35.6 (±4.0)
6.15 (LB 59)	H	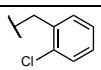	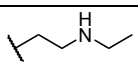	CH_3	10-20	<5

The results in Table 5 suggest that introducing a fluorine atom into the C-2 position (**6.2**, **6.4**, **6.7** and **6.9)** results in improvements in solubility compared to the unsubstituted analogues (**20**, **6.5**, **6.8** and **6.10**). The most significant improvement in solubility is seen in the addition of fluorine to **6.10** (<5 μM) to give **6.9** (>200 μM), resulting in a greater than 40-fold increase in solubility. Compounds with Mannich base side-chains (**6.6** and **6.11**) showed poor solubility (<5 μM) in both kinetic and equilibrium solubility assays.

A line graph comparing the results of the equilibrium and kinetic solubility assays is seen below (Figure 2.17). This graph illustrates the general agreement between these two methods of measuring solubility. From this overlay it is clear that two compounds (**6.4** and **6.12**) can be classified as moderately soluble and two other compounds (**6.2** and **6.9)** classify as highly soluble (i.e. ≥ 150 μM) in the equilibrium solubility assay.

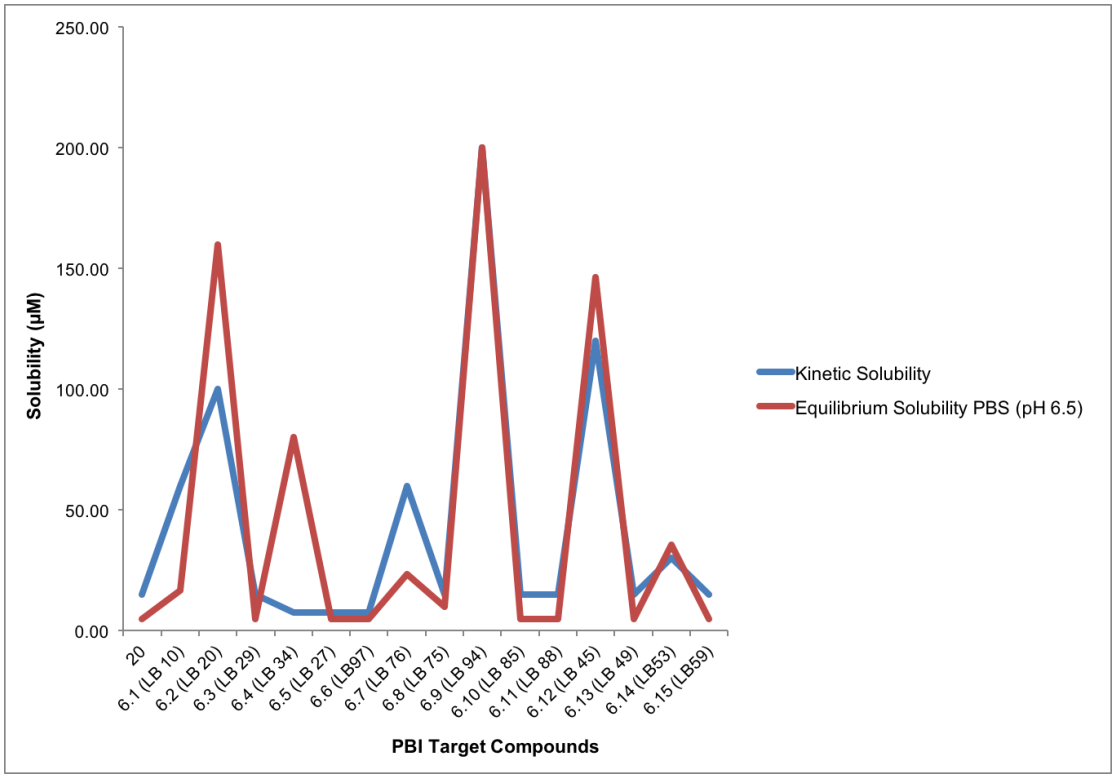

Figure 2.17: Overlay of kinetic solubility data and HPLC-based equilibrium solubility data.

2.9 Determination and Evaluation of Factors Contributing to Solubility

This section investigates the possible factors that contributed towards solubility in the PBIs synthesized. The following factors were considered in this evaluation:

1. Dihedral angle
2. Single crystal XRD analysis
3. Density Functional Theory (DFT) calculations
4. CLogD
5. HPLC retention time
6. Melting point

2.9.1 Dihedral angle

As mentioned previously, various approaches can be used to improve solubility. This project focused on disrupting the molecular planarity of the target molecule by introducing substituents in appropriate positions of the PBI core. The dihedral angle is a convenient, measurable parameter that can be used to measure the disruption of planarity. It can be measured by X-ray crystal analysis or DFT calculations.[45]

2.9.2 Single crystal XRD analysis of 6.4

2.9.2.1 Introduction

This section describes the single crystal X-ray diffraction analysis of **6.4** (LB34). This compound showed good *in vitro* antiplasmodial activity combined with a good cytotoxicity profile, and was therefore selected for structural elucidation in an effort to provide more information regarding the effect of changes in the dihedral angle on solubility.

Single crystals of **6.4** were grown by slow evaporation using an array of solvents. Acetone, ethanol and acetonitrile were the selected solvents and

were chosen based on their polarity. Ethanol gave rise to the appropriate sized crystals. The crystal structure and refinement parameters for **6.4** are seen in Table 6.

Table 6: Crystallographic data for 6.4 obtained from ethanol

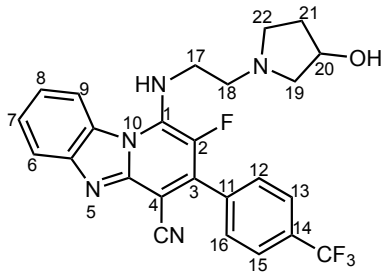

Parameter	Value
Empirical formula	$2(C_{25}H_{21}N_5OF_4).(C_2H_6O)$
Formula weight (g/mol)	1013.00
Temperature (K)	173(2)
Wavelength (Å)	0.71073
Crystal system	Monoclinic
Space group	$P2_1$
Cell parameters (Å, °)	a=14.8505(7) b=9.5610(5) c=18.1279(10)
	α=90 β=111.5666(1) γ=90
Cell volume ($Å^3$)	2392.7(2)
Crystal size (mm)	0.12 × 0.24 × 0.31
Z	2
Calculated density ($g.cm^{-1}$)	1.405
Θ min (°)	1.208
Θ max (°)	28.343
Reflections collected	21121
Final R indices [I > 2σ(I)]	0.0618
R indices (all data)	0.0973
Goodness-of-fit on F^2	1.011

2.9.2.2 General comments

The structure of **6.4** crystallizes in $P2_1$ with Z = 2 (Figure 2.18). The oxygen atom of the hydroxyl group was disordered over two positions. The refined site occupancy factors were found to be 0.549 for O1A and O1B; 0.451 for O2A and O2B. All the fluorine atoms of the CF_3 group were disordered. The refined site occupancy factors are 0.450 for F1A, F2A and F3A; 0.550 for F4A, F5A and F6A; 0.785 for F1B, F2B and F3B; 0.215 for F4B, F5B and F6B. The hydroxyl hydrogen on O1A, O2A, O1B, O2B and O1G could not be located in the different electron density maps and were excluded from the final structure model. The structure was refined to R factor of 0.0618.

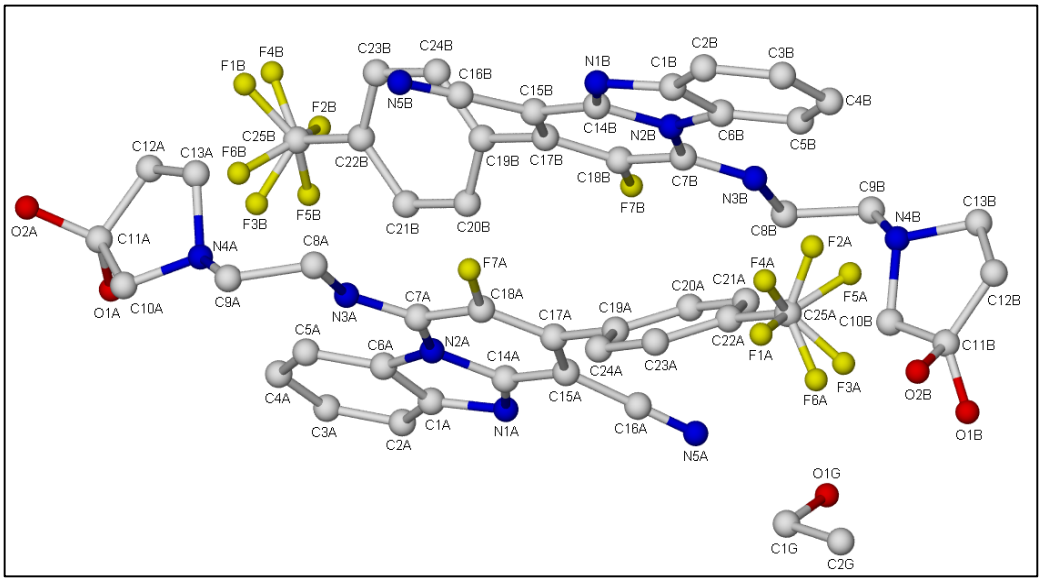

Figure 2.18: The asymmetric unit (ASU) of the **6.4** solvated crystal that was obtained from ethanol.

The ASU consists of two molecules (denoted A and B) that are hydrogen bonded to one ethanol molecule. The linear nitrile group at C16A (C16A-N5A) is coplanar to the PBI core. The structure is stabilized by various hydrogen bonds between the hydroxyl oxygens of pyrrolidinol and ethanol groups, and the nitrile nitrogen (Figure 2.19). These have donor···acceptor distances varying from 2.660 - 3.018 Å. These hydrogen bonds form chains that may be described as $C_3^3(17)$ in Etter's graph system.[71] Weak intermolecular C-H···F bonds (2.6614 – 3.1515 Å), intramolecular C-H···N bonds (2.6421 – 3.4335 Å) and π-π stacking are also observed.

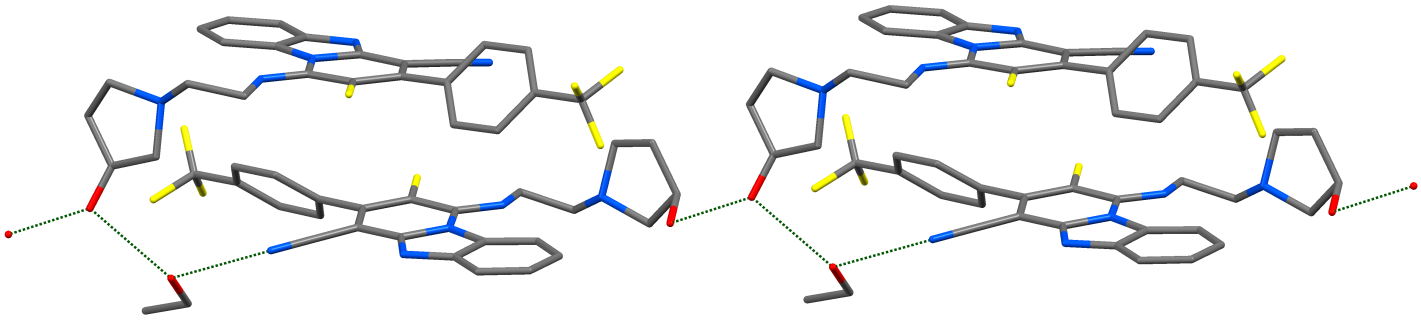

Figure 2.19: The hydrogen bonding between molecules may be described as $C_3^3(17)$.[71]

2.9.3 Density Functional Theory Calculations

2.9.3.1 Introduction

Molecular planarity and symmetry influence the crystal packing of a molecule. Therefore the disruption of molecular planarity/symmetry is hypothesized to decrease the crystal packing energy and result in improved solubility.[45] The structural modifications made at position C-2, as discussed in section 2.7, were performed in an effort to disrupt the molecular planarity of the molecule by increasing the dihedral angle.

2.9.3.2 Calculated dihedral angles

Due to the fact that only one crystal structure was obtained, density functional theory (DFT) calculations (B3LYP/6-31G*)[72] were utilized to obtain the dihedral angles (Figure 2.20) of all the PBI target compounds for the optimized structures, as seen in Table 7.

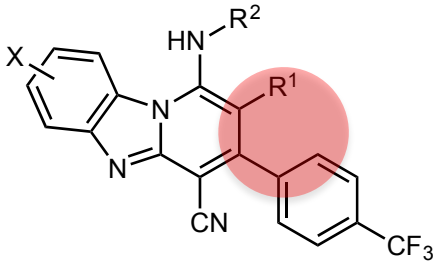

Figure 2.20: Dihedral angles (red) measured in the PBI target compounds.

Table 7: Calculated Dihedral Angles and Physicochemical Properties for PBI Target Compounds

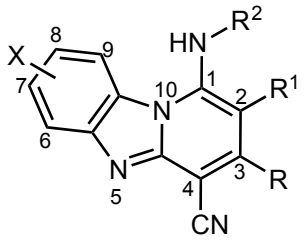

Compound	X	R^1	R^2	R	Calculated Dihedral Angles[a] (deg)	CLogD[b]	HPLC retention time (min)[c]	Melting Point (°C)	Equilibrium Solubility: PBS (pH 6.5) μM
20	H	H	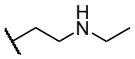	4-CF_3Ph	43.6	3.137	4.08	222 - 224	<5
6.1 (LB 10)	H	CH_3	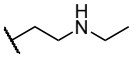	4-CF_3Ph	82.2	3.260	3.53	174 – 177	16.5 (±0.9)
6.2 (LB 20)	H	F	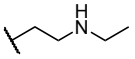	4-CF_3Ph	74.4	3.154	3.75	281 - 286	160
6.3 (LB 29)	H	CH_3	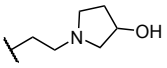	4-CF_3Ph	84.1	3.556	3.38	236 – 238	<5
6.4 (LB 34)	H	F	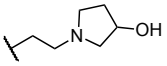	4-CF_3Ph	75.9	3.468	3.51	265 - 267	80
6.5 (LB 27)	H	H	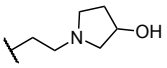	4-CF_3Ph	66.1	3.460	3.56	267 - 269	<5
6.6 (LB 97)	H	F	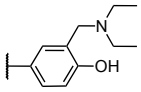	4-CF_3Ph	78.7	4.432	3.98	275 - 280	<5
6.7 (LB 76)	7,8-Cl	F	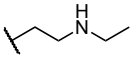	4-CF_3Ph	74.4	3.971	4.74	332 - 338	23.4 (±1.2)
6.8 (LB 75)	7,8-Cl	H	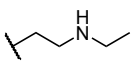	4-CF_3Ph	66.8	4.063	4.29	266 - 268	10
6.9 (LB 94)	7,8-F	F	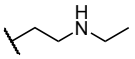	4-CF_3Ph	74.8	2.932	4.14	253 - 260	>200
6.10 (LB 85)	7,8-F	H	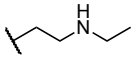	4-CF_3Ph	66.8	2.989	3.48	212 - 215	<5
6.11 (LB 88)	7,8-F	H	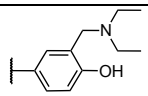	4-CF_3Ph	62.1	4.229	4.15	284 - 288	<5
6.12 (LB 45)	H		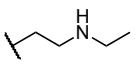	CH_3	67.8	2.389	3.22	174 – 176	146.5 (±2.0)
6.13 (LB 49)	H	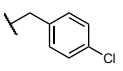	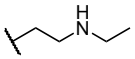	CH_3	67.8	3.104	3.71	189 – 191	<5
6.14 (LB 53)	H		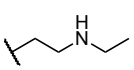	CH_3	68.0	3.093	3.60	162 – 166	35.6 (±4.0)
6.15 (LB 59)	H		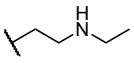	CH_3	59.2	3.072	3.49	200 - 202	<5

[a] Calculated dihedral angle was estimated with Gaussian 09. [b] CLogD values were estimated with StarDrop, version 6.0.3. [c] Kinetex Core reversed-phase column (3.0 mm x 50 mm).

Figure 2.21 displays an overlay of the crystal structure of **6.4** with the corresponding optimized structure. The dihedral angle of the crystal structure of **6.4** was found to be 49.0°. The calculated dihedral angle of the optimized structure was found to be 43.6° (Table 7). The RMSD value for the two superimposed structures was calculated using Mercury CSD 3.5.1[73] and found to be 0.156Å. A relatively low RMSD value such as this gives confidence to the calculated dihedral angles of the optimized structures.

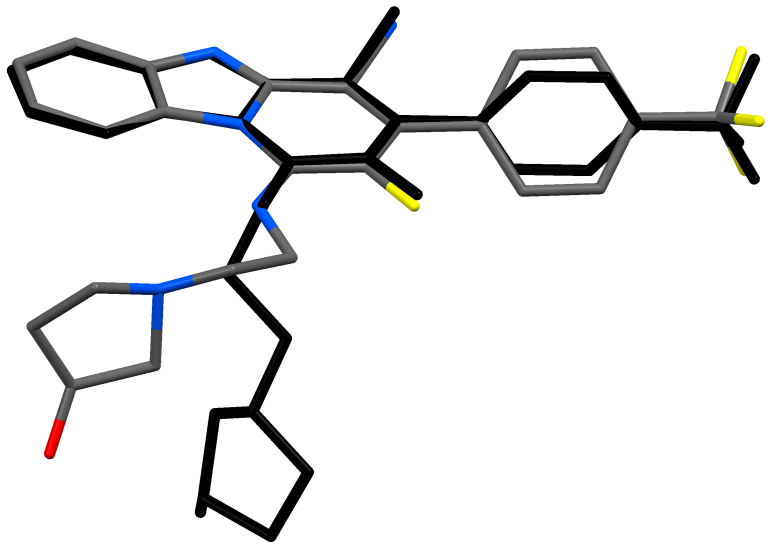

Figure 2.21: Overlay of the crystal structure and the optimized structure (black) of **6.4** obtained using DFT calculations (B3LYP/6-31G*).

As seen in Table 7, most of the C-2 unsubstituted compounds (**20**, **6.5**, **6.8,** and **6.11**) display small dihedral angles (< 67°). The C-2 substituted compounds show an increase in the dihedral angle relative to their unsubstituted analogues.

A trend is observed between equilibrium solubility and dihedral angle (R^2 = 0.1), as seen in Figure 2.22. However, when the three outliers (**6.1**, **6.3** and **6.6**) were excluded, a stronger trend (R^2 = 0.4) was observed. The relatively weak trend confirms that there are many factors that influence solubility and that dihedral angle is just one of them.

The two methyl-substituted analogues (**6.1** and **6.3**) may weaken the trend because the methyl group may be involved in weak hydrogen bonding that may cause tighter crystal packing. This could account for their large dihedral angles but low solubility.

The third outlier, **6.6**, is one of the Mannich base derivatives. Both Mannich bases show poor solubility that may be explained by the aromatic ring of the Mannich base side-chain that is available for further π- π stacking with the rest of the planar PBI core. However, what makes **6.6** different from the other Mannich base (**6.11**) is that it has a fluoro-group substituted at position C-2 and thus the dihedral angle is increased relative to **6.11** (R^1 = H). The weak trend confirms that there are many factors at play when considering solubility, and hydrophobicity is a contributing factor.

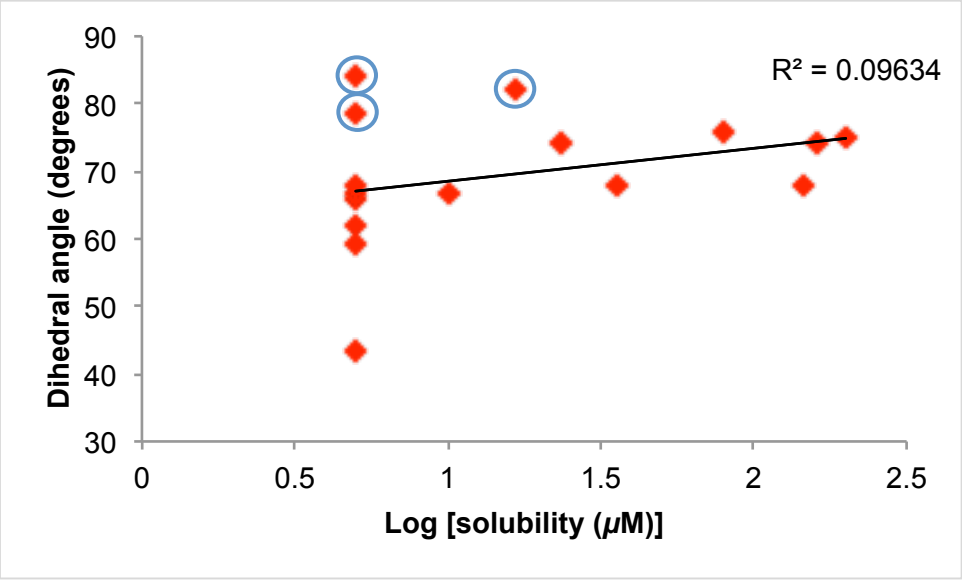

Figure 2.22: Relationship between solubility and calculated dihedral angle of PBI target compounds. Outliers (**6.1**, **6.3** and **6.6**) are circled in blue.

Ishikawa *et al.*[45] found that upon increasing the dihedral angle, the crystal packing energy decreased and this resulted in an increase in solubility and a decrease in melting point. However, from the results in Table 7, no correlation between melting point and solubility or dihedral angle was observed.

2.10 Conclusion

Structural modifications were performed on the parent PBI core and 15 analogues were synthesized. All the analogues were fully characterized using spectroscopic and analytical techniques such as ^{1}H and ^{13}C NMR spectroscopy, mass spectrometry, purity on reverse-phase HPLC and melting point.

All compounds were evaluated for *in vitro* antiplasmodial activity, cytotoxicity and BHI activity. The microsomal metabolic stability of selected compounds was also determined. Equilibrium solubility and kinetic solubility assays were used to determine the effect of structural modifications on solubility.

Most compounds displayed good antiplasmodial activity against the chloroquine sensitive (NF54) strain of *P. falciparum* with activity in the sub-micromolar range. Substitutions at the C-2 position improved solubility, but this was at the expense of antiplasmodial activity.

Compounds that are unsubstituted at the C-2 position generally showed good metabolic stability whereas compounds with a substituent at C-2 showed high levels of metabolic degradation. This position appears to make the PBI core/phenyl ring vulnerable to oxidation, which is largely responsible for the metabolic instability.

DFT calculations were used to obtain optimized structures in order to calculate the dihedral angles of all the analogues with a view to determining the effect of structural modifications on the dihedral angle, and the relation to solubility. The optimized structure of **6.4** was compared to the experimentally determined crystal structure of **6.4** and these structures displayed a RMSD value of 0.156. The calculated dihedral angles showed a moderate correlation (0.4) with solubility. This suggests that there are many factors that influence the solubility of PBIs and the dihedral angle is a contributing factor.

Further SAR studies can be carried out to expand the structural diversity of the analogues. This may aid in finding compounds that combine good *in vitro* potency with acceptable drug-like properties.

CHAPTER 3: CONCLUSION

3.1 General Summary and Conclusion

SAR studies were carried out on the PBI scaffold. Analogues were synthesized in an attempt to address the solubility liability previously identified in the lead compound (**20**).

A straight forward organic synthetic approach was utilized in the synthesis of the PBI target compounds. The identity and purity of these compounds were confirmed through characterization using analytical and spectroscopic techniques such as ^{1}H and ^{13}C NMR Spectroscopy, mass spectrometry (LC-MS), reverse-phase HPLC and melting point.

The solubility of target compounds was experimentally investigated using equilibrium and kinetic solubility assays. All compounds were evaluated for *in vitro* antiplasmodial activity, cytotoxicity and BHI activity. Selected compounds were also evaluated for metabolic stability in mouse and human liver microsomes.

i. Pharmacological evaluation

- Compounds showed good antiplasmodial activity against the chloroquine sensitive (NF54) strain of *Plasmodium falciparum* with activity in the sub-micromolar range.
- Selected compounds with sub-micromolar activity against the chloroquine sensitive (NF54) strain were tested against the chloroquine resistant (K1) strain of *Plasmodium falciparum* and found to be equipotent against both strains, suggesting the absence of cross resistance.
- Substitutions on the benzimidazole moiety of the PBI core improved activity up to 6-fold relative to the lead compound.
- Compounds with the 2-aminoethyl-3-pyrrolidinol side-chain showed improved activities compared to the corresponding *N*-ethylethane-diamino analogues.

- Substitutions at the C-2 position resulted in a decrease in antiplasmodial activity and altered the ability of these compounds to inhibit the formation of *β*-hematin. A plot of antiplasmodial activity and BHI displayed a positive albeit weak correlation between the BHI activity of compounds and antiplasmodial potency. This suggests that BHI is a contributing mechanism to the antiplasmodial activity of these compounds.
- Substitution at the C-2 position resulted in PBI derivatives with low metabolic stability relative to the unsubstituted compounds (Figure 3.1).

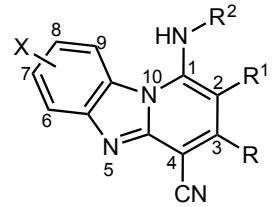

Figure 3.1: General structure of the PBI scaffold.

ii. Solubility

- Solubility was significantly improved upon introduction of a fluorine or methyl substituent at the C-2 position.
- Single crystals of **6.4** were grown and analysed by X-ray diffraction in an effort to measure the dihedral angle and determine whether or not improvements in solubility were related to an increase in dihedral angle.
- DFT calculations were used to obtain the dihedral angles for the optimized structures of all the PBI target compounds in order to determine the effect of structural modifications on dihedral angle and the consequential effect on solubility. The reliability of the optimized structures was confirmed by superimposing the single X-ray crystal structure of **6.4** with its corresponding optimized structure and a RMSD value of 0.156 was obtained.
- The optimized structure of **6.4** suggests that the C-2 substituted compounds displayed an increase in the dihedral angle relative to the corresponding unsubstituted analogues as expected.
- A weak trend (R^2 = 0.4) between equilibrium solubility and dihedral angle suggests that many factors may influence the solubility of PBIs and that dihedral angle is just one of the contributing factors.

3.2 Future Outlook

Further SAR studies to expand the chemical diversity of these compounds could lead to compounds that combine good antiplasmodial potency with desirable drug-like properties. Reactive metabolite studies should be carried out on the Mannich base analogues. As seen in scheme 7, these analogues have the same side chain as the antimalarial drug Amodiaquine. Studies have shown that Amodiaquine undergoes metabolism to form the cytotoxic amodiaquine quinoneimine that has been associated with hepatotoxicity and agranulocytosis.[74,75]

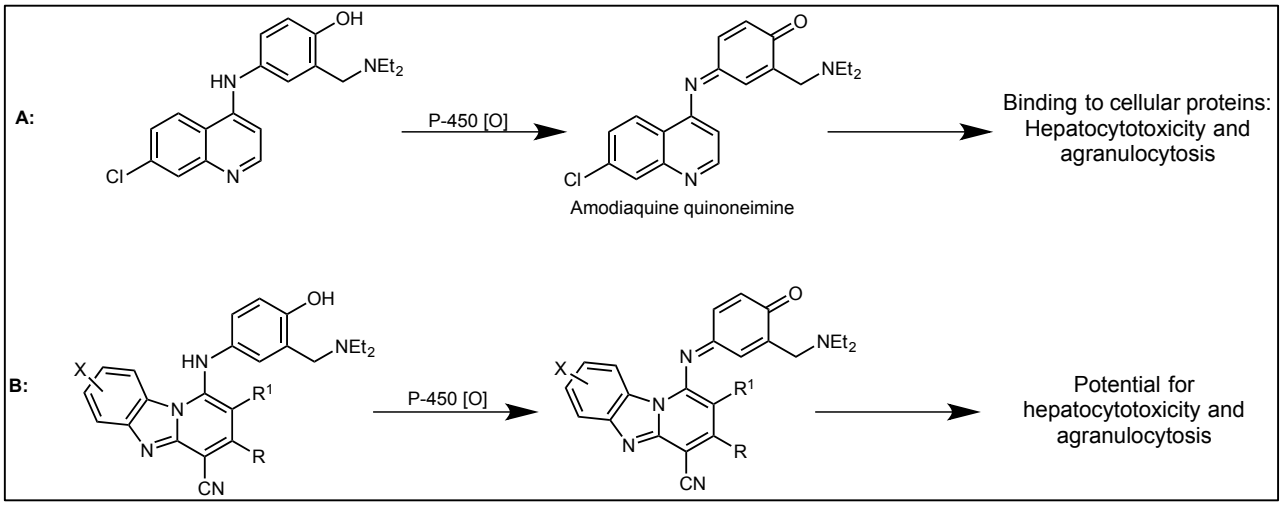

Scheme 7: Metabolism of Amodiaquine to form the reactive metabolite amodiaquine quinoneimine (A); and the Mannich Base side-chain derivatives that have potential to form reactive metabolites (B).

The crystal structure of other analogues, in particular the methyl substituted and the unsubstituted analogues, can be investigated in an effort to compare their dihedral angles with that of the fluorine-substituted crystal structure (**6.4**) obtained in this project and thus provide further validation of the DFT calculated optimized structures (Figure 3.2).

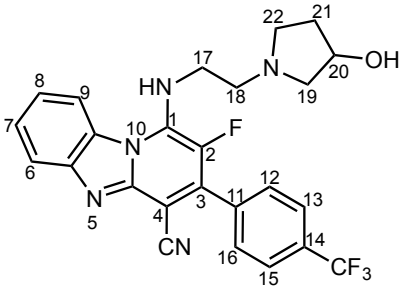

Figure 3.2: Structure of **6.4**

Since the 2-aminoethyl-3-pyrrolidinol analogues were obtained as a racemic mixture, the individual enantiomers can be synthesized and *in vitro* antiplasmodial activity investigated to determine if the individual enantiomers (Figure 3.3) possess different potencies.

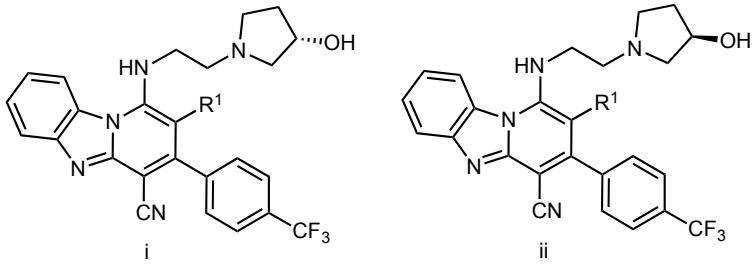

Figure 3.3: The (S)-enantiomer (i) and (R)-enantiomer (ii) of the 2-aminoethyl-3-pyrrolidinol analogues.

From the results found in this study, compound **6.8** displayed the most potent antiplasmodial activity (IC_{50} = 0.02 μM), **6.7** displayed the highest metabolic stability (>90 % remaining after 30 minutes) and **6.9** was found to be the most soluble (>200 μM) in the equilibrium solubility assay (Figure 3.4).

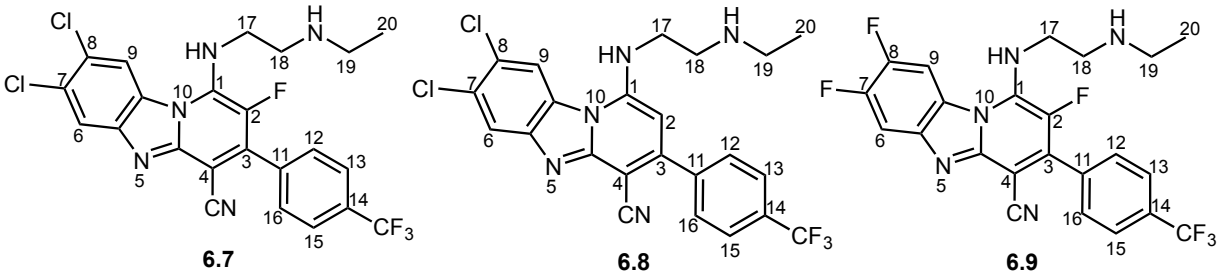

Figure 3.4: The structures of compounds **6.7**, **6.8** and **6.9**.

Although compounds **6.7** and **6.8** outshone in the respective assays, they fell short in the solubility assay (see Table 8). As seen in Table 8, compound **6.4** (Figure 3.2), displayed a combination of good antiplasmodial activity (IC_{50} = 0.19 μM) and moderate solubility (80 μM). Since the benzimidazole moiety of this compound is currently unexplored, these substitutions could potentially improve the activity and metabolic stability as seen in other analogues such as **6.7** - **6.9** (Figure 3.5). Additionally, metabolite identification can be done on this compound in order to identify the metabolites so that they can be synthesized and tested for antiplasmodial activity.

Table 8: Biological and Solubility Data for Selected PBI Target Compounds*

Compound	Antiplasmodial Activity (NF54) IC_{50} (μM)	Metabolic Stability in MLM: % remaining after 30 min	Equilibrium Solubility: PBS (pH 6.5) μM
6.7	0.78	91	23.4 (± 1.2)
6.8	0.02	81	10
6.9	3.95	ND[a]	>200
6.4	0.19	37	80

**Green = good result*; *orange = moderate result; red = poor result*

[a]ND: Not determined

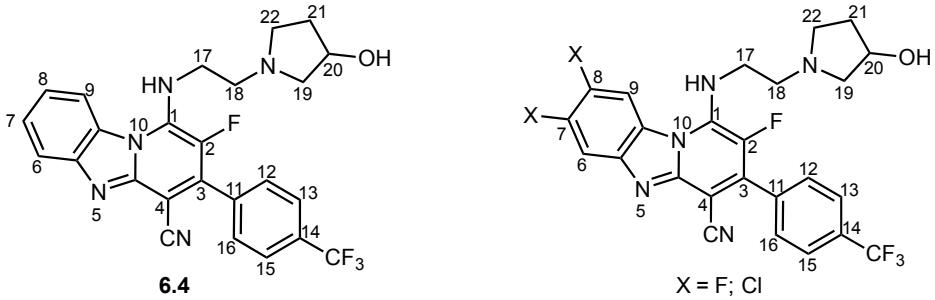

Figure 3.5: Compound **6.4** and proposed structures for future work.

Overall, more structurally diverse analogues are required in order to have more data points and obtain a broader understanding of the observed trends.

CHAPTER 4: EXPERIMENTAL

4.1 Reagents, Solvents and Equipment

All commercially available chemicals were purchased from Sigma-Aldrich, Merck or Combi-Blocks Limited and were of analytical grade, thus used without further purification. Reported compounds were characterized using ^{1}H NMR, ^{13}C NMR, HPLC-MS and melting point determination.

^{1}H NMR spectra were recorded on a Varian Mercury (300 MHz), a Bruker Ultrashield-Plus (400 MHz) spectrometer or a Bruker (600 MHz). Fluorine decoupled ^{13}C NMR spectra were recorded on the same instruments at 101 MHz or 151 MHz and ^{19}F spectra were recorded at 377 MHz. NMR samples were dissolved in deuterated dimethylsulfoxide (DMSO-d_6), methanol (CD_3OD) or chloroform ($CDCl_3$). Chemical shifts (δ) are reported in parts per million (ppm) to 2 decimal places. Coupling constants (*J*) are reported in Hertz (Hz) to one decimal place. Abbreviations used in assigning ^{1}H-NMR signals are: d (doublet), dd (doublet of doublets), ddd (doublet of doublet of doublets), dt (doublet of triplets), m (multiplet), q (quartet), s (singlet), t (triplet) or td (triplet of doublets).

Target compounds' peak purities and mass spectrometry were determined on an Agilent HPLC system equipped with Agilent 1260® Infinity Binary Pump, Agilent 1260® Infinity Diode Array Detector, Agilent 1290® Infinity Column Compartment, Agilent 1260® Infinity Autosampler, Agilent 6120® Quadrupole LC/MS and Peak Scientific® Genius 1050 Nitrogen Generator. The column used was a Kinetex Core C18, 2.6 *μ*m, 3.0 mm (ID) x 50 mm (length) maintained at 40 °C. Table 9 lists the composition and gradient conditions of the mobile phase used at a flow rate of 0.9 mL/min. The injection volume was 2 *μ*L while the mass spectra were obtained both by positive mode Electron Spray Ionization (ESI) and Atmospheric Pressure Chemical Ionization (APCI). The diode array detector was programmed to scan the eluents at an absorption wavelength range of 210-640 nm.

Table 9: HPLC Gradient Conditions

Time (min)	% A	% B	Composition	
			A	B
0.00-1.00	80	20	10mM NH_4OAc in buffer (0.4% acetic acid)	10mM NH_4OAc (0.4% acetic acid) in 90% HPLC grade CH_3OH in H_2O
1.00-3.00	0	100		
3.00-4.50	0	100		
4.50-5.20	80	20		
5.20-6.00	80	20		

Melting points were determined using a Stuart Automatic Melting Point Apparatus, SMP40 (Bibby Scientific) or Reichert-Jung Thermovar hot stage microscope and are uncorrected.

Reactions were monitored by thin layer chromatography (TLC) using Fluka or Merck F254 aluminium-backed pre-coated silica gel plates and were visualized under ultraviolet light at 254 or 366 nm. Silica gel column chromatography was performed using Merck kieselgel 60: 70-230 mesh by gravity column chromatography or flash column chromatography on a Biotage Isolera^{TM} system (Biotage AB, Uppsala, Sweden).

4.2 Synthesis and Characterization

General procedure for the synthesis of compound 2.1

Ethyl(4-trifluromethylbenzoyl)acetate (1.0 equiv.) was added to a stirring solution of methyl iodide (2.0 equiv.) and potassium carbonate (2.0 equiv.) in acetonitrile (9.0 mL). The mixture was heated to 50°C for 2 hours. The mixture was cooled to room temperature and the solvent was removed *in vacuo.* The residue was diluted with ethyl acetate, washed with water, dried with anhydrous sodium sulfate and concentrated *in vacuo.* The residue was purified by flash column chromatography (EtOAc/Hex) to obtain compound **2.1**.

***Ethyl 2-methyl-3-oxo-3-(4-(trifluoromethyl)phenyl)propanoate,* 2.1**

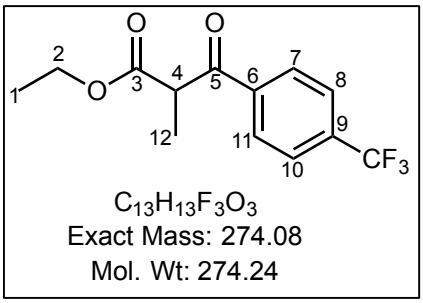

$C_{13}H_{13}F_3O_3$
Exact Mass: 274.08
Mol. Wt: 274.24

Colorless oil (0.554 g, 52 %); R_f 0.27 (10 % EtOAc-Hex); ^{1}H NMR (300 MHz, $CDCl_3$) δ 8.10 (d, *J* = 8.2 Hz, 2H, $ArH^{8,10}$), 7.76 (d, *J* = 8.2 Hz, 2H, $ArH^{7,11}$), 4.38 (q, *J* = 7.1 Hz, 1H, H^4), 4.17 (q, *J* = 7.2 Hz, 2H, H^2), 1.53 (d, *J* = 7.1 Hz, 3H, H^{12}), 1.19 (t, *J* = 7.2 Hz, 3H, H^1); ^{13}C NMR (101 MHz, DMSO-d_6) δ 197.6, 173.1, 141.5 (2C), 136.9, 131.5 (2C), 128.5 (2C), 64.3, 51.5, 16.6, 16.2; MS: *m/z* 275.1 $[M+H]^+$.

General procedure for the synthesis of compound 2.2

Ethyl(4-trifluromethylbenzoyl)acetate (1.0 equiv.) was added to Selectfluor fluorinating agent (2.0 equiv.) in acetonitrile (3.0 mL). The mixture was heated in the microwave at 82°C for 10 minutes. The black precipitate was filtered off and the solvent was removed *in vacuo*. The residue was purified by flash column chromatography (EtOAc-Hex) to acquire compound **2.2**.

***Ethyl 2-fluoro-3-oxo-3-(4-(trifluoromethyl)phenyl)propanoate* 2.2**

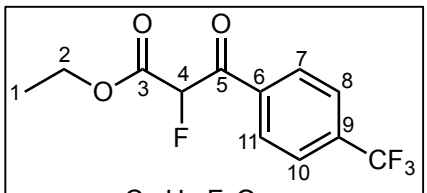

$C_{12}H_{10}F_4O_3$
Exact Mass: 278.06
Mol. Wt: 278.20

Yellow oil (2.315 g, 66 %); R_f 0.33 (10 % EtOAc-Hex); ^{1}H NMR (400 MHz, $CDCl_3$) δ 8.17 (d, *J* = 8.2, 2H, $ArH^{8,10}$), 7.79 (d, *J* = 8.2 Hz, 2H, $ArH^{7,11}$), 5.86 (d, *J* = 48.8 Hz, 1H, H^4), 4.33 (q, *J* = 7.1 Hz, 2H, H^2), 1.29 (t, *J* = 7.1 Hz, 3H, H^1); ^{13}C NMR (101 MHz, $CDCl_3$) δ 188.8, 164.3, 136.0, 129.9, 129.9, 125.9, 125.8, 122.0, 91.3, 89.3, 62.9, 13.9; ^{19}F NMR (377 MHz, $CDCl_3$) δ -63.49, -190.44; MS: *m/z* 277.0 $[M-H]^-$.

General procedure for the synthesis of compounds 2.3

To a suspension of potassium tertiary butoxide (1.2 equiv.) in anhydrous THF (2 mL/mmol), ethyl acetoacetate (1.1 equiv.) and tertiary butanol (0.1 equiv.) were added at 0°C under nitrogen and the clear yellow solution was left to stir for 30 minutes. The appropriate benzyl halide (1.0 equiv.) was added dropwise at 0°C. The reaction was left to stir at 70°C for 8 – 24 hours. The reaction was quenched with water and saturated aqueous sodium bicarbonate. The organic layer was extracted with ethyl acetate (2 x 10 mL), after which the organic extracts were collected and dried with magnesium sulfate and concentrated *in vacuo*. The residue was purified by flash column chromatography (EtOAc-Hex) to obtain the desired intermediates, **2.3.1 – 2.3.4.**

***Ethyl 2-benzyl-3-oxobutanoate* (2.3.1)**

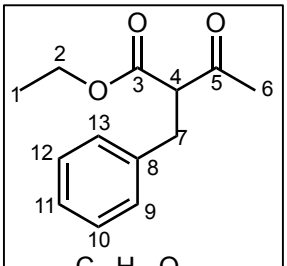

$C_{13}H_{16}O_3$
Exact Mass: 220.11
Mol. Wt: 220.27

Colorless oil (0.342 g, 7 %); R_f 0.46 (20 % EtOAc-Hex); ^{1}H NMR (400 MHz, $CDCl_3$) δ 7.32 – 7.18 (m, 5H, $ArH^{9,10,11,12,13}$), 4.17 (q, *J* = 7.6 Hz, 2H, H^2), 3.80 (t, *J* = 7.6 Hz, 1H, H^4), 3.19 (dd, *J* = 7.6, 1.5 Hz, 2H, H^7), 2.21 (s, 3H, H^6), 1.22 (t, *J* = 7.6 Hz, 3H, H^1); ^{13}C NMR (101 MHz, $CDCl_3$) δ 202.4, 169.1, 138.2, 128.8 (2C), 128.6 (2C), 126.7, 61.4, 61.3, 44.0, 29.5, 14.00; MS: *m/z* 221.1 $[M+H]^+$.

***Ethyl 2-(4-chlorobenzyl)-3-oxobutanoate* (2.3.2)**

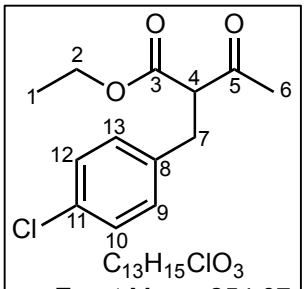

$C_{13}H_{15}ClO_3$
Exact Mass: 254.07
Mol. Wt: 254.71

Yellow oil (2.339 g, 60 %); R_f 0.61 (30 % EtOAc-Hex); ^{1}H NMR (400 MHz, $CDCl_3$) δ 7.29 – 7.25 (m, 2H, $ArH^{10,12}$), 7.15 – 7.12 (m, 2H, $ArH^{9,13}$), 4.17 (q, *J* = 7.2, Hz, 2H, H^2), 3.75 (t, *J* = 7.6 Hz, 1H, H^4), 3.15 (dd, *J* = 7.6, 3.5, 2H, H^7), 2.22 (s, 3H, H^6), 1.23 (t, *J* = 7.2 Hz, 3H, H^1); ^{13}C NMR (101 MHz, $CDCl_3$) δ 201.9, 168.9, 136.7, 131.4, 130.2 (2C), 128.7 (2C), 61.7, 61.2, 33.2, 29.5, 14.0; MS: *m/z* 253.0 $[M-H]^-$.

***Ethyl 2-(3-chlorobenzyl)-3-oxobutanoate* (2.3.3)**

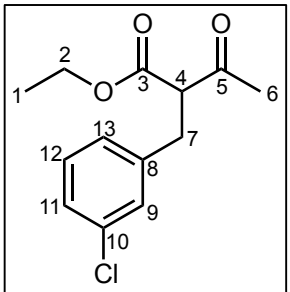

$C_{13}H_{15}ClO_3$
Exact Mass: 254.07
Mol. Wt: 254.71

Yellow oil (3.283 g, 84 %); R_f 0.56 (15 % EtOAc-Hex); ^{1}H NMR (400 MHz, $CDCl_3$) δ 7.23 – 7.19 (m, 4H, $ArH^{9,11,12,13}$), 4.18 (q, *J* = 7.3, 2H, H^2), 3.76 (dd, *J* = 7.6, 7.3 Hz, 1H, H^4), 3.19 – 3.13 (m, 2H, H^7), 2.23 (s, 3H, H^6), 1.23 (t, *J* = 7.3 Hz, 3H, H^1); ^{13}C NMR (101 MHz, $CDCl_3$) δ 201.7, 168.8, 140.3, 134.3, 130.2, 129.8, 127.0, 126.9, 61.6, 61.0, 33.4, 29.5, 14.0; MS: *m/z* 254.07 $[M]^+$.

***Ethyl 2-(2-chlorobenzyl)-3-oxobutanoate* (2.3.4)**

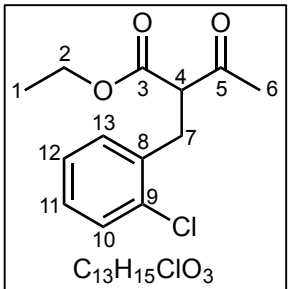

$C_{13}H_{15}ClO_3$
Exact Mass: 254.07
Mol. Wt: 254.71

Yellow oil (2.311 g, 59 %); R_f 0.53 (15 % EtOAc-Hex); ^{1}H NMR (400 MHz, $CDCl_3$) δ 7.38 – 7.35 (m, 1H, ArH^{10}), 7.29 – 7.25 (m, 1H, ArH^{12}), 7.20 – 7.17 (m, 2H, $ArH^{11,13}$), 4.23 – 4.11 (m, 2H, H^2), 3.97 (dd, *J* = 8.3, 6.6 Hz, 1H, H^4), 3.35 – 3.23 (m, 2H, H^7), 2.25 (s, 3H, H^6), 1.23 (t, *J* = 7.1 Hz, 3H, H^1); ^{13}C NMR (101 MHz, $CDCl_3$) δ 202.1, 168.9, 135.8, 134.1, 131.6, 129.6, 128.3, 126.9, 61.5, 58.8, 31.9, 29.6, 14.0; MS: *m/z* 254.06 $[M]^+$.

General procedure for the synthesis of compound 3.2

4-5-Dichloro-*o*-phenylenediamine (1.0 equiv.) was added to ethyl-2-cyanoacetate (3.0 equiv.) in DMF (1.5 mL). The solution was heated to 150°C for 2 hours. The organic layer was extracted with ethyl acetate and the organic extracts were combined, washed with water, brine, dried with anhydrous magnesium sulfate and concentrated *in vacuo*. The residue was purified by flash column chromatography (EtOAc-Hex) to obtain the required compound **3.1**.

***2-(5,6-dichloro-1H-benzo[d]imidazol-2-yl)acetonitrile* (3.2)**

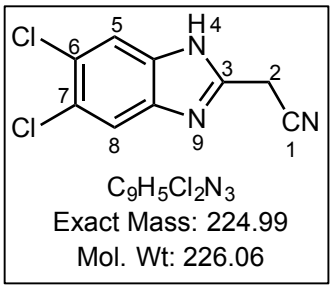

$C_9H_5Cl_2N_3$
Exact Mass: 224.99
Mol. Wt: 226.06

Red/brown solid (1.645 g, 57 %); %); m.p. 274 - 278 ^{o}C; R_f 0.35 (50 % EtOAc-Hex); ^{1}H NMR (400 MHz, DMSO-d_6) δ 12.91 (s, 1H, NH), 7.86 (s, 2H, ArH^{5,8}), 4.43 (s, 2H, H^{2}); ^{13}C NMR (101 MHz, DMSO-d_6) δ 148.4, 145.2, 143.4, 120.4, 116.7, 116.0, 113.5, 110.2, 18.9; HPLC-MS (APCI/ESI): Purity = 99%, t_R = 3.18 min, MS: *m/z* 226.0 $[M+H]^+$.

General procedure for the synthesis of compound 3.3

A mixture of 4,5-difluorobenzene-1,2-diamine (1.0 equiv.) and ethyl-2-cyanoacetate (2.0 equiv.) was heated in the microwave at 110°C for 15 minutes. The residue was purified by flash column chromatography (EtOAc-Hex) to obtain the required compound **3.2**.

***2-(5,6-difluoro-1H-benzo[d]imidazol-2-yl)acetonitrile* (3.3)**

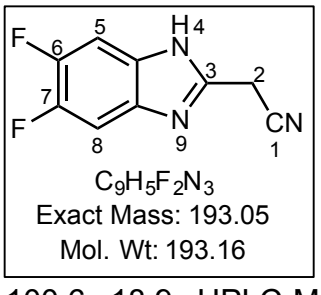

$C_9H_5F_2N_3$
Exact Mass: 193.05
Mol. Wt: 193.16

Red/brown solid (0.485 g, 60 %); m.p. 267 - 269 ^{o}C; R_f 0.38 (70 % EtOAc-Hex); ^{1}H NMR (400 MHz, DMSO-d_6) δ 12.80 (s, 1H, NH), 7.67 – 7.59 (m, 2H, ArH^{5,8}), 4.39 (s, 2H, H^{2}); ^{13}C NMR (101 MHz, DMSO-d_6) δ 148.5, 148.3, 147.4, 146.1, 146.0, 116.8, 106.1, 100.6, 18.9; HPLC-MS (APCI/ESI): Purity = 99%, t_R = 1.32 min, MS: *m/z* 194.1 $[M+H]^+$.

General procedure for the synthesis of the hydroxy intermediates (4.1 – 4.11)

A mixture of the appropriate 2-benzimidazole acetonitrile (1.0 equiv.), ammonium acetate (2 equiv.) and the appropriate *β*-keto ester (1.2 equiv.) was heated to reflux at 145°C for 1-4 hours. The suspension was cooled to 75°C before acetonitrile (10 mL) was added and the mixture was allowed to stir for 15 minutes. The mixture was cooled to room temperature and cooled on ice. The cold mixture was filtered and the precipitate washed with cold acetonitrile (4x10 mL), dried *in vacuo* and used without further purification.

***1-hydroxy-2-methyl-3-(4-(trifluoromethyl)phenyl)benzo[4,5]imidazo[1,2-a]pyridine-4-carbonitrile* (4.1)**

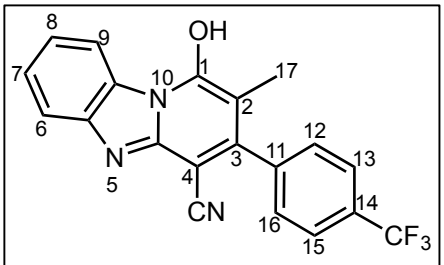

$C_{20}H_{12}F_3N_3O$
Exact Mass: 367.09
Mol. Wt: 367.33

Obtained from **2.1** (0.787 g, 2.87 mmol, 1.2 equiv.), **3.1** (0.376 g, 2.39 mmol, 1.0 equiv.) and NH_4OAc (0.369 g, 4.79 mmol, 2.0 equiv.) as a brown solid (0.132 g, 28 %); m.p. 299 - 301 °C; R_f 0.48 (50 % EtOAc-Hex); ^{1}H NMR (400 MHz, DMSO-d_6) δ 13.58 (s, 1H, OH), 8.66 (dt, *J* = 8.2, 1.0 Hz, 1H, ArH^9), 7.93 (d, *J* = 8.0 Hz, 2H, ArH^{13,15}), 7.65 (d *J* = 8.0 Hz, 2H, ArH^{12,16}), 7.58 – 7.55 (m, 2H, ArH^{6,7}), 7.45 – 7.36 (m, 1H, ArH^8), 1.88 (s, 3H, H^{17}); ^{13}C NMR (101 MHz, DMSO-d_6) δ 159.3, 148.3, 145.9, 141.8, 132.3, 129.9 (2C), 129.4, 128.1, 127.3, 126.0, 126.0 (2C), 123.3, 122.9, 117.1, 116.8, 111.8, 111.6, 13.6; HPLC-MS (APCI/ESI): Purity = 99%, t_R = 4.48 min, MS: *m/z* 368.1 $[M+H]^+$.

***2-fluoro-1-hydroxy-3-(4-(trifluoromethyl)phenyl)benzo[4,5]imidazo[1,2-a]pyridine-4-carbonitrile* (4.2)**

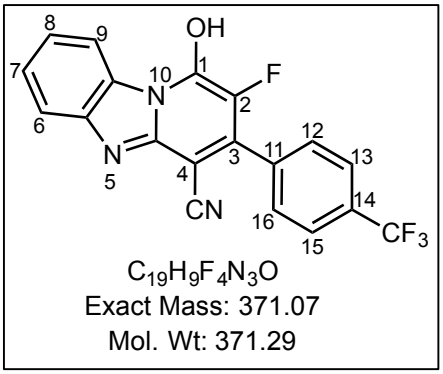

$C_{19}H_9F_4N_3O$
Exact Mass: 371.07
Mol. Wt: 371.29

Obtained from **2.2** (0.626 g, 2.25 mmol, 1.2 equiv.), **3.1** (0.295 g, 1.88 mmol, 1.0 equiv.) and NH_4OAc (0.289 g, 3.75 mmol, 2.0 equiv.) as a brown solid (0.416 g, 57 %); m.p. 343 - 348 °C; R_f 0.43 (50 % EtOAc-Hex); ^{1}H NMR (400 MHz, DMSO-d_6) δ 13.81 (s, 1H, OH), 8.60 (dt, J = 8.2, 1.0 Hz, 1H, ArH^9), 7.98 (d, J = 7.8 Hz, 2H, ArH^{13,15}), 7.82 (d, J = 7.8 Hz, 2H, ArH^{12,16}), 7.60 – 7.57 (m, 2H, ArH^{6,7}), 7.43 (ddd, J = 8.0, 8.0, 4.0 Hz 1H, ArH^8); ^{13}C NMR (101 MHz, DMSO-d_6) δ 152.5, 152.2, 144.6, 139.6, 137.3, 135.7, 134.7, 134.6, 132.8, 130.7, 128.4, 128.4, 127.7, 126.1, 126.1, 123.0, 116.6, 116.4, 112.2; HPLC-MS (APCI/ESI): Purity = 97%, t_R = 4.20 min, MS: *m/z* 372.0 $[M+H]^+$.

1-Hydroxy-3-(4-(trifluoromethyl)phenyl)benzo[4,5]imidazo[1,2-*a*]pyridine-4-carbonitrile (4.3)

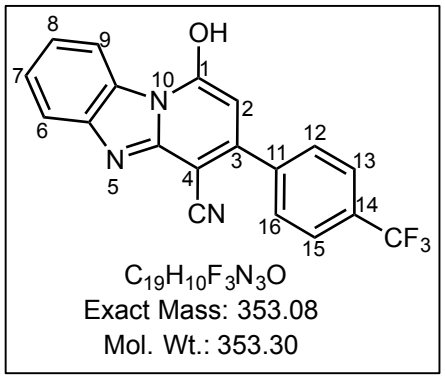

$C_{19}H_{10}F_3N_3O$
Exact Mass: 353.08
Mol. Wt.: 353.30

Obtained from ethyl(4-trifluromethylbenzoyl)-acetate (0.994 g, 3.82 mmol, 1.2 equiv.), **3.1** (0.500 g, 3.18 mmol, 1.0 equiv.) and NH_4OAc (0.490 g, 6.36 mmol, 2.0 equiv.) as a silver tan powder (0.850 g, 76%); R_f 0.61 (70 % EtOAc-Hex); m.p. 341 - 342 °C; ^{1}H NMR (400 MHz, DMSO-d_6) δ 8.59 (d, J = 8.1 Hz, 1H, ArH^9), 7.91 (d, J = 8.2 Hz, 2H, ArH^{13,15}), 7.85 (d, J = 8.2 Hz, 2H, ArH^{12,16}), 7.56 (m, 2H, ArH^{6,7}), 7.40 (t, J = 8.1 Hz, 1H, ArH^8), 6.09 (s, 1H, H^2); ^{13}C NMR (100 MHz, DMSO-d_6) δ 158.3, 151.5, 147.9, 141.4, 132.4, 130.4, 129.6, 128.1, 127.3 (C2), 126.0 (C2), 123.1 (C2), 117.0, 116.7, 112.1(C2) and 105.2; MS: *m/z* 354 $[M+H]^+$.

***7,8-dichloro-2-fluoro-1-hydroxy-3-(4-(trifluoromethyl)phenyl)benzo-[4,5]imidazo[1,2-a]pyridine-4-carbonitrile* (4.4)**

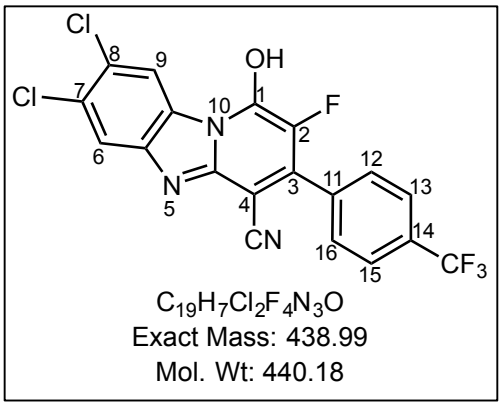

$C_{19}H_7Cl_2F_4N_3O$
Exact Mass: 438.99
Mol. Wt: 440.18

Obtained from **3.2** (0.670 g, 2.96 mmol, 1.0 equiv.), **2.2** (0.990 g, 3.56 mmol, 1.2 equiv.) and NH_4OAc (0.457 g, 5.93 mmol, 2.0 equiv.) as a dark green solid (0.663 g, 51 %); m.p. 299 - 301 °C; R_f 0.35 (50 % EtOAc-Hex); ^1H NMR (400 MHz, DMSO-d_6) δ 8.65 (s, 1H, ArH^9), 7.94 (d, *J* = 7.8 Hz, 2H, $ArH^{13,15}$), 7.79 (d, *J* = 7.8 Hz, 2H, $ArH^{12,16}$), 7.76 (s, 1H, ArH^6); ^{13}C NMR (101 MHz, DMSO-d_6) δ 165.7, 152.5, 139.4 (2C), 136.6 (2C), 130.7, 129.6, 128.7, 125.9, 125.9, 122.2, 119.9, 116.9 (2C), 115.6, 106.5, 101.1, 88.6; HPLC-MS (APCI/ESI): Purity = 99%, t_R = 4.84 min, MS: *m/z* 440.8 $[M+H]^+$.

***7,8-dichloro-1-hydroxy-3-(4-(trifluoromethyl)phenyl)benzo-[4,5]imidazo[1,2-a]pyridine-4-carbonitrile* (4.5)**

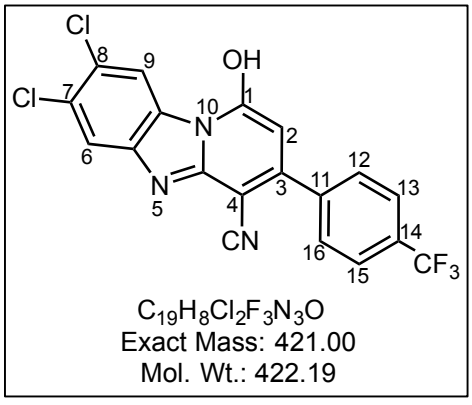

$C_{19}H_8Cl_2F_3N_3O$
Exact Mass: 421.00
Mol. Wt.: 422.19

Obtained from **3.2** (0.504 g, 2.23 mmol, 1.0 equiv.), ethyl(4-trifluromethyl-benzoyl)acetate (0.55 mL, 2.68 mmol, 1.2 equiv.) and NH_4OAc (0.343 g, 4.46 mmol, 2.0 equiv.) as a brown solid (0.787 g, 84 %); m.p. 305 - 307 °C; R_f 0.41 (60 % EtOAc-Hex); ^1H NMR (400 MHz, DMSO-d_6) δ 8.66 (s, 1H, ArH^9), 7.91 (d, *J* = 8.1 Hz, 2H, $ArH^{13,15}$), 7.84 (d, *J* = 8.1 Hz, 2H, $ArH^{12,16}$), 8.66 (s, 1H, ArH^6), 6.05 (s, 1H, H^2). ^{13}C NMR (101 MHz, DMSO-d_6) δ 158.5, 151.9, 150.0, 141.6, 134.7, 130.4, 130.0, 129.6 (2C), 129.2, 128.1, 126.0, 126.0, 124.2, 123.2, 117.3, 117.2, 114.0, 104.4; HPLC-MS (APCI/ESI): Purity = 95%, t_R = 5.36 min, MS: *m/z* 422.1 $[M+H]^+$.

***2,7,8-trifluoro-1-hydroxy-3-(4-(trifluoromethyl)phenyl)benzo-[4,5]imidazo[1,2-a]pyridine-4-carbonitrile* (4.6)**

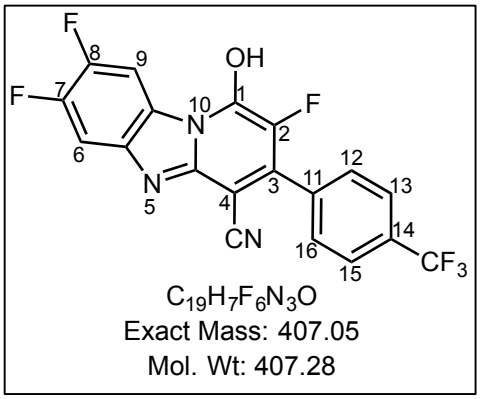

$C_{19}H_7F_6N_3O$
Exact Mass: 407.05
Mol. Wt: 407.28

Obtained from **3.3** (0.460 g, 2.38 mmol, 1.0 equiv.), **2.2** (0.795 g, 2.86 mmol, 1.2 equiv.) and NH_4OAc (0.367 g, 4.76 mmol, 2.0 equiv.) as a dark green solid (0.498 g, 51 %); m.p. 292 - 296 °C; R_f 0.26 (50 % EtOAc-Hex); ^1H NMR (400 MHz, DMSO-d_6) δ 8.45 (dd, J = 8.0, 4.0 Hz, 1H, ArH^9), 7.92 (d, J = 8.1 Hz, 2H, $ArH^{13,15}$), 7.78 (d, J = 8.1 Hz, 2H, $ArH^{12,16}$), 7.57 (dd, J = 8.0, 4,0 Hz, 1H, ArH^6); ^{13}C NMR (101 MHz, DMSO-d_6) δ 152.9, 152.6, 150.1, 149.9, 137.2, 136.6, 136.1, 135.9, 130.7, 130.0, 129.7, 125.8, 125.8, 123.2, 118.5, 104.2, 104.0, 103.1, 102.9; HPLC-MS (APCI/ESI): Purity = 99%, t_R = 5.06 min, MS: *m/z* 406.1 $[M-H]^-$.

***7,8-difluoro-1-hydroxy-3-(4-(trifluoromethyl)phenyl)benzo-[4,5]imidazo[1,2-a]pyridine-4-carbonitrile* (4.7)**

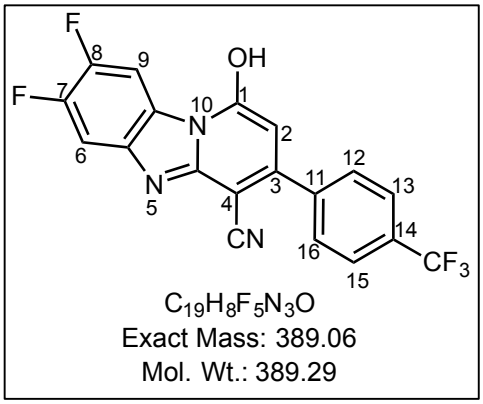

$C_{19}H_8F_5N_3O$
Exact Mass: 389.06
Mol. Wt.: 389.29

Obtained from **3.3** (0.244 g, 1.26 mmol, 1.0 equiv.), ethyl(4-trifluromethyl-benzoyl)acetate (0.30 mL, 1.52 mmol, 1.2 equiv.) and NH_4OAc (0.194 g, 2.52 mmol, 2.0 equiv.) as a grey/brown solid (0.306 g, 62 %); m.p. 289 - 294 °C; R_f 0.61 (70 % EtOAc-Hex); ^1H NMR (400 MHz, DMSO-d_6) δ 8.52 (dd, J = 10.0, 7.0 Hz, 1H ArH^9), 7.91 (d, J = 8.1 Hz, 2H, $ArH^{13,15}$), 7.84 (d, J = 8.1 Hz, 2H, $ArH^{12,16}$), 7.63 (dd, J = 10.0, 7.0 Hz, 1H ArH^6), 6.11 (s, 1H, ArH^2). ^{13}C NMR (101 MHz, DMSO- d_6) δ 158.1, 151.8, 149.1, 141.3, 130.5, 130.2, 129.6, 129.1, 129.0, 126.1, 126.1, 123.7, 123.6, 116.7, 105.7, 105.5, 105.1, 101.2, 101.0; HPLC-MS (APCI/ESI): Purity = 99%, t_R = 5.05 min, MS: *m/z* 388.0 $[M-H]^-$.

***2-benzyl-1-hydroxy-3-methylbenzo[4,5]imidazo[1,2-a]pyridine-4-carbonitrile* (4.8)**

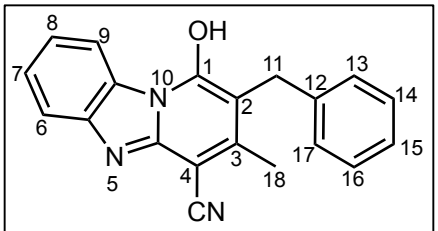

$C_{20}H_{15}N_3O$
Exact Mass: 313.12
Mol. Wt: 313.36

Obtained from **2.3** (0.262 g, 1.19 mmol, 1.2 equiv.), **3.1** (0.156 g, 0.99 mmol, 1.0 equiv.) and NH_4OAc (0.153 g, 1.98 mmol, 2.0 equiv.) as a brown solid (0.243 g, 78 %); m.p. 245 - 249 °C R_f 0.58 (50 % EtOAc-Hex); ^1H NMR (400 MHz, DMSO-d_6) δ 13.45 (s, 1H, OH), 8.60 (dt, *J* = 8.1, 1.0 Hz, 1H, ArH^9), 7.54 – 7.49 (m, 2H, $ArH^{6,7}$), 7.35 (ddd, *J* = 8.0, 8.0, 4.0 Hz 1H, ArH^8), 7.27 – 7.21 (m, 4H, $ArH^{13,14,16,17}$), 7.17 – 7.12 (m, 1H, ArH^{15}), 3.97 (s, 2H, H^{11}), 2.35 (s, 3H, H^{18}); ^{13}C NMR (101 MHz, DMSO-d_6) δ 159.2, 147.5, 146.0, 140.9, 132.3, 128.7 (2C), 128.4 (2C), 128.3, 127.0, 126.2, 122.6, 117.3, 116.7, 114.9, 111.7 (2C), 31.6, 18.8; HPLC-MS (APCI/ESI): Purity = 99%, t_R = 4.43 min, MS: *m/z* 314.1 $[M+H]^+$.

***2-(4-chlorobenzyl)-1-hydroxy-3-methylbenzo[4,5]imidazo[1,2-a]pyridine-4-carbonitrile* (4.9)**

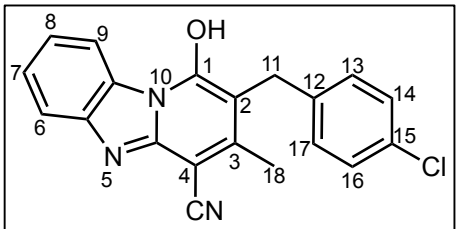

$C_{20}H_{14}ClN_3O$
Exact Mass: 347.08
Mol. Wt: 347.80

Obtained from **2.3** (2.339 g, 9.18 mmol, 1.2 equiv.), **3.1** (1.202 g, 7.65 mmol, 1.0 equiv.) and NH_4OAc (1.180 g, 15.31 mmol, 2.0 equiv.) as a light brown solid (1.904 g, 72 %); m.p. 109 - 114 °C; R_f 0.78 (50 % EtOAc-Hex); ^1H NMR (400 MHz, DMSO-d_6) δ 8.58 (ddd, *J* = 8.1, 1.2, 0.7 Hz, 1H, ArH^9), 7.54 – 7.44 (m, 2H, $ArH^{6,7}$), 7.30 – 7.24 (m, 5H, $ArH^{8,13,14,16,17}$), 3.95 (s, 2H, H^{11}), 2.34 (s, 3H, H^{18}); ^{13}C NMR (101 MHz, DMSO-d_6) δ 172.4, 159.6, 147.6, 147.4, 140.5, 135.2, 132.3, 130.7, 130.3, 128.9, 128.6, 126.4, 126.0, 121.6, 118.2, 116.5, 112.7, 112.5, 31.1, 18.8; HPLC-MS (APCI/ESI): Purity = 83%, t_R = 5.33 min, MS: *m/z* 348.0 $[M+H]^+$.

***2-(3-chlorobenzyl)-1-hydroxy-3-methylbenzo[4,5]imidazo[1,2-a]pyridine-4-carbonitrile* (4.10)**

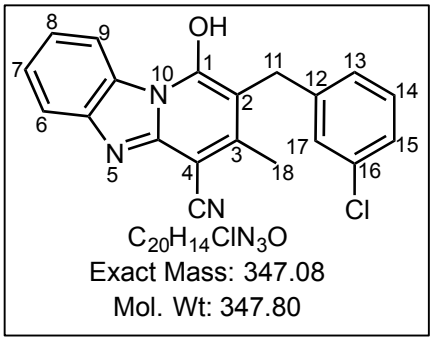

Obtained from **2.3** (3.179 g, 12.48 mmol, 1.2 equiv.), **3.1** (1.634 g, 10.40 mmol, 1.0 equiv.) and NH_4OAc (1.603 g, 20.80 mmol, 2.0 equiv.) as a brown solid (3.294 g, 91 %); m.p. 211 - 215 °C; R_f 0.60 (50 % EtOAc-Hex); ^1H NMR (400 MHz, DMSO-d_6) δ 8.59 (dt, J = 8.1, 1.0 Hz, 1H, ArH^9), 7.54 – 7.45 (m, 2H, $ArH^{6,7}$), 7.31 – 7.26 (m, 3H, $ArH^{8,15,17}$), 7.23 - 7.16 (m, 2H, $H^{13,14}$), 3.98 (s, 2H, H^{11}), 2.35 (s, 3H, H^{18}); ^{13}C NMR (101 MHz, DMSO-d_6) δ 172.4, 159.6, 147.8, 147.3, 144.1, 133.4, 130.5 (2C), 128.8, 128.2, 127.2, 126.4, 126.2, 121.7, 118.1, 116.5, 112.6, 112.3, 31.4, 18.8; HPLC-MS (APCI/ESI): Purity = 87%, t_R = 4.88 min, MS: *m/z* 348.0 $[M+H]^+$.

***2-(2-chlorobenzyl)-1-hydroxy-3-methylbenzo[4,5]imidazo[1,2-a]pyridine-4-carbonitrile* (4.11)**

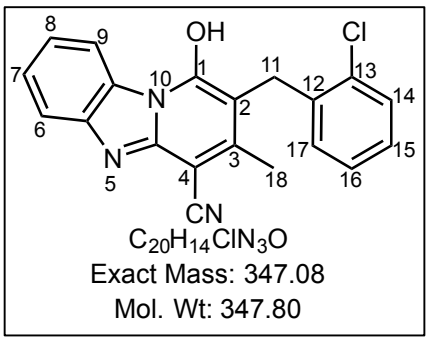

Obtained from **2.3** (2.240 g, 8.79 mmol, 1.2 equiv.), **3.1** (1.152 g, 7.33 mmol, 1.0 equiv.) and NH_4OAc (1.130 g, 14.66 mmol, 2.0 equiv.) as a grey/brown solid (2.176 g, 85 %); m.p. 319 - 325 °C; R_f 0.80 (50 % EtOAc-Hex); ^1H NMR (400 MHz, DMSO-d_6) δ 13.34 (s, 1H, OH), 8.59 (d, J = 8.2 Hz, 1H, ArH^9), 7.58 – 7.50 (m, 2H, $ArH^{6,7}$), 7.45 (d, J = 7.8 Hz, 1H, ArH^{14}), 7.38 – 7.33 (m, 1H, ArH^8), 7.23 – 7.13 (m, 2H, $ArH^{15,16}$), 6.97 (d, J = 7.6 Hz, 1H, ArH^{17}), 4.05 (s, 2H, H^{11}), 2.30 (s, 3H, H^{18}); ^{13}C NMR (101 MHz, DMSO-d_6) δ 159.1, 148.4, 147.4, 146.4, 137.7, 133.6, 132.4, 129.5, 129.1, 128.4, 128.0, 127.6, 127.0, 122.7, 117.1, 116.7, 112.8, 111.8, 29.4, 18.6; HPLC-MS (APCI/ESI): Purity = 99%, t_R = 4.82 min, MS: *m/z* 348.0 $[M+H]^+$.

General procedure for the synthesis of the chlorinated intermediates (5.1 – 5.11)

A mixture of the appropriate hydroxy intermediate (1.0 equiv.) and $POCl_3$ (20 equiv.) was heated to 130°C for 2-8 hours. Excess $POCl_3$ was removed by distillation, cold water (20 mL) was added to the brown residue and the mixture was stirred at room temperature for 15 minutes. The mixture was neutralized with saturated sodium bicarbonate solution and filtered. The solid was washed with cold water (4x10 mL), dried *in vacuo* and used without further purification.

1-chloro-2-methyl-3-(4-(trifluoromethyl)phenyl)benzo[4,5]imidazo[1,2-a]pyridine-4-carbonitrile **(5.1)**

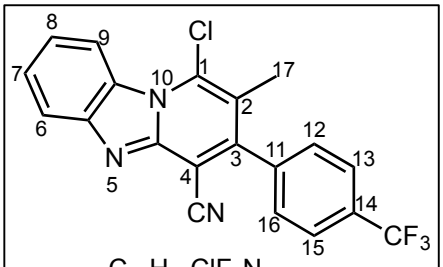

$C_{20}H_{11}ClF_3N_3$
Exact Mass: 385.06
Mol. Wt: 385.77

Obtained from **4.1** (0.312 g, 0.85 mmol, 1.0 equiv.) and $POCl_3$ (1.58 mL, 17.0 mmol, 20 equiv.) as a yellow/brown solid (0.300 g, 92 %); m.p. 289 - 291°C; R_f 0.59 (30 % EtOAc-Hex); ^{1}H NMR (400 MHz, DMSO-d_6) δ 8.78 (d, J = 8.0 Hz, 1H,H^9), 8.02 – 7.98 (m, 3H, $H^{6,13,15}$), 7.78 (d, J = 8.0 Hz, 2H, $ArH^{12,16}$), 7.69 (t, J = 7.7 Hz, 1H, ArH^7), 7.53 (t, J = 8.0 Hz, 1H, ArH^8), 2.20 (s, 3H, H^{17}); ^{13}C NMR (101 MHz, DMSO-d_6) δ 150.6, 146.2, 145.0, 140.4, 133.8, 130.3, 130.2, 127.3, 126.3 (2C), 126.2, 122.8 (2C), 120.3, 118.1, 116.5, 114.9 (2C), 99.9, 16.9; HPLC-MS (APCI/ESI): Purity = 95%, t_R = 4.44 min; MS: *m/z* 386.1 $[M+H]^+$.

1-chloro-2-fluoro-3-(4-(trifluoromethyl)phenyl)benzo[4,5]imidazo[1,2-a]pyridine-4-carbonitrile **(5.2)**

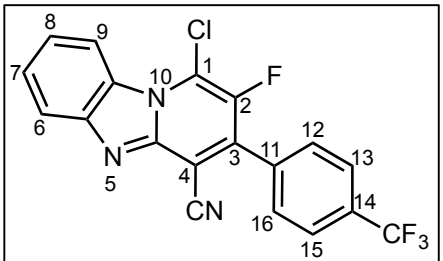

$C_{19}H_8ClF_4N_3$
Exact Mass: 389.03
Mol. Wt: 389.74

Obtained from **4.2** (0.730 g, 1.88 mmol, 1.0 equiv.) and $POCl_3$ (5.25 mL, 56.3 mmol, 30 equiv.) as a yellow/brown solid (0.642 g, 84 %); m.p. 281 - 285 °C; R_f 0.58 (30 % EtOAc-Hex); ^{1}H NMR (400 MHz, DMSO-d_6) δ 8.73 (dt, J = 8.6, 1.0 Hz, 1H, ArH^9), 8.08 – 8.02

(m, 3H, ArH^{6,13,15}), 7.96 (d, *J* = 8.0 Hz, 2H, ArH^{12,16}), 7.73 (ddd, *J* = 8.6, 7.1, 1.0 Hz, 1H, ArH^{7}), 7.58 (ddd, *J* = 8.6, 7.1, 1.0 Hz, 1H, ArH^{8}); ^{13}C NMR (101 MHz, DMSO-d_6) δ 145.6, 145.5, 144.9, 144.7, 143.3, 132.4, 131.1, 130.6, 127.8, 127.6, 126.3, 126.2, 126.0, 126.0, 123.4, 123.1, 116.7, 115.8, 112.2; ^{19}F NMR (377 MHz, DMSO-d_6) δ -61.30, -155.54; HPLC-MS (APCI/ESI): Purity = >99%, t_R = 5.13 min, MS: *m/z* 390.1 $[M+H]^+$.

1-Chloro-3-(4-(trifluoromethyl)phenyl)benzo[4,5]imidazo[1,2-*a*]pyridine-4-carbonitrile (5.3)

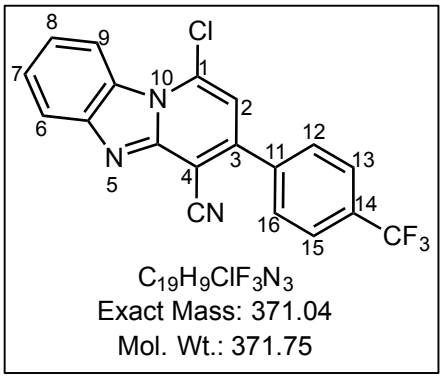

$C_{19}H_9ClF_3N_3$
Exact Mass: 371.04
Mol. Wt.: 371.75

Obtained from **4.3** (0.500 g, 1.42 mmol, 1.0 equiv.) and $POCl_3$ (2.63 mL, 28.3 mmol, 20 equiv.) as a yellow solid (0.481 g, 91%); R_f 0.53 (40 % EtOAc-Hex); M. pt. 247-248^{o}C; ^{1}H NMR (400 MHz, DMSO-d_6) δ 8.66 (d, *J* = 8.4 Hz, 1H, ArH^{9}), 8.01 (m, 5H, ArH ^{6,12,13,15,16}), 7.67 (t, *J* = 8.4 Hz, 1H, ArH^{7}), 7.58 (s, 1H, H^{2}), 7.51 (t, *J* = 8.4 Hz, 1H, ArH^{8}); ^{13}C NMR (100 MHz, DMSO-d_6) δ 148.2, 147.7, 144.9, 139.4, 135.2, 131.0, 130.4, 129.7, 127.5, 126.3 (2C), 123.1 (2C), 120.7, 116.3, 115.4, 112.8 (2C) and 97.5; MS: *m/z* 372:374 (3:1) $[M+H]^+$.

***1,7,8-trichloro-2-fluoro-3-(4-(trifluoromethyl)phenyl)benzo[4,5]imidazo-[1,2-a]pyridine-4-carbonitrile* (5.4)**

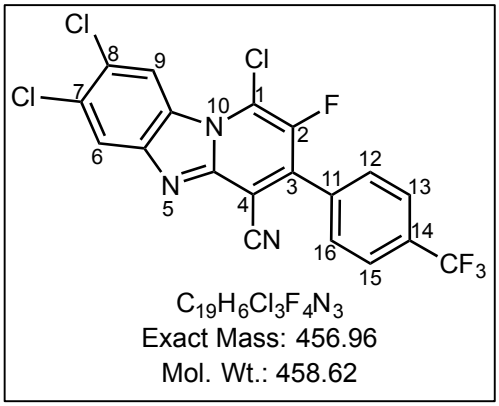

$C_{19}H_6Cl_3F_4N_3$
Exact Mass: 456.96
Mol. Wt.: 458.62

Obtained from **4.4** (0.740 g, 1.68 mmol, 1.0 equiv.) and $POCl_3$ (3.13 mL, 33.62 mmol, 20 equiv.) as a green solid (0.617 g, 80 %); m.p. 279 - 284 °C; R_f 0.89 (30 % EtOAc-Hex); ^{1}H NMR (400 MHz, DMSO-d_6) δ 8.92 (s, 1H, ArH^{9}), 8.41 (s, 1H, ArH^{6}), 8.08 (d, *J* = 8.0 Hz, 2H, ArH^{13,15}), 7.97 (d, *J* = 8.0 Hz, 2H, ArH^{12,16}); ^{13}C NMR (101 MHz, DMSO-d_6) δ 146.5, 146.1, 144.6, 143.7, 140.8, 140.6, 134.0, 131.1, 130.6, 130.4, 129.8, 126.5, 125.7, 121.7, 117.5, 117.0,

114.1, 113.7, 99.1; HPLC-MS (APCI/ESI): Purity = 99%, t_R = 5.51 min, MS: *m/z* 460.0 $[M+H]^+$.

1,7,8-Trichloro-3-(4-(trifluoromethyl)phenyl)benzo[4,5]imidazo[1,2-a]pyridine-4-carbonitrile (5.5)

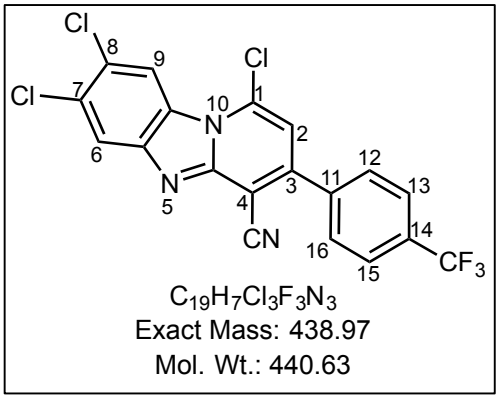

$C_{19}H_7Cl_3F_3N_3$
Exact Mass: 438.97
Mol. Wt.: 440.63

Obtained from **4.5** (0.758 g, 1.80 mmol, 1.0 equiv.) and $POCl_3$ (3.35 mL, 35.90 mmol, 20 equiv.) as a brown solid (0.850 g, 107 %); m.p. 253 - 255 °C; R_f 0.80 (70 % EtOAc-Hex); ^{1}H NMR (400 MHz, DMSO-d_6) δ 8.86 (s, 1H, ArH^9), 8.34 (s, 1H, ArH^6), 8.03 (m, 4H, ArH^{12,13,15,16}), 7.70 (s, 1H, H^2); ^{13}C NMR (150 MHz, DMSO-d_6) δ 149.5, 149.4, 144.3, 139.1, 135.4, 134.7, 130.9, 130.4, 130.2, 128.9, 126.4 (2C), 125.2, 125.1, 123.4, 121.2, 117.5, 115.0, 113.6; HPLC-MS (APCI/ESI): Purity = 99%, t_R = 5.53 min, MS: *m/z* 440.0 $[M+H]^+$.

1-chloro-2,7,8-trifluoro-3-(4-(trifluoromethyl)phenyl)benzo[4,5]imidazo-[1,2-a]pyridine-4-carbonitrile (5.6)

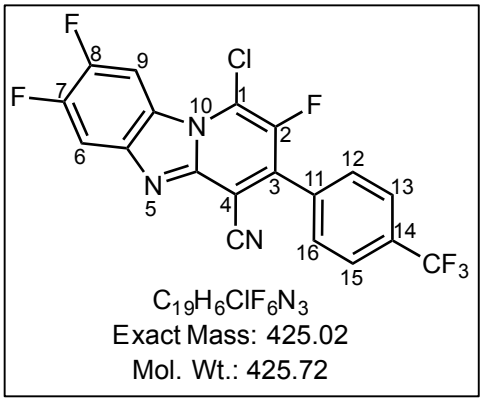

$C_{19}H_6ClF_6N_3$
Exact Mass: 425.02
Mol. Wt.: 425.72

Obtained from **4.6** (0.850 g, 2.09 mmol, 1.0 equiv.) and $POCl_3$ (3.89 mL, 41.70 mmol, 20 equiv.) as a green/brown solid (1.2208 g, 137 %); m.p. 253 - 260 °C; R_f 0.66 (50 % EtOAc-Hex); ^{1}H NMR (400 MHz, DMSO-d_6) δ 8.53 (dd, *J* = 10.0, 7.0 Hz, 1H, ArH^9), 7.98 (d, *J* = 8.3 Hz, 2H, ArH1^{3,15}), 7.80 (d, *J* = 8.3 Hz, 2H, ArH^{12,16}), 7.67 (dd, *J* = 10.0, 7.0 Hz, 1H, ArH^6); ^{13}C NMR (101 MHz, DMSO-d_6) δ 152.1, 151.8, 145.6, 139.6, 137.3, 135.5, 135.1, 134.9, 131.1, 130.6 (2C), 126.2, 126.1, 123.1, 115.9, 105.8, 105.5, 101.3, 101.1; HPLC-MS (APCI/ESI): Purity = 95%, t_R = 5.19 min, MS: *m/z* 426.0 $[M+H]^+$.

***1-chloro-7,8-difluoro-3-(4-(trifluoromethyl)phenyl)benzo[4,5]imidazo[1,2-a]pyridine-4-carbonitrile* (5.7)**

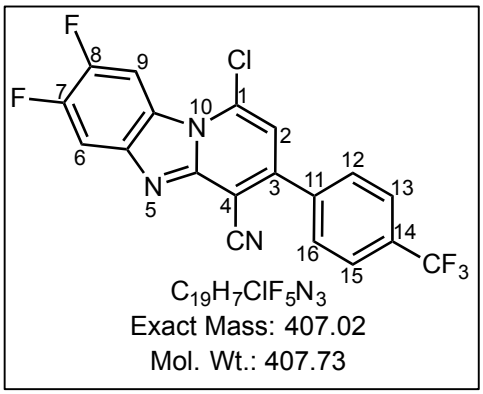

$C_{19}H_7ClF_5N_3$
Exact Mass: 407.02
Mol. Wt.: 407.73

Obtained from **4.7** (0.766 g, 1.97 mmol, 1.0 equiv.) and $POCl_3$ (3.67 mL, 39.40 mmol, 20 equiv.) as a brown solid (0.700 g, 87 %); m.p. 237 - 242 °C; R_f 0.77 (70 % EtOAc-Hex); ^{1}H NMR (400 MHz, DMSO-d_6) δ 8.74 (dd, J = 11.0, 7.6 Hz, 1H, ArH^9), 8.13 (dd, J = 11.0, 7.6 Hz, 1H, ArH^6), 8.02 (s, 4H, ArH^{12,13,15,16}), 7.64 (s, 1H, ArH^2); ^{13}C NMR (150 MHz, DMSO-d_6) δ 148.5, 141.2, 141.1, 139.3, 134.8, 130.4 (2C), 126.4, 126.4, 125.8, 125.1, 125.0, 115.1, 113.3, 107.4, 107.2, 105.0, 104.8, 97.6; HPLC-MS (APCI/ESI): Purity = 96%, t_R = 5.19 min, MS: *m/z* 408.0 $[M+H]^+$.

***2-benzyl-1-chloro-3-methylbenzo[4,5]imidazo[1,2-a]pyridine-4-carbonitrile* (5.8)**

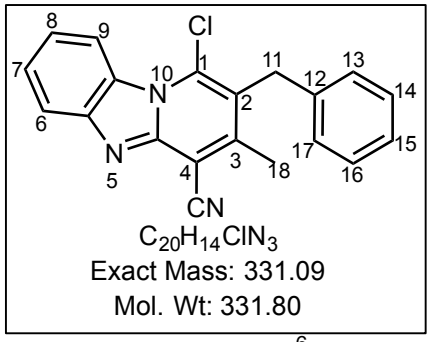

$C_{20}H_{14}ClN_3$
Exact Mass: 331.09
Mol. Wt: 331.80

Obtained from **4.8** (0.297 g, 0.95 mmol, 1.0 equiv.) and $POCl_3$ (2.65 mL, 28.4 mmol, 30 equiv.) as a green/brown solid (0.328 g, 104 %); m.p. 167 - 171 °C; R_f 0.63 (30 % EtOAc-Hex); ^{1}H NMR (400 MHz, DMSO-d_6) δ 8.70 (dt, *J* = 8.6, 0.9 Hz, 1H, ArH^9), 7.95 (dt, *J* = 8.6, 0.9 Hz, 1H, ArH^6), 7.64 (ddd, *J* = 8.6, 7.1, 0.9 Hz, 1H, ArH^7), 7.46 (ddd, *J* = 8.6, 7.1, 0.9 Hz, 1H, ArH^8), 7.33 – 7.29 (m, 2H, ArH^{13,17}), 7.25 – 7.21 (m, 3H, ArH^{14,15,16}), 4.34 (s, 2H, H^{11}), 2.57 (s, 3H, H^{18}); ^{13}C NMR (101 MHz, DMSO-d_6) δ 150.2, 146.7, 144.6, 137.7, 134.7, 130.6, 129.1 (3C), 128.2, 127.0 (2C), 122.4, 121.3, 112.0, 116.6, 115.3, 99.9, 34.6, 20.0; HPLC-MS (APCI/ESI): Purity = 95%, t_R = 4.71 min, MS: *m/z* 332.1 $[M+H]^+$.

***1-chloro-2-(4-chlorobenzyl)-3-methylbenzo[4,5]imidazo[1,2-a]pyridine-4-carbonitrile* (5.9)**

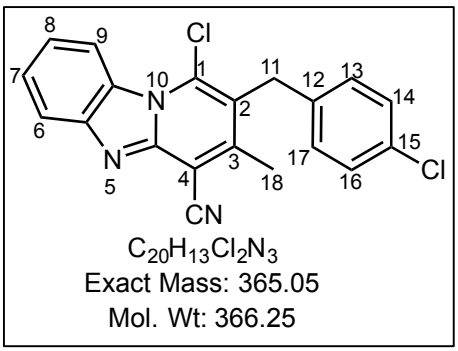

$C_{20}H_{13}Cl_2N_3$
Exact Mass: 365.05
Mol. Wt: 366.25

Obtained from **4.9** (0.348 g, 5.30 mmol, 1.0 equiv.) and $POCl_3$ (14.8 mL, 159.1 mmol, 30 equiv.) as a green/brown solid (2.107 g, 109 %); m.p. 202 - 208 °C; R_f 0.41 (30 % EtOAc-Hex); ^{1}H NMR (400 MHz, DMSO-d_6) δ 8.72 (dt, J = 8.5, 0.9 Hz, 1H, ArH^9), 7.98 – 7.93 (m, 1H, ArH^6), 7.68 – 7.64 (m, 1H, ArH^7), 7.50 – 7.46 (m, 1H, ArH^8), 7.37 – 7.34 (m, 2H, ArH^{14,16}), 7.25 (d, J = 8.4 Hz, 2H, ArH^{13,17}), 4.33 (s, 2H, H^{11}), 2.55 (s, 3H, H^{18}); ^{13}C NMR (101 MHz, DMSO-d_6) δ 158.8, 151.6, 150.3, 144.3, 136.8, 135.6, 135.0, 130.1, 129.1, 128.6, 127.1, 127.0, 122.9, 122.5, 119.8, 116.7, 105.3, 99.6, 33.9, 20.1; HPLC-MS (APCI/ESI): Purity = 86%, t_R = 4.91 min, MS: *m/z* 366.0 $[M+H]^+$.

***1-chloro-2-(3-chlorobenzyl)-3-methylbenzo[4,5]imidazo[1,2-a]pyridine-4-carbonitrile* (5.10)**

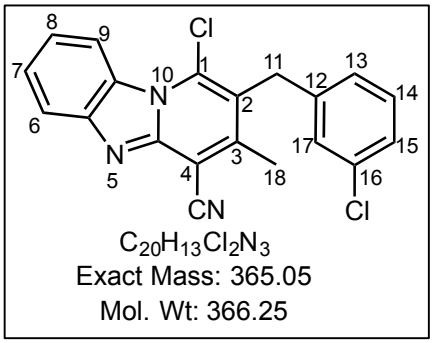

$C_{20}H_{13}Cl_2N_3$
Exact Mass: 365.05
Mol. Wt: 366.25

Obtained from **4.10** (3.000 g, 12.21 mmol, 1.0 equiv.) and $POCl_3$ (22.8 mL, 244.2 mmol, 20 equiv.) as a brown solid (2.987 g, 67 %); m.p. 174 - 180 °C; R_f 0.46 (30 % EtOAc-Hex); ^{1}H NMR (400 MHz, DMSO-d_6) δ 8.69 (dt, J = 8.4, 0.9 Hz, 1H, ArH^9), 7.95 (dt, J = 8.4, 0.9 Hz, 1H, ArH^6), 7.64 (ddd, J = 8.4, 7.2, 0.9 Hz, 1H, ArH^7), 7.46 (ddd, J = 8.4, 7.2, 0.9 Hz, 1H, ArH^8), 7.33 – 7.28 (m, 3H, ArH^{13,15,17}), 7.19 – 7.17 (m, 1H, ArH^{14}), 4.35 (s, 2H, H^{11}), 2.56 (s, 3H, H^{18}); ^{13}C NMR (101 MHz, DMSO-d_6) δ 149.9, 146.8, 144.8, 140.4, 134.9, 134.0, 130.9, 130.6, 128.1, 127.1, 126.9, 126.9, 122.3, 120.4, 120.0, 116.6, 115.3, 100.0, 34.3, 20.0; HPLC-MS (APCI/ESI): Purity = 89%, t_R = 4.94 min, *m/z* 366.0 $[M+H]^+$.

***1-chloro-2-(2-chlorobenzyl)-3-methylbenzo[4,5]imidazo[1,2-a]pyridine-4-carbonitrile* (5.11)**

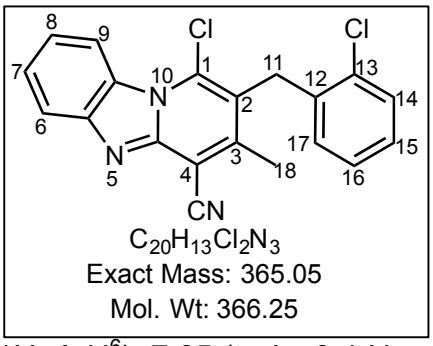

$C_{20}H_{13}Cl_2N_3$
Exact Mass: 365.05
Mol. Wt: 366.25

Obtained from **4.11** (0.933 g, 2.68 mmol, 1.0 equiv.) and $POCl_3$ (5.0 mL, 53.64 mmol, 20 equiv.) as a yellow/brown solid (0.985 g, 100 %); m.p. 268 - 271 °C; R_f 0.67 (30 % EtOAc-Hex); ^{1}H NMR (400 MHz, DMSO-d_6) δ 8.69 (d, J = 8.4 Hz, 1H, ArH^9), 7.97 (d, J = 8.4 Hz, 1H, ArH^6), 7.65 (t, J = 8.4 Hz, 1H, ArH^7), 7.54 (dd, J = 8.0, 1.4 Hz, 1H, ArH^{14}), 7.47 (ddd, J = 8.4, 7.0, 1.2 Hz, 1H, ArH^8), 7.30 (t, J = 7.0 Hz, 1H, ArH^{15}), 7.20 (t, J = 7.0 Hz, 1H, ArH^{16}), 6.97 (d, J = 7.0 Hz, 1H, ArH^{17}), 4.36 (s, 2H, H^{11}), 2.54 (s, 3H, H^{18}); ^{13}C NMR (101 MHz, DMSO-d_6) δ 149.9, 146.9, 144.9, 140.7, 135.0, 133.6, 130.6, 129.9, 129.0, 128.9, 128.1, 127.0, 122.4, 120.1, 120.0, 116.5, 115.2, 100.2, 32.7, 19.7; HPLC-MS (APCI/ESI): Purity = 97%, t_R = 4.83 min, MS: *m/z* 366.0 $[M+H]^+$.

General procedure for the synthesis of target compounds (6.1 – 6.5; 6.7 – 6.10; 6.12 - 6.15)

The appropriate amine (2.0 equiv.) was added to a stirring solution of the appropriate chlorinated intermediate (1.0 equiv.) and triethylamine (2.0 equiv.) in THF (4.0 mL). The solution was heated in the microwave at 80°C for 20-40 minutes. The solvent was removed *in vacuo* and the residue was purified by flash column chromatography (MeOH-DCM). The resulting solid was recrystallized from acetone.

***1-((2-(ethylamino)ethyl)amino)-2-methyl-3-(4-(trifluoromethyl)phenyl)-benzo[4,5]imidazo[1,2-a]pyridine-4-carbonitrile* (6.1)**

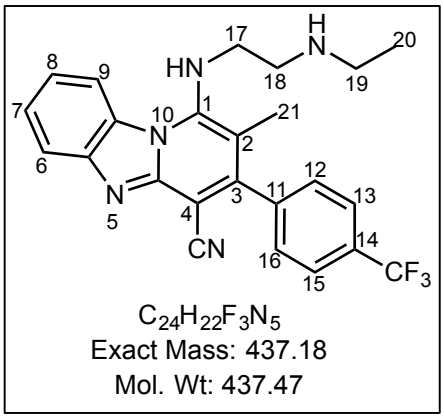

$C_{24}H_{22}F_3N_5$
Exact Mass: 437.18
Mol. Wt: 437.47

Obtained from **5.1** (0.278 g, 0.72 mmol, 1.0 equiv.), *N*-ethylethylenediamine (0.376 mL, 1.44 mmol, 2.0 equiv.) and triethylamine (0.20 mL, 1.44 mmol, 2.0 equiv.) as a yellow/orange solid (0.204 g, 65 %); m.p. 174 – 177 °C; R_f 0.31 (5 % MeOH-DCM); ^{1}H NMR (400 MHz, $CDCl_3$) δ 8.35 (d, *J* = 8.4 Hz, 1H, ArH^9), 7.98 (d, *J* = 8.2 Hz, 1H, ArH^6), 7.79 (d, *J* = 8.1 Hz, 2H, $ArH^{13,15}$), 7.57 – 7.50 (m, 3H, $ArH^{7,12,16}$), 7.34 (t, *J* = 8.4 Hz, 1H, ArH^8), 6.02 (s, 1H, NH), 3.50 (t, *J* = 5.4 2H, H^{17}), 3.04 – 2.98 (m, 2H, H^{18}), 2.80 (q, *J* = 7.1 Hz, 2H, H^{19}), 2.15 (s, 3H, H^{21}), 1.22 (t, *J* = 7.1 Hz, 3H, H^{20}); ^{13}C NMR (101 MHz, $CDCl_3$) δ 151.8, 148.3, 147.6, 145.4, 140.5, 131.4, 131.1, 129.3, 128.7, 126.2, 125.8, 125.8, 122.5, 121.1, 119.9, 115.8, 115.0, 104.4, 92.3, 48.5, 46.5, 43.6, 15.3, 15.0; HPLC-MS (APCI/ESI): Purity = 96%, t_R = 3.53 min, MS: *m/z* 438.2 $[M+H]^+$.

***1-((2-(ethylamino)ethyl)amino)-2-fluoro-3-(4-(trifluoromethyl)phenyl)-benzo[4,5]imidazo[1,2-a]pyridine-4-carbonitrile* (6.2)**

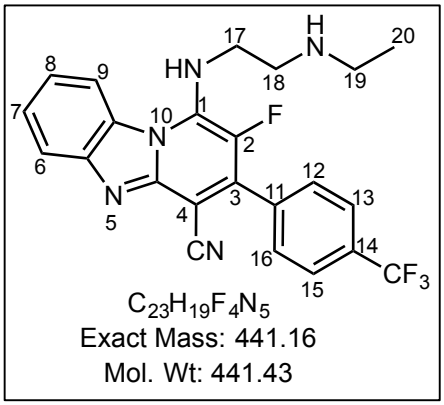

$C_{23}H_{19}F_4N_5$
Exact Mass: 441.16
Mol. Wt: 441.43

Obtained from **5.2** (0.240 g, 0.59 mmol, 1.0 equiv.), N-ethylethylenediamine (0.29 mL, 1.18 mmol, 2.0 equiv.) and triethylamine (0.16 mL, 1.18 mmol, 2.0 equiv.) as a yellow solid (0.050 g, 19 %); m.p. 281 - 286 °C; R_f 0.17 (8 % MeOH-DCM); ^{1}H NMR (400 MHz, DMSO-d_6) δ 7.74 (d, *J* = 8.2 Hz, 2H, $H^{6,9}$), 7.49 (d, *J* = 8.1 Hz, 4H, $H^{12,13,15,16}$), 7.19 – 7.14 (m, 2H, $H^{7,8}$), 4.52 (t, *J* = 9.5 Hz, 2H, H^{17}), 4.12 (t, *J* = 9.5 Hz, 2H, H^{18}), 3.65 (q, *J* = 7.2 Hz, 2H, H^{19}), 1.27 (t, *J* = 7.2 Hz, 3H, H^{20}); ^{13}C NMR (101 MHz, MeOD) δ 148.3, 144.9, 143.8, 143.7, 143.6, 143.4, 134.3, 134.0, 131.8,

131.4, 131.1, 129.9, 125.1, 125.0, 122.9, 122.6, 122.4, 110.9, 96.1, 49.1 42.5, 42.4, 11.9; ^{19}F NMR (377 MHz, MeOD) δ -64.48, -166.23; HPLC-MS (APCI/ESI): Purity = 99%, t_R = 3.75 min, MS: *m/z* 442.1 $[M+H]^+$.

***1-((2-(3-hydroxypyrrolidin-1-yl)ethyl)amino)-2-methyl-3-(4-(trifluoro-methyl)phenyl)benzo[4,5]imidazo[1,2-a]pyridine-4-carbonitrile* (6.3)**

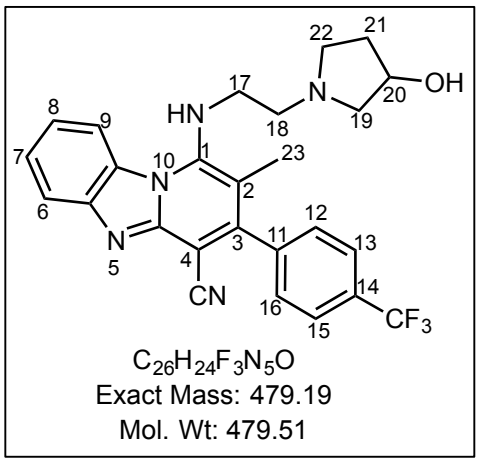

$C_{26}H_{24}F_3N_5O$
Exact Mass: 479.19
Mol. Wt: 479.51

Obtained from **5.1** (0.215 g, 0.56 mmol, 1.0 equiv.), 1-(2-aminoethyl)-3-pyrroldinol (0.109 g, 0.84 mmol, 1.5 equiv.) and triethylamine (0.15 mL, 1.11 mmol, 2.0 equiv.) as an orange/brown solid (0.150 g, 56 %); m.p. 236 – 238 °C; R_f 0.26 (5 % MeOH-DCM); ^{1}H NMR (400 MHz, DMSO-d_6) δ 8.40 (d, *J* = 8.4 Hz, 1H, ArH^9), 7.96 (d, *J* = 7.8 Hz, 2H, ArH^{13,15}), 7.86 (d, *J* = 7.8 Hz, 1H, ArH^6), 7.71 (d, *J* = 7.8 Hz, 2H, ArH^{12,16}), 7.57 (ddd, *J* = 8.4, 7.6, 1.2 Hz, 1H, ArH^7), 7.39 (ddd, *J* = 8.4, 7.6, 1.2 Hz, 1H, ArH^8), 4.71 - 4.64 (m, 1H, H^{20}), 4.10 (s, 1H, NH), 3.48 (t, *J* = 5.7 Hz, 2H, H^{17}), 2.66 (t, *J* = 5.7 Hz, 2H, H^{18}), 2.57 – 2.48 (m, 2H, H^{21}), 2.29 – 2.23 (m, 2H, H^{22}), 2.07 (s, 3H, H^{23}), 1.92 - 182 (m, 1H, H^{19}), 1.55 – 1.43 (m, 1H, H^{19}); ^{13}C NMR (101 MHz, DMSO-d_6) δ 152.0, 149.5, 148.0, 145.3, 141.8, 130.2, 130.0, 129.7, 129.0, 126.3, 126.1, 126.1, 123.2, 121.1, 119.1, 116.8, 116.3, 105.8, 90.1, 62.5, 56.1, 55.3, 52.3, 45.8, 34.9, 15.2; HPLC-MS (APCI/ESI): Purity = 99%, t_R = 3.56 min, MS: *m/z* 480.2 $[M+H]^+$.

***2-fluoro-1-((2-(3-hydroxypyrrolidin-1-yl)ethyl)amino)-3-(4-(trifluoromethyl)phenyl)benzo[4,5]imidazo[1,2-a]pyridine-4-carbonitrile* (6.4)**

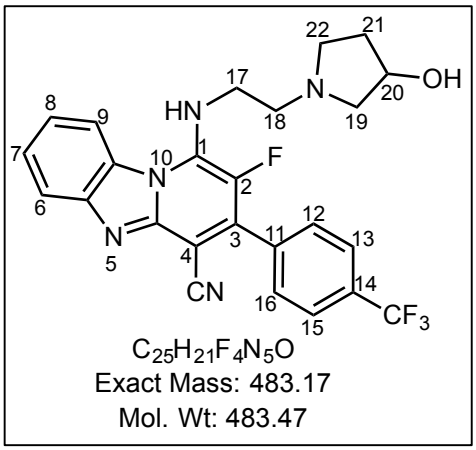

$C_{25}H_{21}F_4N_5O$
Exact Mass: 483.17
Mol. Wt: 483.47

Obtained from **5.2** (0.614 g, 1.50 mmol, 1.0 equiv.), 1-(2-aminoethyl)-3-pyrroldinol (0.294 g, 2.26 mmol, 1.5 equiv.) and triethylamine (0.42 mL, 3.00 mmol, 2.0 equiv.) as a yellow solid (0.323 g, 44 %); m.p. 265 - 267 °C; R_f 0.34 (5 % MeOH-DCM); ^{1}H NMR (400 MHz, DMSO-d_6) δ 8.54 (d, *J* = 8.4 Hz, 1H, ArH^9), 7.96 (d, *J* = 8.0 Hz, 2H, ArH^{13,15}), 7.86 (d, *J* = 8.0 Hz, 2H, ArH$^{12, 16}$), 7.82 (d, *J* = 8.4 Hz, 1H, ArH^6), 7.55 (t, *J* = 8.4 Hz, 1H, ArH^7), 7.34 (t, *J* = 8.4 Hz, 1H, ArH^8), 4.35 – 4.25 (m, 1H, H^{20}), 3.92 – 3.82 (m, 2H, H^{17}), 3.01 – 2.95 (m, 2H, H^{18}), 2.94 – 2.89 (m, 2H, H^{21}), 2.72 – 2.66 (m, 2H, H^{22}), 2.08 – 2.02 (m, 1H, H^{19}), 1.74 – 1.65 (m, 1H, H^{19}). ^{13}C NMR (101 MHz, DMSO-d_6) δ 147.2, 145.7, 141.3, 141.1, 136.5, 133.1, 130.9, 130.2, 130.1, 126.2, 125.9, 125.9, 123.2 120.7, 118.7, 117.2, 117.2, 115.5, 62.5, 55.4, 55.4, 52.4, 44.3, 44.2, 34.7; HPLC-MS (APCI/ESI): Purity = 99%, t_R = 3.51 min, MS: *m/z* 484.2 $[M+H]^+$.

***1-((2-(3-hydroxypyrrolidin-1-yl)ethyl)amino)-3-(4-(trifluoromethyl)phenyl)-benzo[4,5]imidazo[1,2-a]pyridine-4-carbonitrile* (6.5)**

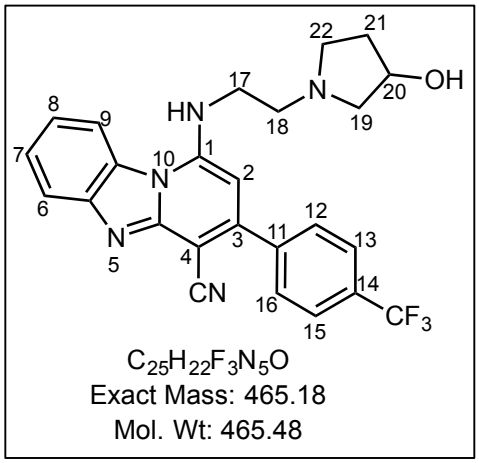

$C_{25}H_{22}F_3N_5O$
Exact Mass: 465.18
Mol. Wt: 465.48

Obtained from **5.3** (0.300 g, 0.81 mmol, 1.0 equiv.), 1-(2-aminoethyl)-3-pyrroldinol (0.158 g, 1.21 mmol, 1.5 equiv.) and triethylamine (0.20 mL, 1.61 mmol, 2.0 equiv.) as a yellow solid (0.122 g, 32 %); m.p. 267 - 269 °C; R_f 0.24 (5 % MeOH-DCM); ^{1}H NMR (400 MHz, DMSO-d_6) δ 8.43 (d, *J* = 8.4 Hz, 1H, ArH^9), 8.00 – 7.93 (m, 4H, ArH^{12,13,15,16}), 7.89 – 7.86 (m, 1H,

ArH[6]), 7.60 (ddd, *J* = 8.4, 7.2, 0.9 Hz, 1H, ArH[7]), 7.41 (ddd, *J* = 8.4, 7.2, 0.9 Hz, 1H, ArH[8]), 6.29 (s, 1H, H[2]), 4.71 (s, 1H, NH), 4.37 – 4.28 (m, 1H, H[20]), 3.72 (t, *J* = 6.3 Hz, 2H, H[17]), 3.05 – 3.02 (m, 2H, H[18]), 3.00 – 2.94 (m, 2H, H[21]), 2.79 – 2.68 (m, 2H, H[22]), 2.16 – 2.02 (m, 1H, H[19]), 1.78 – 1.66 (m, 1H, H[19]); ^{13}C NMR (101 MHz, DMSO-d_6) δ 150.6, 149.3, 149.0, 145.4, 141.9, 130.4, 130.1, 128.3, 126.4, 126.1, 126.1, 125.9, 123.2, 121.2, 119.1, 117.6, 115.0, 90.8, 82.8, 62.6, 55.4, 53.3, 52.6, 49.1, 34.7; HPLC-MS (APCI/ESI): Purity = 99%, t_R = 3.38 min, MS: m/z 466.2 $[M+H]^+$.

*7,8-dichloro-1-((2-(ethylamino)ethyl)amino)-2-fluoro-3-(4-(trifluoromethyl)phenyl)benzo[4,5]imidazo[1,2-a]pyridine-4-carbonitrile (***6.7)**

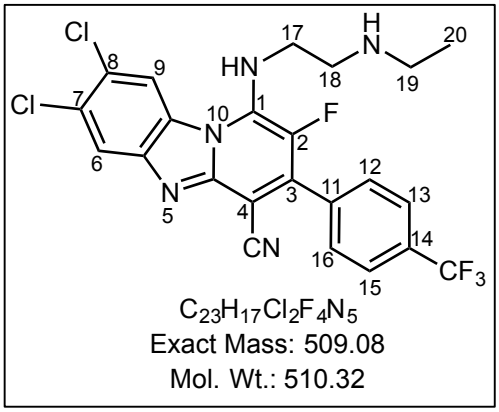

Obtained from **5.4** (0.600 g, 1.31 mmol, 1.0 equiv.), N-ethylethylenediamine (0.28 mL, 2.62 mmol, 2.0 equiv.) and triethylamine (0.36 mL, 2.62 mmol, 2.0 equiv.) as a yellow solid (0.185 g, 28 %); m.p 332 - 338 °C; R_f 0.08 (20 % MeOH-DCM); ^{1}H NMR (400 MHz, DMSO-d_6) δ 7.73 (d, *J* = 7.8 Hz, 4H, ArH[6, 9,15,16]), 7.45 (d, *J* = 7.8 Hz, 2H, ArH[12,16]) , 4.51 (t, *J* = 9.4 Hz, 2H, H[17]), 4.12 (t, *J* = 9.4 Hz, 2H, H[18]), 3.65 (q, *J* = 7.1 Hz, 2H, H[19]), 1.27 (t, *J* = 7.1 Hz, 3H, H[20]); ^{13}C NMR (101 MHz, DMSO-d_6) δ 148.4, 143.7, 143.4, 143.1, 143.0, 134.9, 133.7, 131.5, 130.6, 130.3, 130.0, 129.7 (2C), 125.8, 125.7, 125.0, 123.0, 120.2, 95.9, 48.8, 48.0, 42.6, 13.3; HPLC-MS (APCI/ESI): Purity= 98%, t_R = 4.74 min, MS: *m/z* 510.1 $[M+H]^+$.

***7,8-dichloro-1-((2-(ethylamino)ethyl)amino)-3-(4-(trifluoromethyl)phenyl)-benzo[4,5]imidazo[1,2-a]pyridine-4-carbonitrile* (6.8)**

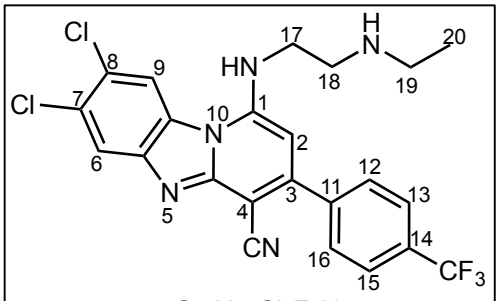

$C_{23}H_{18}Cl_2F_3N_5$
Exact Mass: 491.09
Mol. Wt.: 492.33

Obtained from **5.5** (0.413 g, 0.93 mmol, 1.0 equiv.), N-ethylethylenediamine (0.20 mL, 1.87 mmol, 2.0 equiv.) and triethylamine (0.26 mL, 1.87 mmol, 2.0 equiv.) as a yellow solid (0.112 g, 24 %); m.p 266 - 268 °C; R_f 0.40 (8 % MeOH-DCM); ^{1}H NMR (400 MHz, DMSO-d_6) δ 8.95 (s, 1H, ArH^9), 7.87 (d, *J* = 8.4 Hz, 2H, ArH^{13,15}), 7.84 (d, *J* = 8.4 Hz, 2H, ArH^{12,16}), 7.71 (s, 1H, ArH^6), 5.72 (s, 1H, H^2), 3.58 (t, *J* = 6.2 Hz, 2H, H^{17}), 3.25 (t, *J* = 6.2 Hz, 2H, H^{18}), 3.05 (q, *J* = 7.3 Hz, 2H, H^{19}), 1.24 (t, *J* = 7.3 Hz, 3H, H^{20}); ^{13}C NMR (101 MHz, DMSO-d6) δ 154.3, 152.7, 148.0, 145.5, 143.8, 130.4, 129.6 (2C), 129.5, 129.0, 126.2, 125.7, 125.7, 123.7, 120.6, 119.8, 117.7, 116.6, 91.8, 48.1, 44.8, 42.8, 12.0; HPLC-MS (APCI/ESI): Purity= 99%, t_R = 4.29 min, MS: *m/z* 492.1 $[M+H]^+$.

***1-((2-(ethylamino)ethyl)amino)-2,7,8-trifluoro-3-(4-(trifluoromethyl)-phenyl)benzo[4,5]imidazo[1,2-a]pyridine-4-carbonitrile* (6.9)**

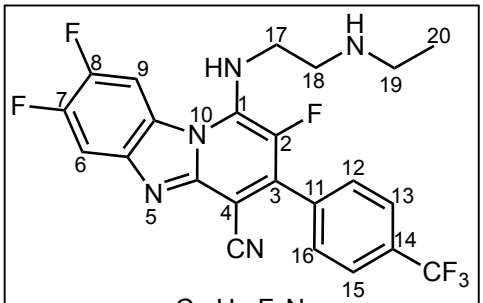

$C_{23}H_{17}F_6N_5$
Exact Mass: 477.14
Mol. Wt: 477.41

Obtained from **5.6** (0.579 g, 1.36 mmol, 1.0 equiv.), N-ethylethylenediamine (0.29 mL, 2.72 mmol, 2.0 equiv.) and triethylamine (0.38 mL, 2.72 mmol, 2.0 equiv.) as a yellow solid (0.033 g, 5 %); m.p 253 - 260 °C; R_f 0.13 (20 % MeOH-DCM); ^{1}H NMR (400 MHz, DMSO-d_6) δ 7.70 (d, *J* = 8.0 Hz, 2H, ArH^{13,15}), 7.42 (d, *J* = 8.0 Hz, 2H, ArH^{12,16}), 7.10 (t, *J* = 9.9 Hz, 2H, ArH^{6,9}), 4.46 (t, 2H, *J* = 9.2, H^{17}), 4.02 (t, *J* = 9.2 Hz, 2H, H^{18}), 3.57 (q, *J* = 7.1 Hz, 2H, H^{19}), 1.23 (t, *J* = 7.1 Hz, 3H, H^{20}); ^{13}C NMR (101 MHz, DMSO-d_6) δ 156.2, 148.9, 144.3, 142.4, 142.3, 138.2, 133.6, 130.5 (2C), 128.9, 128.6, 128.3, 126.1, 125.0 (2C), 123.4, 102.2 (2C), 89.0, 48.4, 47.7, 42.5, 13.1; HPLC-MS (APCI/ESI): Purity= 99%, t_R = 4.14 min, MS: *m/z* 478.1 $[M+H]^+$.

1-((2-(ethylamino)ethyl)amino)-7,8-difluoro-3-(4-(trifluoromethyl)phenyl)-benzo[4,5]imidazo[1,2-a]pyridine-4-carbonitrile **(6.10)**

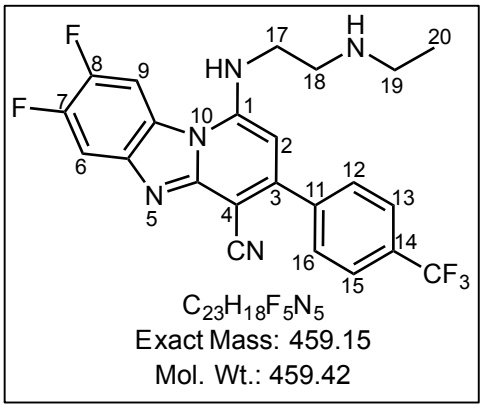

$C_{23}H_{18}F_5N_5$
Exact Mass: 459.15
Mol. Wt.: 459.42

Obtained from **5.7** (0.250 g, 0.61 mmol, 1.0 equiv.), N-ethylethylenediamine (0.13 mL, 1.22 mmol, 2.0 equiv.) and triethylamine (0.17 mL, 1.22 mmol, 2.0 equiv.) as a yellow solid (0.200 g, 71 %); m.p 212 - 215 °C; R_f 0.41 (20 % MeOH-DCM); ^{1}H NMR (400 MHz, DMSO-d_6) δ 8.75 (dd, J = 11.5, 8.0 Hz, 1H, ArH^9), 7.84 (m, 4H, ArH^{12,13,15,16}), 7.52 (dd, J = 11.5, 8.0 Hz, 1H, ArH^6), 5.68 (s, 1H, ArH^2), 3.56 (t, J = 6.1 Hz, 2H, H^{17}), 3.23 (t, J = 6.1 Hz, 2H, H^{18}), 3.01 (q, J = 7.2 Hz, 2H, H^{19}), 1.22 (t, J = 7.2 Hz, 3H, H^{20}); ^{13}C NMR (101 MHz, DMSO-d_6) δ 153.6, 152.2, 147.9, 146.8, 146.7, 143.9, 142.6, 141.6, 141.5, 129.6, 129.5, 125.7, 125.7, 120.5, 105.2, 105.0, 103.2, 103.0, 91.0, 48.2, 44.7, 42.9, 12.4; HPLC-MS (APCI/ESI): Purity= 99%, t_R = 3.84 min, MS: *m/z* 460.2 [M+H]$^+$.

2-benzyl-1-((2-(ethylamino)ethyl)amino)-3-methylbenzo[4,5]imidazo-[1,2a]pyridine-4-carbonitrile **(6.12)**

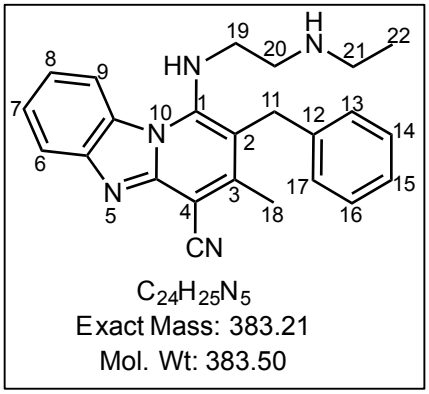

$C_{24}H_{25}N_5$
Exact Mass: 383.21
Mol. Wt: 383.50

Obtained from **5.8** (0.293 g, 0.88 mmol, 1.0 equiv.), N-ethylethylenediamine (0.19 mL, 1.80 mmol, 2.0 equiv.) and triethylamine (0.25 mL, 1.77 mmol, 2.0 equiv.) as an orange solid (0.023 g, 7 %); m.p. 174 – 176 °C; R_f 0.10 (5 % MeOH-DCM); ^{1}H NMR (400 MHz, DMSO-d_6) δ 8.28 (dt, J = 8.4, 1.0 Hz, 1H, ArH^9), 7.83 (dt, J = 8.4, 1.0 Hz, 1H, ArH^6), 7.53 (ddd, J = 8.4, 7.1, 1.1 Hz, 1H, ArH^7), 7.36 – 7.29 (m, 3H, ArH^{8,13,17}), 7.24 – 7.16 (m, 3H, ArH^{14,15,16}), 4.27 (s, 2H, H^{11}), 3.21 (t, J = 5.9 Hz, 2H, H^{19}), 2.66 (t, J = 5.9 Hz, 2H, H^{20}), 2.49 (s, 3H, H^{18}), 2.45 (q, J = 7.1 Hz, 2H, H^{21}), 0.97 (t, J = 7.1 Hz, 3H, H^{22}); ^{13}C NMR (101 MHz, DMSO-d_6) δ 151.0, 149.1, 148.3, 145.1, 139.8, 129.4, 129.1 (3C), 128.1, 126.8 (2C), 126.1, 120.9, 119.0, 117.0, 116.5, 110.3, 49.0, 47.2, 43.5, 32.0,

19.8, 15.7; HPLC-MS (APCI/ESI): Purity = 99%, t_R = 3.22 min, *m/z* 384.2 $[M+H]^+$.

2-(4-chlorobenzyl)-1-((2-(ethylamino)ethyl)amino)-3-methylbenzo-[4,5]imidazo [1,2-a]pyridine-4-carbonitrile **(6.13)**

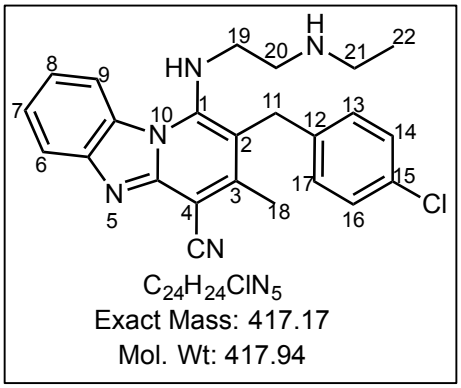

Obtained from **5.9** (0.600 g, 1.64 mmol, 1.0 equiv.), N-ethylethylenediamine (0.35 mL, 3.28 mmol, 2.0 equiv.) and triethylamine (0.45 mL, 3.28 mmol, 2.0 equiv.) as a yellow solid (0.137 g, 20 %); m.p. 189 – 191 °C; R_f 0.33 (5 % MeOH-DCM); ^{1}H NMR (400 MHz, DMSO-d_6) δ 8.30 (d, *J* = 8.4 Hz, 1H, ArH^9), 7.83 (d, *J* = 8.4 Hz, 1H, ArH^6), 7.53 (t, *J* = 8.4 Hz, 1H, ArH^7), 7.37 – 7.32 (m, 3H, ArH^{8,14,16}), 7.20 (d, *J* = 8.4 Hz, 2H, ArH^{13,17}), 4.26 (s, 2H, H^{11}), 3.22 – 3.19 (m, 2H, H^{19}), 2.67 (t, *J* = 5.9 Hz, 2H, H^{20}), 2.49 – 2.43 (m, 5H, H^{18,21}), 0.97 (t, *J* = 7.1 Hz, 3H, H^{22}); ^{13}C NMR (101 MHz, DMSO-d_6) δ 155.9, 150.9, 149.7, 148.1, 138.7, 131.6, 131.2, 129.8, 129.2, 127.4, 122.2, 121.0, 119.1, 115.8, 115.7, 102.5, 101.1, 89.7, 48.7, 45.9, 44.1, 31.2, 18.7, 13.7; HPLC-MS (APCI/ESI): Purity = 99%, t_R = 3.71 min, MS: *m/z* 418.1 $[M+H]^+$.

2-(3-chlorobenzyl)-1-((2-(ethylamino)ethyl)amino)-3-methylbenzo-[4,5]imi dazo[1,2-a]pyridine-4-carbonitrile **(6.14)**

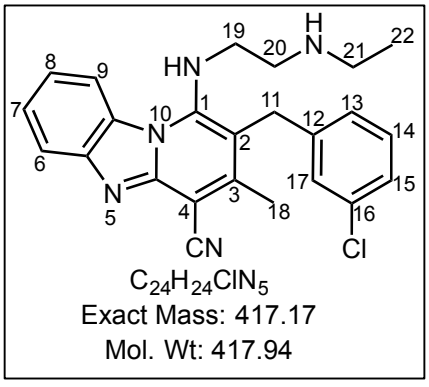

Obtained from **5.10** (0.600 g, 1.64 mmol, 1.0 equiv.), N-ethylethylenediamine (0.35 mL, 3.28 mmol, 2.0 equiv.) and triethylamine (0.46 mL, 3.28 mmol, 2.0 equiv.) as an orange solid (0.212 g, 31 %); m.p. 162 – 166 °C; R_f 0.23 (5 % MeOH-DCM); ^{1}H NMR (400 MHz, DMSO-d_6) δ 8.28 (d, *J* = 8.0 Hz, 1H, ArH^9), 7.83 (d, *J* = 8.0 Hz, 1H, ArH^6), 7.53 (ddd, *J* = 8.0, 7.1, 1.1 Hz, 1H, ArH^7), 7.36 – 7.27 (m, 4H, ArH^{8,14,15,17}), 7.11 (dt, *J* = 7.4, 1.5 Hz, 1H, ArH^{13}), 4.28 (s, 2H, H^{11}), 3.21 (t, *J* = 6.0 Hz, 2H, H^{19}), 2.65 (t, *J* = 6.0 Hz, 2H, H^{20}), 2.47 (s, 3H, H^{18}), 2.44 (q, *J* = 7.5 Hz, 2H, H^{21}), 0.97 (t, *J* = 7.5 Hz, 3H, H^{22}); ^{13}C NMR (101 MHz, DMSO-

d_6) δ 150.8, 149.2, 148.4, 145.2, 142.6, 133.8, 130.9 (2C), 129.5, 128.1, 126.8 (2C), 126.0, 120.8, 119.0, 117.0, 116.5, 109.4, 49.1, 47.2, 43.5, 31.8, 19.8, 15.6; HPLC-MS (APCI/ESI): Purity = 99%, t_R = 3.60 min, MS: *m/z* 418.1 $[M+H]^+$.

***2-(2-chlorobenzyl)-1-((2-(ethylamino)ethyl)amino)-3-methylbenzo-[4,5]imidazo[1,2-a]pyridine-4-carbonitrile* (6.15)**

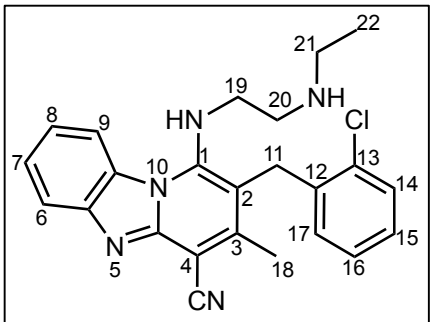

$C_{24}H_{24}ClN_5$
Exact Mass: 417.17
Mol. Wt: 417.94

Obtained from **5.11** (0.450 g, 1.23 mmol, 1.0 equiv.), N-ethylethylenediamine (0.26 mL, 2.46 mmol, 2.0 equiv.) and triethylamine (0.34 mL, 2.46 mmol, 2.0 equiv.) as a yellow solid (0.103 g, 20 %); m.p 200 - 202 °C; R_f 0.44 (5 % MeOH-DCM); ^{1}H NMR (400 MHz, DMSO-d_6) δ 8.33 (d, *J* = 8.4 Hz, 1H, ArH^9), 7.85 (d, *J* = 8.4 Hz, 1H, ArH^6), 7.57 – 7.51 (m, 2H, ArH^{7,14}), 7.36 (ddd, *J* = 8.4, 7.1, 1.2 Hz, 1H, ArH^8), 7.29 (td, *J* = 7.6, 1.7 Hz, 1H, ArH^{15}), 7.21 (td, *J* = 7.6, 1.4 Hz, 1H, ArH^{16}), 6.91 (d, *J* = 7.6 Hz, 1H, ArH^{17}), 4.29 (s, 2H, H^{11}), 3.23 (t, *J* = 5.9 Hz, 2H, H^{19}), 2.69 (t, *J* = 5.9 Hz, 2H, H^{20}), 2.44 (q, *J* = 7.1 Hz, 2H, H^{21}), 2.40 (s, 3H, H^{18}), 0.96 (t, *J* = 7.1 Hz, 3H, H^{22}); ^{13}C NMR (101 MHz, DMSO-d_6) δ 151.0, 149.2, 148.4, 145.3, 137.0, 133.7, 129.8, 129.5, 129.0, 128.6, 128.0, 126.1 (2C), 120.9, 119.1, 116.8, 116.4, 108.4, 49.0, 47.2, 43.4, 30.6, 19.4, 15.5; HPLC-MS (APCI/ESI): Purity= 99%, t_R = 3.49 min, MS: *m/z* 418.1 $[M+H]^+$.

General procedure for the synthesis of target compounds 6.6 and 6.11

4-Amino-*α*-diethylamino-*o*-cresol (2.0 equiv.) was added to a stirring solution of the appropriate chlorinated intermediate (1.0 equiv.) and triethylamine (2.0 equiv.) in THF (4.0 mL) and DMF (0.15 mL). The solution was heated in the microwave at 80°C for 40-60 minutes. The solvent was removed *in vacuo.* The reaction mixture was diluted in DCM, washed with water, brine and dried over anhydrous magnesium sulphate. The solution was concentrated *in vacuo* and the residue was purified using Biotage Isolera One® column chromatography, SiO_2 (25 g cartridge), EtOAc/Hexane, with fractions being

collected at 280nm and monitored at 254nm. Fractions were combined, the solvent was removed *in vacuo* and the resulting solid was further purified by recrystallization from acetone.

***1-((3-((diethylamino)methyl)-4-hydroxyphenyl)amino)-2-fluoro-3-(4-(trifluoromethyl)phenyl)benzo[4,5]imidazo[1,2-a]pyridine-4-carbonitrile* (6.6)**

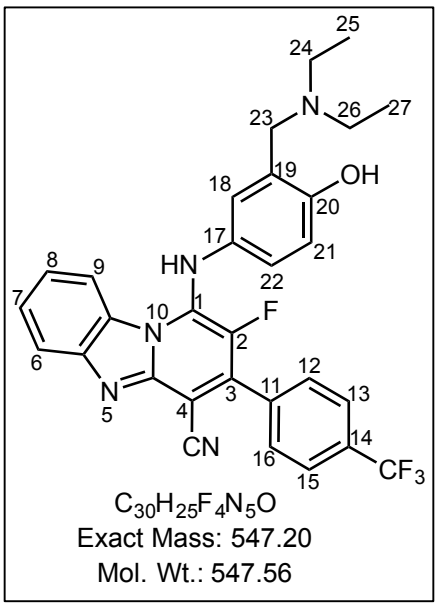

$C_{30}H_{25}F_4N_5O$
Exact Mass: 547.20
Mol. Wt.: 547.56

Obtained from **5.2** (0.198 g, 0.51 mmol, 1.0 equiv.), 4-amino-*α*-diethylamino-*o*-cresol (0.197 g, 1.02 mmol, 2.0 equiv.) and triethylamine (0.14 mL, 1.02 mmol, 2.0 equiv.) as a yellow solid (0.033 g, 11 %); m.p 275 - 280 °C; R_f 0.49 (20 % MeOH-DCM); ^{1}H NMR (400 MHz, DMSO-d_6) δ 8.66 (d, 1H, ArH^9), 7.88 (d, *J* = 8.1 Hz, 2H, ArH^{13,15}), 7.74 (d, *J* = 8.1 Hz, 2H, ArH^{12,16}), 7.59 (d, *J* = 7.8 Hz, 1H, ArH^6), 7.37 (t, *J* = 7.8 Hz, 1H, ArH^7), 7.10 (t, *J* = 7.8 Hz, 1H, ArH^8), 6.92 – 6.81 (m, 2H, ArH^{18,22}), 6.75 (d, *J* = 8.5 Hz, 1H, ArH^{21}), 4.02 (s, 2H, H^{23}), 2.92 (q, *J* = 8.0 Hz, 4H, H^{24,26}), 1.15 (t, *J* = 8.0 Hz, 3H, H^{25,27}); ^{13}C NMR (101 MHz, DMSO-d_6) δ 152.4, 151.4, 149.3, 144.8, 144.7, 142.8, 137.8, 131.5, 130.9, 129.7, 129.4, 126.0, 125.6 (2C), 124.9, 123.5, 123.3, 122.5, 119.8, 118.9, 117.1, 116.2, 115.7, 106.5, 98.3, 52.1, 46.7, 31.1, 29.8, 9.6; HPLC-MS (APCI/ESI): Purity= 99%, t_R = 3.98 min, MS: *m/z* 548.1 $[M+H]^+$.

***1-((3-((diethylamino)methyl)-4-hydroxyphenyl)amino)-7,8-difluoro-3-(4-(trifluoromethyl)phenyl)benzo[4,5]imidazo[1,2-a]pyridine-4-carbonitrile* (6.11)**

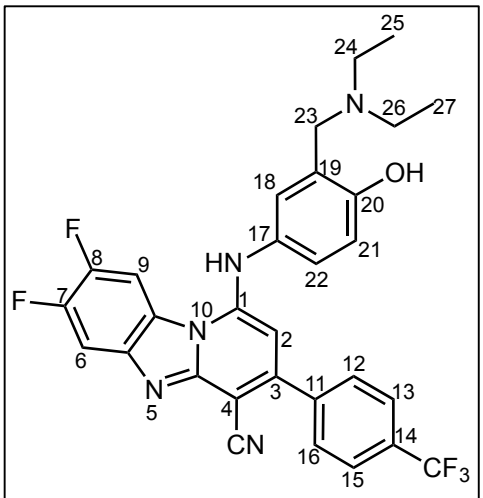

$C_{30}H_{24}F_5N_5O$
Exact Mass: 565.19
Mol. Wt.: 565.55

Obtained from **5.7** (0.405 g, 0.99 mmol, 1.0 equiv.), 4-amino-*α*-diethylamino-*o*-cresol (0.386 g, 1.99 mmol, 2.0 equiv.) and triethylamine (0.28 mL, 1.99 mmol, 2.0 equiv.) as a yellow solid (0.145 g, 26 %); m.p 284 - 288 °C; R_f 0.65 (20 % MeOH-DCM); ^{1}H NMR (400 MHz, DMSO-d_6) δ 8.76 (dd, *J* = 11.5, 8.7 Hz, 1H, ArH^9), 7.80 (d, *J* = 8.2 Hz, 2H, ArH^{13,15}), 7.69 (d, *J* = 8.2 Hz, 2H, ArH^{12,16}), 7.55 (dd, *J* = 11.5, 8.7 Hz, 1H, ArH^6), 7.06 (d, *J* = 2.6 Hz, 1H, ArH^{18}), 6.99 (dd, *J* = 8.5, 2.6 Hz, 1H, ArH^{22}), 6.86 (d, *J* = 8.5 Hz, 1H, ArH^{21}), 5.59 (s, 1H, ArH^2), 4.08 (s, 2H, H^{23}), 2.97 (q, *J* = 7.2 Hz, 4H, H^{24,26}), 1.16 (t, *J* = 7.2 Hz, 6H, H^{25,27}); ^{13}C NMR (101 MHz, DMSO-d_6) δ 153.8, 151.0, 149.3, 149.2, 147.8, 146.8, 144.9, 143.8, 141.8, 141.6, 129.4, 129.2, 126.2, 126.0, 125.8, 125.8, 125.1, 123.3, 120.3, 116.7, 105.0, 104.8, 103.5, 103.3, 92.6, 55.4, 51.9, 47.0, 25.6, 9.6; HPLC-MS (APCI/ESI): Purity= 97%, t_R = 4.15 min, MS: *m/z* 566.2 $[M+H]^+$.

4.3 Assay Protocols

4.3.1. Antiplasmodial activity assay

This procedure was designed for use with culture adapted *P. falciparum* strains and clinical isolates. On one 96-well plate, 6 drugs were tested in duplicate. Standard strains used were *P. falciparum*, NF54 (sensitive to all known drugs) and *Plasmodium falciparum*, K1 (chloroquine and pyrimethamine resistant).

Antimalarial drugs were dissolved in DMSO at 10mg/mL. If insoluble, other solvents were used according to the recommendations of the supplier. For the assays, 4X fresh dilutions of all drugs in screening medium were prepared. Blood smears of stock cultures of the two strains were prepared and parasitemia was determined (parasitemia < 3% was not used). Drug stock solutions were diluted with screening medium to the right start concentrations.

Serial drug dilutions were prepared with a multichannel pipette. 100 μL was taken from wells of row B and transferred, after gentle mixing, to wells of row C. After mixing, 100 μL was transferred from wells of row C to wells of row D and so forth to row H. The 100 μL removed from wells of row H were discarded. A two-fold serial dilution of drugs was thus obtained. For too active compounds the highest concentration was appropriately lowered. Wells of rows A served as controls without drug.

100 μL of infected blood (parasitemia of 0.3%, 2.5% hematocrit) were added to all wells with a multipette. Only the control wells (A9-12) received uninfected blood of 2.5% hematocrit. The plates were incubated in an incubation chamber at 37°C in an atmosphere containing the special gas mixture (93% N_2, 4% CO_2, 3% O_2).

After 48 hours 50 μL [3H]-hypoxanthine (= 0.5 μCi) solution was added to each well of the plate. The plates were incubated for another 24 hours. The plates were then harvested with a BetaplateTM cell harvester (Wallac, Zurich, Switzerland), which transferred the red blood cells onto a glass fiber filter and washed with distilled water. The dried filters were inserted into a plastic foil

with 10 mL of scintillation fluid and counted in a BetaplateTM liquid scintillation counter (Wallac, Zurich, Switzerland). The results were recorded as counts per minute (cpm) per well at each drug concentration. Data was transferred into a graphic programme (e.g. EXCEL) and expressed as percentage of the untreated controls. The 50% inhibitory concentration (IC_{50}) value was evaluated by Logit regression analysis.

Definition of test score: no activity: IC_{50} > 1000 ng/mL; low activity: IC_{50} 50-1000 ng/mL; good activity: IC_{50} < 50 ng/mL. Chloroquine and artesunate are used for each assay as positive controls.

4.3.2 Cytotoxicity assay

Test samples were screened for *in vitro* cytotoxicity against a mammalian cell-line, Chinese Hamster Ovarian (CHO) using the 3-(4,5-dimethylthiazol-2-yl)-2,5-diphenyltetrazoliumbromide (MTT)-assay. The MTT-assay is used as a colorimetric assay for cellular growth and survival. The tetrazolium salt, MTT, was used to measure all growth and chemosensitivity. The test samples were tested in triplicate on one occasion.

The test samples were prepared to a 20 mg/mL stock solution in 100% DMSO. Test compounds were stored at -20°C until use. Dilutions were prepared on the day of the experiment. Emetine was used as the reference drug in all experiments. The initial concentration of emetine was 100 μg/mL, which was serially diluted in complete medium with 10-fold dilutions to give 6 concentrations, the lowest being 0.001 μg/mL. The same dilution technique was applied to all the test samples. The highest concentration of solvent to which the cells were exposed to had no measurable effect on the cell viability (data not shown). The 50% inhibitory concentration (IC_{50}) values were obtained from full dose-response curves, using a non-linear dose-response curve fitting analysis via GraphPad Prism v.4 software.

4.3.3 β-Hematin inhibition assay

Stock solutions of controls and test compounds were made to 20 mM in DMSO. A solution containing water/305.5 *μ*M NP40/DMSO at a v/v ratio of 70%/20%/10%, respectively was added to every well in columns 1-11 while 140 *μ*L of water and 40 *μ*L of 305.5 *μ*M NP40 were added to column 12 to mediate the formation of β-hematin. Twenty microliters of drug (20 mM) was added to column 12 and 100 *μ*L of this solution serially diluted to column 2, and column 1 was left as a blank (0 *μ*M of compound). In case the compound was colored (for instance AQ), a pre-reading of the plate was done by measuring absorbance at 405 nm on a SpectraMax plate reader. A 178.8 *μ*L aliquot of hematin stock was suspended in 20 mL of a 1 M acetate buffer, pH 4.9 and 100 *μ*L of this hematin suspension added into each well. Plates were then incubated for ±5 hours at 37°C after which 32 *μ*L of pyridine solution (20% water, 20% acetone, 10% 2M HEPES buffer (pH 7.4), 50% pyridine) was added, followed by addition of 60 *μ*L of acetone to all wells. Plates were again read at 405 nm and IC_{50} values plotted in GraphPad.

4.3.4 Microsomal metabolic stability assay

The metabolic stability of the compounds was assessed in mouse liver microsomes, using the one point assay described in the Standard Operating Procedure 4.2_NL_20120829 TO assay (pre-clinical pharmacology laboratory at Groote Schuur Hospital).

Briefly, the metabolic stability was determined after 30 minutes incubation of the compounds with mouse liver microsomes. After protein precipitation, the supernatant was analyzed by LC-MS-MS (4000 Q-TRAP AB Sciex) with MRM methods using a Phenomenex Kinetex PFP, 2.1 mm x 50 mm, 2.6 *μ*m particles. The incubations were performed in triplicates and controls were also included (propranolol, midazolam and MMV390048). Results were reported

as % remaining after 30 minutes incubation and as predicted half-life, using the Obach's formula.

4.3.5 Kinetic solubility assay

All target compounds were assessed for kinetic solubility using a 96-well clear polystyrene plate. The compounds were dissolved in HPLC grade DMSO to make 10 mM stock solutions. The pre-dilution plate was prepared by making serial dilutions of the stock solution in DMSO, in triplicate, to obtain concentrations ranging from 0.25 to 8.0 mM.

From the pre-dilution plate, the assay plate is prepared by making secondary dilutions in DMSO and 0.01M pH 7.4 PBS, also in triplicate. These dilutions are made such that the final volume in each assay plate well is 200 μL and the concentrations of the wells range from 0 to 200 μM. The plates were then covered and left to incubate at room temperature for 2 hours. Absorbance measurements were taken at 620 nm with a SpectraMax 340PC mircoplate reader (Molecular Devices, Sunnydale, CA). The analysis wavelength of 620 nm was chosen since few samples are known to absorb at this wavelength and thus it minimizes the chance of false readings resulting from absorbance by the compound in solution. A plot of absorbance vs. concentration is used to identify the limit of solubility.

4.3.6 Equilibrium solubility assay

Aqueous solubility was measured using the DMSO-dry down method, adapted from Zhou *et al.*[76] Briefly, the high and medium calibration standards (220 μM, 100 μM) in duplicate, as well as the samples (200 μM) in triplicate, were added to a 96-well plate, from a 10mM stock solution in DMSO. DMSO was then evaporated in a MiVac sample concentrator (SP Scientific, Cape Town, South Africa) operated at full vacuum, 37°C, for two hours. DMSO was then added to the standards, and after vortexing the plate, the high standard was used to prepare a low (11 μM) calibration standard in DMSO. Phosphate buffered saline (pH 7.4) was added to the sample wells and the plate was

incubated for 24 hours at 25°C with shaking. The plate was then centrifuged at 2500 g for 30 minutes and the supernatants transferred to another plate for analysis.

Aqueous solubility was determined from UV peak areas of the samples relative to the standards using best-fit calibration curves in Microsoft Excel 2013. HPLC-DAD analysis was performed using an Agilent 1200 Rapid Resolution HPLC, coupled with an Agilent 1200 diode array detector (ABSciex, Johannesburg, South Africa). For elution, 0.1% formic acid in water and 0.1% formic acid in acetonitrile were used as mobile phases A and B respectively. A Kinetex C_{18} (50mm x 2.1 mm), packed with 2.6 μM fused-core particles (Separations, Johannesburg, South Africa) was used for the chromatography. Agilent Chemstation was used for instrument control and data processing.

4.3.7 Single crystal XRD analysis

Single-crystal X-ray diffraction data were collected on a Bruker KAPPA APEX II DUO diffractometer using graphite-monochromated Mo-Kα radiation (χ = 0.71073 Å). Data collection was carried out at 173(2) K. Temperature was controlled by an Oxford Cryostream cooling system (Oxford Cryostat). Cell refinement and data reduction were performed using the program SAINT[77]. The data were scaled and absorption correction performed using SADABS[78]. The structure was solved by direct methods using SHELXS-97[78] and refined by full-matrix least-squares methods based on F^2 using SHELXL-2014[78] and using the graphics interface program X-Seed[79,80]. The programs X-Seed and POV-Ray[81] were both used to prepare molecular graphic images.

4.3.8 DFT calculations

All calculations were performed using Gaussian 09 and Jaguar[82] from the Schrödinger Suite 2012. Visualizations were performed using the graphical interface Maestro 7.9.[83]

CHAPTER 5: REFERENCES

(1) World Health Organization. *World Malaria Report 2015*; 2015.

(2) World Health Organization. *World Malaria Report 2016*; 2016.

(3) Kappe, S. H. I.; Kaiser, K.; Matuschewski, K. The Plasmodium Sporozoite Journey: A Rite of Passage. *Trends Parasitol.* **2003**, *19* (3), 135–143.

(4) Phillips, R. S. Current Status of Malaria and Potential for Control. *Clin. Microbiol. Rev.* **2001**, *14* (1), 208–226.

(5) Greenwood, B. M.; Fidock, D. A.; Kyle, D. E.; Kappe, S. H. I.; Alonso, P. L.; Collins, F. H.; Duffy, P. E. Malaria: Progress, Perils, and Prospects for Eradication. *J. Clin. Invest.* **2008**, *118* (4), 1266–1276.

(6) Cho, S.; Kim, S.; Kim, Y.; Park, Y. Optical Imaging Techniques for the Study of Malaria. *Trends Biotechnol.* **2012**, *30* (2), 71–79.

(7) Cowman, A. F.; Crabb, B. S. Invasion of Red Blood Cells by Malaria Parasites. *Cell* **2006**, *124*, 755–766.

(8) Sherman, I. W. Biochemistry of Plasmodium (Malarial Parasites). *Microbiol. Rev.* **1979**, *43* (4), 453–495.

(9) Mohandas, N.; An, X. Malaria and Human Red Blood Cells. *Med. Microbiol. Immunol.* **2013**, *201* (4), 593–598.

(10) Steck, E. A. *The Chemotherapy of Protozoan diseases.V.1, Sects 1-2*; Washington DC, 1972.

(11) Delgado, J. N.; Remers, W. A. *Wilson and Gisvold's Text Book of Organic Medicine and Pharmaceutical Chemistry*, 10th ed.; Lippincott Williams & Wilkins, 1998.

(12) Coatney, G. R. Pitfalls in a Disocvery: The Chronicle of Chloroquine. *Am. J. Trop. Med. Hyg.* **1963**, *12* (November), 121–128.

(13) Young, M. D.; Moore, D. V. Chloroquine Resistance in Plasmodium Falciparum. *Am. J. Trop. Med. Hyg.* **1961**, *10*, 317–320.

(14) Greenwood, B.; Mutabingwa, T. Malaria in 2002. *Nature* **2002**, *415*, 670–672.

(15) Wellems, T. E.; Plowe, C. V. Chloroquine-Resistant Malaria. *J. Infect. Dis.* **2001**, *184*, 770–776.

(16) Dorsey, G.; Fidock, D.; Wellems, T.; Rosenthal, P. *Antimalarial Chemotherapy. Mechanisms of Action, Resistance and New Directions in Drug Discovery*; Humana Press Inc.: Humana, Totowa, New Jersey, 2001.

(17) Cui, L.; Su, X. Discovery, Mechanisms of Action and Combination Therapy of Artemisinin. *Expert. Rev. Anti. Infect .Ther.* **2009**, *7* (8), 999–1013.

(18) Lin, J. T.; Juliano, J. J.; Wongsrichanalai, C. Drug-Resistant Malaria: The Era of ACT. *Curr. Infect. Dis. Rep.* **2010**, *12* (3), 165–173.

(19) World Health Organization. *Antimalarial Drug Combination Therapy: Report of a WHO Technical Consultation*; Geneva, 2001.

(20) World Health Organization. *World Malaria Report 2013*; 2013.

(21) WHO. *Global Report on Antimalrial Drug Efficacy and Drug Resistance 2000-2010*; WHO Press: Geneva, 2010.

(22) World Health Organization. *Status Report on Artemisinin Resistance*; 2014; Vol. 13.

(23) Looasreesuwon, S.; Canfield, C. J.; Chulay, J. D.; Hutchinson, D. B. A. Malarone (Atovaquone and Proguanil Hydrochloride): A Review of Its Clinical Development for Treatment of Malaria. *Am. J. Trop. Med. Hyg.* **1999**, *60* (4), 533–541.

(24) Tan, K. R.; Magill, A. J.; Parise, M. E.; Arguin, P. M. Doxycycline for Malaria Chemoprophylaxis and Treatment: Report from the CDC Expert Meeting on Malaria Chemoprophylaxis. *Am. J. Trop. Med. Hyg.* **2011**, *84* (4), 517–531.

(25) World Health Organization. *Guidelines for the Treatment of Malaria*; 2006.

(26) Al-Ali, H. The Evolution of Drug Discovery: From Phenotypes to Targets, and Back. *Med. Chem. Commun.* **2016**, *7*, 788–798.

(27) Kotz, J. Phenotypic Screening, Take Two. *SciBX* **2012**, *5* (15), 1–3.

(28) Carr, R. A. E.; Congreve, M.; Murray, C. W.; Rees, D. C. Fragment-Based Lead Discovery: Leads by Design. *Drug Discov. Today* **2005**, *10* (14), 987–992.

(29) Butera, J. A. Phenotypic Screening as a Strategic Component of Drug Discovery Programs Targeting Novel Antiparasitic and

Antimycobacterial Agents: An Editorial. *J. Med. Chem.* **2013**, *56* (20), 7715–7718.

(30) Swinney, D. C.; Anthony, J. How Were New Medicines Discovered? *Nat. Rev. Drug Discov.* **2011**, *10* (7), 507–519.

(31) Njoroge, M.; Njuguna, N. M.; Mutai, P.; Ongarora, D. S. B.; Smith, P. W.; Chibale, K. Recent Approaches to Chemical Discovery and Development Against Malaria and the Neglected Tropical Diseases Human African Trypanosomiasis and Schistosomiasis. *Chem. Rev.* **2014**, *114*, 11138–11163.

(32) Wells, T. N. C. Is the Tide Turning for New Malaria Medicines? *Science* **2010**, *329* (5996), 1153–1154.

(33) Hart, C. P. Finding the Target after Screening the Phenotype. *Drug Discov. Today* **2005**, *10* (7), 513–519.

(34) Sykes, M. L.; Avery, V. M. Approaches to Protozoan Drug Discovery: Phenotypic Screening. *J. Med. Chem.* **2013**, *56* (20), 7727–7740.

(35) Jeffery, D. A.; Bogyo, M. Chemical Proteomics and Its Application to Drug Discovery. *Curr. Opin. Biotechnol.* **2003**, *14* (1), 87–95.

(36) Cong, F.; Cheung, A. K.; Huang, S.-M. A. Chemical Genetics–Based Target Identification in Drug Discovery. *Annu. Rev. Pharmacol. Toxicol* **2012**, *52*, 57–78.

(37) Guiguemde, W. A.; Shelat, A. A.; Garcia-Bustos, J. F.; Diagana, T. T.; Gamo, F. J.; Guy, R. . Global Phenotypic Screening for Antimalarials. *Chem. Biol.* **2012**, *19* (1), 116–129.

(38) Yayon, A.; Timberg, R.; Friedman, S.; Ginsburg, H. Effects of Chloroquine on the Feeding Mechanism of the Intraerythrocytic Human Malarial Parasite Plasmodium Falciparum. *J. Protozool.* **1984**, *31* (3), 367–372.

(39) Egan, T. J. Haemozoin Formation. *Mol. Biochem. Parisitol.* **2008**, *157* (2), 127–136.

(40) Sigala, P. A.; Crowley, J. R.; Hsieh, S.; Henderson, J. P.; Goldberg, D. E. Direct Tests of Enzymatic Heme Degradation by the Malaria Parasite Plasmodium Falciparum. *J. Biol. Chem.* **2012**, *287* (45), 37793–37807.

(41) Egan, T. J.; Marques, H. M. The Role of Haem in the Activity of Chloroquine and Related Antimalarial Drugs. *Coord. Chem. Rev.* **1999**,

192, 493–517.

(42) Basilico, N.; Pagani, E.; Monti, D.; Olliaro, P.; Taramelli, D. A Microtitre-Based Method for Measuring the Haem Polymerization Inhibitory Activity (HPIA) of Antimalarial Drugs. *J. Antimicrob. Chemother.* **1998**, *42* (1), 55–60.

(43) Kerns, E. H.; Di, L. *Drug-like Properties: Concepts, Structures Design and Methods*; Elsevier Inc.: Burlington, MA, USA, 2008.

(44) Bhattachar, S. N.; Deschenes, L. A.; Wesley, J. A. Solubility: It's Not Just for Physical Chemists. *Drug Discov. Today* **2006**, *11* (21/22), 1012–1018.

(45) Ishikawa, M.; Hashimoto, Y. Improvement in Aqueous Solubility in Small Molecule Drug Discovery Programs by Disruption of Molecular Planarity and Symmetry. *J. Med. Chem.* **2011**, *54*, 1539–1554.

(46) Jain, N.; Yalkowsky, S. H. Estimation of the Aqueous Solubility 1: Application to Organic Nonelectrolytes, J. *J. Pharm. Sci.* **2001**, *90* (2), 234–252.

(47) Wu, W.; Mckown, L. A.; Reitz, A. B. Metabolism of the New Anxiolytic Agent, a pyrido[1,2-A]benzimidazole (PBI) Analog (RWJ-53050), in Rat and Human Hepatic S9 Fractions, and in Dog; Identification of Cytochrome p450 Isoforms Mediated in the Human Microsomal Metabolism. *Eur. J. Drug Metab. Phannacokinet.* **2006**, *31* (4), 277–283.

(48) Thomas, G. *Medicinal Chemistry, An Introduction*, 2nd ed.; John Wiley & Sons, Ltd.: Chichester, Uk, 2007.

(49) Hasler, J. A.; Estabrook, R.; Murray, M.; Pikuleva, I.; Waterman, M.; Capdevila, J.; Holla, V.; Helvig, C.; Falck, J. R.; Farrell, G.; Kaminsky, L. S.; Spivack, S. D.; Boitier, E.; Beaune, P. Human Cytochromes P450. *Mol. Aspects Med.* **1999**, *20*, 1–137.

(50) Zhang, Y.; Bachmeier, C.; Miller, D. W. In Vitro and in Vivo Models for Assessing Drug Efflux Transporter Activity. *Adv Drug Deliv Rev* **2003**, *55*, 31–51.

(51) Brandon, E. F. A.; Raap, C. D.; Meijerman, I.; Beijnen, J. H.; Schellens, J. H. M. An Update on in Vitro Test Methods in Human Hepatic Drug Biotransformation Research: Pros and Cons. *Toxicol. Appl. Pharmacol.* **2003**, *189*, 233–246.

(52) Dalvie, D.; Obach, R. S.; Kang, P.; Prakash, C.; Loi, C.; Hurst, S.; Nedderman, A.; Goulet, L.; Smith, E.; Bu, H.; Smith, D. A. Assessment of Three Human in Vitro Systems in the Generation of Major Human Excretory and Circulating Metabolites. *Chem. Res. Toxicol.* **2009**, *22*, 357–368.

(53) González Cabrera, D.; Douelle, F.; Younis, Y.; Feng, T. S.; Le Manach, C.; Nchinda, A. T.; Street, L. J.; Scheurer, C.; Kamber, J.; White, K. L.; Montagnat, O. D.; Ryan, E.; Katneni, K.; Zabiulla, K. M.; Joseph, J. T.; Bashyam, S.; Waterson, D.; Witty, M. J.; Charman, S. A.; Wittlin, S.; Chibale, K. Structure-Activity Relationship Studies of Orally Active Antimalarial 3,5-Substituted 2-Aminopyridines. *J. Med. Chem.* **2012**, *55*, 11022–11030.

(54) Ellis, G. P. *The Chemistry of Heterocyclic Compounds, Synthesis of Fused Heterocycles*, Volume 47.; Ellis, G. P., Ed.; John Wiley & Sons, Ltd.: Chichester, UK, 1992.

(55) Refaat, H. M. Synthesis of Potential Anticancer Derivatives of pyrido[1,2-A]benzimidazoles. *Med. Chem. Res.* **2012**, *21* (7), 1253–1260.

(56) Takeshita, H.; Watanabe, J.; Kimura, Y.; Kawakami, K.; Takahashi, H.; Takemura, M.; Kitamura, A.; Someya, K.; Nakajima, R. Novel Pyridobenzimidazole Derivatives Exhibiting Antifungal Activity by the Inhibition of B-1,6-Glucan Synthesis. *Bioorganic Med. Chem. Lett.* **2010**, *20* (13), 3893–3896.

(57) Pieroni, M.; Tipparaju, S. K.; Lun, S.; Song, Y.; Sturm, A. W.; Bishai, W. R.; Kozikowski, A. P. Pyrido[1,2-A]benzimidazole-Based Agents Active Against Tuberculosis (TB), Multidrug-Resistant (MDR) TB and Extensively Drug-Resistant (XDR) TB. *ChemMedChem* **2011**, *6* (2), 334–342.

(58) Kotovskaya, S. K.; Baskakova, Z. M.; Charushin, V. N.; Chupakhin, O. N.; Belanov, E. F.; Bormotov, N. I.; Balakhnin, S. M.; Serova, O. A. Synthesis and Antiviral Activity of Fluorinated pyrido[1,2-A]benzimidazoles. *Pharm. Chem. J.* **2005**, *39* (11), 574–578.

(59) Maryanoff, B. E.; Ho, W.; Mccomsey, D. F.; Reitz, A. B.; Grow, P. P.; Nortey, S.; Shank, R. P.; Dubinsky, B.; Taylor, R. J.; Gardocki, J. F.

Potential Anxiolytic Agents. Pyrido[1,2-A]benzimidazoles: A New Structural Class of Ligands for the Benzodiazepine Binding Site on GABA-A Receptors. *J. Med. Chem.* **1995**, *38*, 16–20.

(60) Khare, S.; Roach, S. L.; Barnes, S. W.; Hoepfner, D.; Walker, J. R.; Chatterjee, A. K.; Neitz, R. J.; Arkin, M. R.; McNamara, C. W.; Ballard, J.; Lai, Y.; Fu, Y.; Molteni, V.; Yeh, V.; McKerrow, J. H.; Glynne, R. J.; Supek, F. Utilizing Chemical Genomics to Identify Cytochrome B as a Novel Drug Target for Chagas Disease. *PLoS Pathog* **2015**, *11* (7), 1–22.

(61) Ryzvanovich, G. A.; Begunov, R. S.; Rachinskaya, O. A.; Muravenko, O. V.; Sokolov, A. A. Synthesis and Intercalation Ability of New Pyrido[1,2-A]benzimidazoles. *Pharm. Chem. J.* **2011**, *45* (3), 141–143.

(62) Lyons, D. M.; Huttunen, K. M.; Browne, K. A.; Ciccone, A.; Trapani, J. A.; Denny, W. A.; Spicer, J. A. Inhibition of the Cellular Function of Perforin by 1-Amino-2,4-dicyanopyrido[1,2-A]benzimidazoles. *Bioorg. Med. Chem.* **2011**, *19* (13), 4091–4100.

(63) Ndakala, A. J.; Gessner, R. K.; Gitari, P. W.; October, N.; White, K. L.; Hudson, A.; Fakorede, F.; Shackleford, D. M.; Keiser, M.; Yeates, C.; Charman, S. A.; Chibale, K. Antimalarial Pyrido[1,2- A]benzimidazoles. *J. Med. Chem.* **2011**, *54*, 4581–4589.

(64) Singh, K.; Okombo, J.; Brunschwig, C.; Ndubi, F.; Barnard, L.; Wilkinson, C.; Njogu, P. M.; Njoroge, M.; Laing, L.; Machado, M.; Reader, J.; Botha, M.; Nondaba, S.; Birkholtz, L.; Lauterbach, S.; Churchyard, A.; Coetzer, T. L.; Burrows, J. N.; Yeates, C.; Denti, P.; Wiesner, L.; Egan, T. J.; Wittlin, S.; Chibale, K. Antimalarial Pyrido[1,2 - a]Benzimidazoles: Lead Optimization, Parasite Life Cycle Stage Pro Fi Le, Mechanistic Evaluation, Killing Kinetics, and in Vivo Oral E Ffi Cacy in a Mouse Model. *J. Med. Chem.* **2017**, *60*, 1432–1448.

(65) Xiao, J.-C.; Shreeve, J. M. Microwave-Assisted Rapid Electrophilic Fluorination of 1,3-Dicarbonyl Derivatives with Selectfluor. *J. Fluor. Chem.* **2005**, *126*, 475–478.

(66) Pieroni, M.; Tipparaju, S. K.; Lun, S.; Song, Y.; Sturm, A. W.; Bishai, W. R.; Kozikowski, A. P. Pyrido[1,2- A]benzimidazole-Based Agents Active

Against Tuberculosis (TB), Multidrug-Resistant (MDR) TB and Extensively Drug-Resistant (XDR) TB. *ChemMedChem* **2011**, *6* (2), 334–342.

(67) Ncokazi, K. K.; Egan, T. J. A Colorimetric High-Throughput β-Hematin Inhibition Screening Assay for Use in the Search for Antimalarial Compounds. *Anal. Biochem.* **2005**, *338* (2), 306–319.

(68) Kerns, E. H.; Di, L.; Carter, G. T. In Vitro Solubility Assays in Drug Discovery. *Curr. Drug Metab.* **2008**, *9*, 879–885.

(69) Bard, B.; Martel, S.; Carrupt, P. A. High Throughput UV Method for Estimation of Thermodynamic Solubility and the Determination of the Solubility in Biorelevant Media. *Eur. J. Pharm. Sci.* **2008**, *33*, 230–240.

(70) Moos, W. H.; Green, G. D. Recent Advances in the Generation of Molecular Diversity. *Annu. Rep. Med. Chem.* **1993**, *28*, 315.

(71) Etter, M. C.; MacDonald, J. C.; Bernstein, J. Graph-Set Analysis of Hydrogen-Bond Patterns in Organic Crystals. *Acta Cryst.* **1990**, *B46*, 256–262.

(72) Frisch M.J., Trucks G.W., Schlegel H.B., Scuseria G.E., R. M. A.; Cheeseman J.R., Scalmani G., Barone V., Mennucci B., P.; G.A., Nakatsuji H., Caricato M., Li X., Hratchian H.P., I. A. F.; Bloino J., Zheng G., Sonnenberg J.L., Hada M., Ehara M., T. K.; Fukuda R., Hasegawa J., Ishida M., Nakajima T., Honda Y., K.; O., Nakai H., Vreven T., Montgomery Jr J.A., Peralta J.E., O. F.; Bearpark M., Heyd J.J., Brothers E., Kudin K.N., S. V. N.; Kobayashi R., Normand J., Raghavachari K., Rendell A., B. J. C.; Iyengar S.S., Tomasi J., Cossi M., Rega N., Millam N.J., K. M.; Knox J.E., Cross J.B., Bakken V., Adamo C., Jaramillo J., G.; R., Stratmann R.E., Yazyev O., Austin A.J., Cammi R., P. C.; Ochterski J.W., Martin R.L., Morokuma K., Zakrzewski V.G., V.; G.A., Salvador P., Dannenberg J.J., Dapprich S., Daniels A.D., F.; O. Foresman J.B., Ortiz J.V., Cioslowski J., F. D. J. Gaussian 09. Gaussian, Inc.: Wallingford, CT, 2009.

(73) Macrae, C. F.; Bruno, I. J.; Chisholm, J. A.; Edgington, P. R.; McCabe, P.; Pidcock, E.; Rodriguez-Monge, L.; Taylor, R.; van de Streek, J.; Wood, P. A. Mercury CSD 3.5.1 New Features for the Visualization and Investigation of Crystal Structures. *J. Appl. Crystallogr.* **2008**, *41*, 466–

470.

(74) Neill, P. M. O.; Mukhtar, A.; Stocks, P. A.; Randle, L. E.; Hindley, S.; Ward, S. A.; Storr, R. C.; Bickley, J. F.; Neil, I. A. O.; Maggs, J. L.; Hughes, R. H.; Winstanley, P. A.; Bray, P. G.; Park, B. K. Isoquine and Related Amodiaquine Analogues : A New Generation of Improved 4-Aminoquinoline Antimalarials. *J. Med. Chem.* **2003**, *46* (23), 4933–4945.

(75) Maggs, J. L.; Tingle, M. D.; Kitteringham, N. R.; Park, B. K. Drug-Protein Conjugates--XIV. Mechanisms of Formation of Protein-Arylating Intermediates from Amodiaquine, a Myelotoxin and Hepatotoxin in Man. *Biochem. Pharmacol.* **1988**, *37* (2), 303–311.

(76) Zhou, L.; Yang, L.; Tilton, S.; Wang, J. Development of a High Throughput Equilibrium Solubility Assay Using Miniaturized Shake-Flask Method in Early Drug Discovery. *J. Pharm. Sci* **2007**, *96* (11), 3052–3071.

(77) SAINT Version 7.60a. Bruker AXS Inc.: Madison, WI, USA, 2006.

(78) Sheldrick, G. M. SHELXS-97, SHELXL-2014 and SADABS Version 2.05. University of Göttingen, Germany 1997.

(79) Barbour, L. J. X-Seed - A Software Tool for Supramolecular Crystallography. *J. Supramol. Chem.* **2001**, *1* (4), 189–191.

(80) Atwood, J. L. and Barbour, L. J. Molecular Graphics: From Science to Art. *Cryst. Growth Des.* **2003**, *3* (1), 3–8.

(81) POV-Ray http://www.povray.org.

(82) Jaguar Version 7.9. Schrodinger.: LLC, New York, NY 2012.

(83) Maestro Version 7.9. Schrodinger: LLC, New York 2012.